ABSTRACT

Title of Document: DEVELOPING A NEW MODEL OF THE GROEL FUNCTIONAL CYCLE AND ITS IMPLICATIONS FOR THE GROEL-OPTIMIZED SUBSTRATE PROTEIN REFOLDING

Xiang Ye, Doctor of Philosophy, 2014

Directed By: Professor George H. Lorimer, Department of Chemistry and Biochemistry

Despite years of research work, many aspects of the fundamentally important GroEL functional cycle are still in dispute. The work of this dissertation mainly focuses on three major disputes in the field: the identity of the rate determining step (RDS), the physiological order of arrival of ligands (ATP, SP and GroES) to the GroEL *trans* ring, and the role of the symmetric GroEL-$GroES_2$ "football" complex in the overall chaperonin cycle. With multiple carefully designed spectroscopic probes, a pre-steady state survey has been conducted on the kinetics of the GroEL functional cycle. From the survey, a two cycle model emerges: in the absence of SP, ADP release is the RDS of the *asymmetric cycle* and consequently, the asymmetric GroEL-$GroES_1$,"bullet" which precedes this step, is the pre-dominant species. In this mode, the machine turns over very slowly, minimizing futile ATP consumption. Due to the slow release of ADP, the system turns over in a well defined manner with the two rings operating 180^o out of phase of

each other, analogous to a two-stroke motor. In the *symmetric cycle*, which operates in the presence of SP, the release of ADP is greatly accelerated while the intrinsic ATPase activity of GroEL remains unaffected. Consequently ATP hydrolysis becomes the RDS and the symmetric GroEL-$GroES_2$ "football" becomes the predominant species. Contrary to previous chaperonin dogma, the symmetric complex is a highly dynamic species exchanging its two bound ligands, GroES and encapsulated SP from both rings with a half time ~1sec. Switching to a parallel processing machine, the chaperonins turns over rapidly, ultimately driven by stochastic hydrolysis of ATP which causes the symmetric complex to undergo breakage of symmetry (BoS). With such a dynamic system, folding in the 'folding cage' seems less important in GroEL-mediated SP refolding as suggested by the passive refolding model. Instead, GroEL may play a more active role in achieving its central biological function as indicated by this two cycle model. This may be the very reason why employing even as low as one GroEL ring per ten SP can achieve SP refolding to a similar extent as using a stoichiometric amount.

DEVELOPING A NEW MODEL OF THE GROEL FUNCTIONAL CYCLE AND ITS IMPLICATIONS FOR THE GROEL-OPTIMIZED SUBSTRATE PROTEIN REFOLDING

By

Xiang Ye

Dissertation submitted to the Faculty of the Graduate School of the
University of Maryland, College Park, in partial fulfillment
of the requirements for the degree of
Doctor of Philosophy
2014

Advisory Committee:
Professor George H. Lorimer, Chair
Professor Dorothy Beckett
Professor Douglas Julin
Professor Nicole LaRonde
Professor Wade Winkler

Acknowledgements

My particular thanks to my advisor, Dr. George Lorimer, for his outstanding mentorship and excellent grasp of the development of the field which not only transformed me in these six years but also granted me the opportunity to be part of the research work that rewrites the history of chaperonin. Thanks also to my committee for their time and effort in helping me complete this degree.

Thanks to all my lab mates: Dong Yang, Nicolas Corsepius, and Xue Fei for their inspirative collaborations with me which tremendously enhance the quality and quantity of my work. Especially thanks to Nicolas Corsepius for generously sharing his computational idea with me and I really learned a lot from him.

Finally, thanks to my parents. Though for the most part they stay on the other side of the globe, without their support and understanding, I cannot move so far from home and from where I started six years ago.

Table of Contents

List of Figures

Chapter 1: Introduction and Specific Aims

Proteins are a group of macromolecules with complex structures and diverse biochemical functions. For most proteins, their normal functions depend on a delicate balance between stability and plasticity of their structures [1-4]. Therefore, proteins are usually marginally stable, with the free energy difference separating the folded native state and the unfolded denatured states as small as several times of the thermal energy ($R*T$) [5]. Though protein folding is thermodynamically favorable under physiological conditions, some proteins, once unfolded, may be unable to refold back to their native conformation by themselves. They are frequently caught in local minimum on their rugged folding landscape which either leads to irreversible formation of aggregates or to folding on a time scale longer than that of biological significance [6]. As a result, it is of vital importance for cells to maintain their proteo-homeostasis and control their protein products in order to survive [7].

To fulfill such task, an integrated network of a large array of specialized protein molecules has evolved, and among them the most studied are molecular chaperones (assisting protein refolding or preventing formation of aggregation) and the ubiquitin-proteasome system to remove irreversible aggregates or other targeted proteins [7]. Of particular interest is the chaperonin of *E. coli*, GroEL, a ring-structured molecular chaperone, which is also among the best studied and the most remarkable molecular machine [8-10].

GroEL can rescue its mis-folded, hydrophobic-residue-exposed substrate protein (SP) by undergoing a complex, multi-stepped cycle driven by ATP hydrolysis which is usually referred to as the GroEL functional cycle or ATPase cycle [10-11]. To understand

how the GroEL-optimized SP refolding is achieved, it is essential to map out the whole functional cycle. However, despite much effort, many aspects of this cycle are still in dispute [10, 12-13]. Three major sources of dispute are introduced and briefly review in this chapter, and the work presented in this dissertation leads to proposal of a new comprehensive model that can account for seemingly contradictory results reported in literature. But before introducing the GroEL functional cycle, I give a brief description on the overall architecture of GroEL and GroES, and various domain movements induced by ligand binding to the chaperonin molecule.

1.1 The Structures of GroEL and GroES

GroEL is a ring-shaped homo-tetradecamer, with two seven-member rings stacked back to back (Figure 1-1). Each subunit of GroEL is of 57kDa in size and comprises three domains: the apical, the intermediate, and the equatorial domain. In the apical domain, the SP binding site is identified at the inner top rim of the ring just between Helix H and Helix I [14-15] (Figure 1-1 left bottom). Interestingly, the same site is also where GroES, the co-chaperonin binds [15]. This is believed to be critical for SP encapsulation and SP refolding by chaperonins.

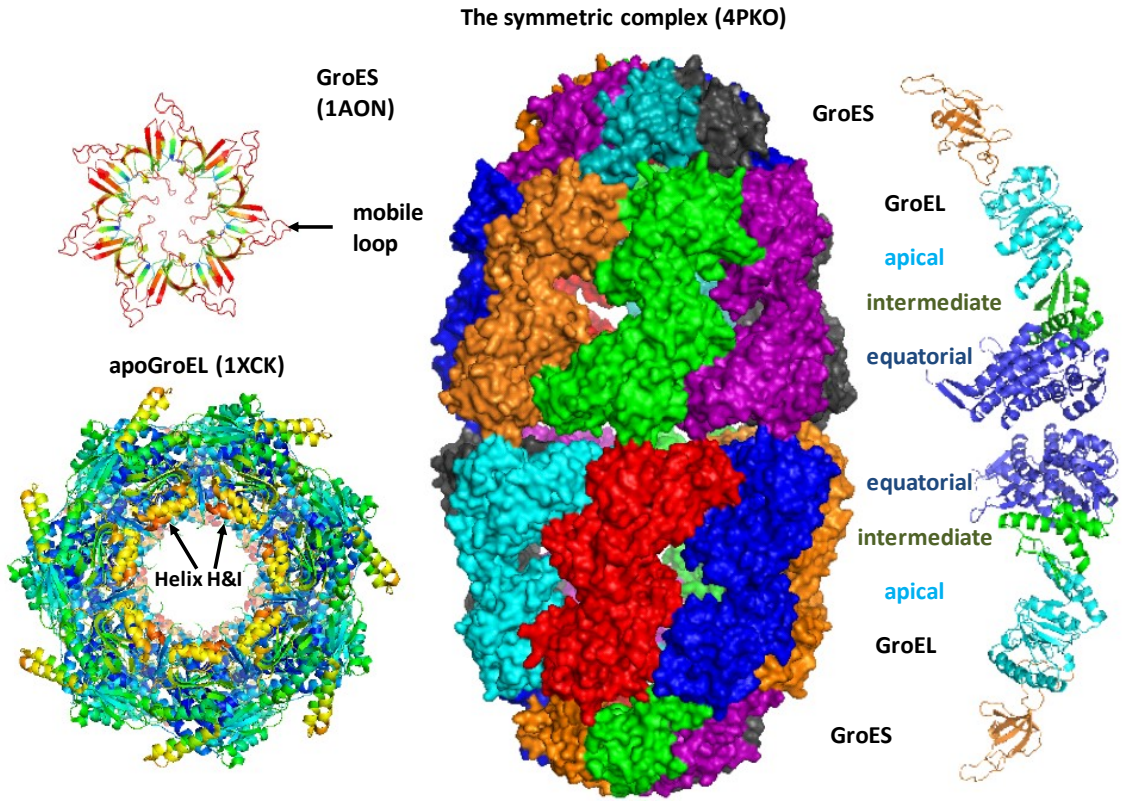

Figure 1-1: The crystal structures of GroEL, GroES, and the symmetric complex. The space filling model in the middle column shows the overall architecture of the symmetric GroEL:ES_2 complex solved by my colleague Xue Fei [16] with individual subunit colored differently. **Right**: a column of two pairs of GroEL and GroES subunit taken from the symmetric complex structure. The three domains of the GroEL subunit are colored differently. **Left**: top views of GroES heptmer (top) and apo-GroEL (bottom) [17]. Both structures are colored according to the b-factor of the main chain carbon (from red to blue, b-factor decreases). It appears that the two helices involved in SP and GroES binding (helix H and I) have exceptionally high b-factors possibly due to residual contaminating SPs. The pdb code for each structure is also included in parenthesis following the name of the molecule.

The equatorial domain contains the nucleotide binding pocket [18] and forms multiple interactions with that of the opposite ring. Those inter-ring interactions are vital for maintaining the two-ring structure and responsible for transmitting allosteric signals across the ring [18]. In Chapter 7, I present experimental work on a mutant in the ring interface that unambiguously demonstrates the influence of inter-ring allostery on GroEL function. The intermediate domain connects the other two domains, and acts as the hinge

point for the large inter-domain rigid-body movements transmitting allosteric signals caused by ligand binding (discussed in greater detail in the next section).

GroES, the cochaperonin, is a dome-shaped homo-heptamer with subunit size of 10kDa (Figure 1-1). Each subunit of GroES has a flexible loop (mobile loop) protruding out toward the bottom of GroES dome which anchors the cochaperonin onto its binding site on GroEL apical domain [19].

1.2 GroEL domain movements accompanying ligand binding

Understanding the domain movements initiated by ligand binding is critical for understanding the mechanism by which GroEL mediates SP refolding in the presence of ATP and GroES. These movements have been worked out by comparing the structures of apo GroEL [18] and GroEL/GroES 1:1 complex (asymmetric complex) (X-ray crystal structure) [14] along with structure of GroEL with ATP in binding sites (cryo-EM structure) [20], and can be satisfactorily described as rigid-body movements. A new high resolution crystal structure of ADP bound GroEL was solved last year and reveals very interesting features that were not accessible with the low resolution cryo-EM ATP-GroEL structure [21].

In the absence of nucleotide, the GroEL tetradecamer adopts a relatively compact conformation and is assigned as the 'Taut' or T state according to allosteric formulation [22]. This state has low affinity for nucleotide and high affinity for SP. SP binding sites are in the hydrophobic groove formed between Helix H and I of each subunit [15]. The exposure of hydrophobic residues of SP is considered as the most important factor for being recognized by GroEL and accounts for the broad substrate specificity of GroEL [23].

Nucleotide binding (ATP or ADP) to the binding pocket at the base of the equatorial domain breaks multiple salt-bridges that stabilize the T state and sets free relevant structural elements for GroES binding and SP encapsulation. Comparing the crystal structure of apo-GroEL with both the cryo-EM struture of ATP-bound GroEL and the crystal structure of ADP-bound GroEL shows that upon nucleotide binding, the M-helix of intermediate domain moves downward and partially closes the nucleotide binding pocket. Such domain movement is used to explain why the affinity for nucleotide is enhanced in this state [20-21]. The structural rearrangements are not just confined to the nucleotide binding site but are also transmitted to the apical domain via the intermediate domain. Hinging on Pro137 and Gly410 of intermediate domain, the apical domain undergoes a 25 degree anti-clockwise twist and the top part of it is set loose and become asymmetric due to breakage of multiple salt-bridges that stabilize the symmetric T state [21]. The most important result is that the seven SP binding sites are dispersed and presented upward which is believed to be the origin of lower SP affinity and forceful unfolding. The resulted new state is predominantly populated in the presence of nucleotide and termed the R state.

The large scale domain movements induced by nucleotide binding set the stage for subsequent GroES binding. While the crystal structure of asymmetric complex shows no great difference in the ring unoccupied by GroES binding (*trans* ring) from apo-GroEL T state structure, the opposite ring (*cis*-ring), capped by GroES, adopts a very different conformation from either T state or R state, thus termed as R' state [14]. In this state, the largest change occurs in the apical domain which, as a whole, moves upward 60 degree horizontally and shifts 90 degree vertically. Such a great transition is attributed to

GroES binding. GroES association with GroEL can best be described as a 'lid on a pot' model and in this manner creates an enclosed chamber which is believed to be critical for SP refolding, though dispute exists as to the role played by this enclosed chamber in SP refolding.

Though GroEL structures at different allosteric states provide invaluable insight into the mechanism of GroEL-mediated SP refolding, the gaps between these static pictures need to be filled by kinetic studies on GroEL with a cohort of its allosteric effectors. In reality, in combination with the structural information, results of kinetic studies of the sort greatly facilitate our understanding of the complex and intriguing GroEL ATPase functional cycle.

1.3 Overview of the GroEL functional Cycle

To understand the mechanism by which GroEL assists SP refolding, it is essential to decode the complex chaperonin functional cycle driven by ATP hydrolysis because it is via this cycle that SP refolding is achieved by the chaperonins. The overall structure of the cycle can be worked out from the ligand-induced domain movements introduced in last section along with well designed kinetic studies: firstly, GroEL captures denatured SP in its apo T state which has higher affinity for SP, then nucleotide binding, especially ATP, shifts the GroEL conformation to R state and weakens SP binding preparing for SP encapsulation. SP encapsulation is finally accomplished by the binding of GroES which, with GroEL, forms an enclosed chamber. Encapsulated SP is released after ATP is hydrolyzed which primes the GroES of the opposite ring to dissociate [9-10].

However, despite decades of intense study, a comprehensive detailed model of the cycle is still elusive mainly because the *GroE* system is extremely complex and any effort to characterize it has to take into account many different factors. The complexity of the chaperonins has two origins (Figure 1-2): on the one hand, due to the two-ring structure of GroEL, there are two layers of communication: allostery between subunits of the same ring and allostery between the two rings. On the other hand, there are five important allosteric factors that can influence GroEL ATPase, i.e. GroES, ATP·Mg^{2+}, ADP·Mg^{2+}, K^+, and SP; and these five factors are cross-correlated in affecting each other's role in GroE function, weaving an overwhelmingly complex tapestry of communication [22-26].

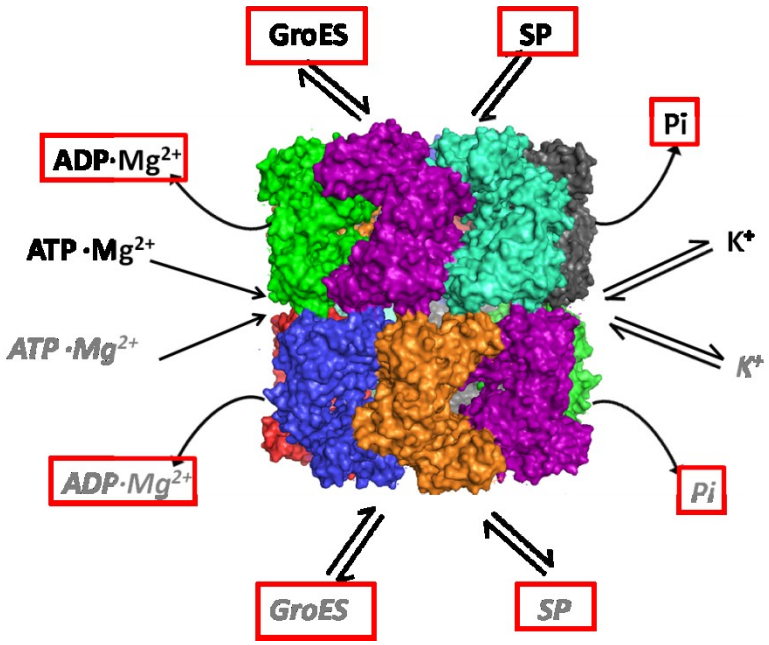

Figure 1-2: Ligands that are involved in the GroEL functional cycle. Those marked with blue rectangles are steps monitored in this dissertation.

Among all five allosteric effectors, GroES and ATP are most studied because they are obligatory for many SPs to be refolded by GroEL [27]. One of the hallmarks of

GroEL ATPase cycle is its 'positive-nested-in-negative' cooperativity regarding steady-state ATP hydrolysis: the ATP turnover rate of GroEL rises at increasing, relatively low [ATP], but then decreases as [ATP] is further increased, and finally reaches a plateau [28]. Addition of GroES into the assay solution can further reduce the turnover rate by 50% to 70%. In light of the double multi-subunit ring structure, Horvitz and his colleague propose a nested-cooperativity model to account for such unusual behavior of ATP hydrolysis [22, 28]. In this model, there are two layers of allostery corresponding to the two layers of GroEL architecture: a concerted Monod-Wyman-Changeaux (MWC) mode [29] is used to describe the transition from T to R state of subunit within a ring, and a sequential Koshland-Nemethy-Filmer (KNF) mode [30] for transition between rings from T/T to R/R via an intermediate T/R. It turns out that both T and R states can bind and hydrolyze ATP though the actual numbers vary from study to study, probably because of the difficulties in defining these allosteric states [31-32]. As for the unusual ATP turnover decrease as [ATP] increase behavior, though it has long being speculated as a result of inter-ring communication by many studies [22, 33-34], the very structural element responsible for such inter-ring allostery is unambiguously identified by the work presented in Chapter 8.

Different from ATP and GroES that attract most of the attention, the other three allosteric effectors are generally ignored. It is well known that potassium is required for ATP hydrolysis and can enhance nucleotide affinity [26], but throughout the literature, $[K^+]$ varies from 5mM to 200mM depending on the group from which the work was published [27, 33, 35-36]. A similar situation is also found with SP: though it is already known that SP can accelerate GroEL ATP turnover [10, 37] and can exert many other

effects in different ways depending the nature of the experiment [10, 32]. The purity of GroEL sample used in the literature can vary tremendously. The role of $ADP \cdot Mg^{2+}$ is probably the most elusive, especially the rate at which it is release by GroEL, which makes the first dispute regarding the GroEL functional cycle that this dissertation intends to address. Some groups claim ADP release is fast and thus ATP hydrolysis is the only rate-determining step [36, 38] whereas others believe ADP release is slow and is *the* rate-determining step [39-41]. Both sides have experimental results to bolster their claim. As I present in Chapter 3 and 4, such bewildering situation can be largely attributed to the lack of appreciation of the role played by both potassium and SP as GroEL activity modulators.

1.4 Two different models depicting the GroEL functional cycle

As can be expected from the fact that no agreement has been reached on the rate-determining step of the cycle, there is no universally accepted model either. Nevertheless, based on experimental results accumulated from decades of study, there are two major competing models that differ from each other mainly in terms of the predominant folding-active chaperonin species: a two-stroke motor model proposes that the two GroEL rings function alternately almost 180 degree out of phase with each other and predicts the asymmetric GroEL:ES_1 complex to be the predominant species [42]; and a football model with the two GroEL rings function simultaneously and, of course, the symmetric GroEL:ES_2 complex as the predominant species [43-46]. Intriguingly, the disputes over the two models reflect how complex the chaperonin system is and witnesses how our understanding on GroEL functionality evolves.

The ‘football’ model was initially proposed based on the observation of football-shaped $GroEL_1$:$GroES_2$ symmetric particles in the presence of ATP under transmission electro-microscope (TEM) [43]. This model envisions ATP hydrolysis as the rate-determining step which leads to accumulation of chaperonin complex immediately before this step, the GroEL:ES_2 symmetric particles observed by TEM [44, 47]. Later studies showed that this complex is capable of mediating SP refolding [48-49] and two model substrates, maltose binding protein (MBP) [50] and rhodanese [51] have been observed to be encapsulated in both rings.

However, Ulrich Hartl’s group reported that the symmetric complex was an artifact formed only under certain unnatural conditions and the predominant physiological species should be the asymmetric complex [52-53]. Despite the fact that no other group could reach the same conclusion [54], the ‘bullet’ model, with the bullet-shaped $GroEL_1$:$GroES_1$ asymmetric particles as the folding active species, gained the upper hand. This can be at least partially attributed to a couple of studies performed by Arthur Horwich’s group. In one such study, they reported that when one GroEL ring (the *cis* ring) was occupied by ATP and GroES (the ‘ÁTP’ bullet), the other ring (the *trans* ring) was incompetent to accepting either ATP or GroES; only after ATP was hydrolyzed to ADP, turning the ‘ATP’ bullet into to ‘ADP’ bullet, could the *trans*-ring recruit ATP followed by GroES [55]. They attribute such mutually exclusive ligand binding event between the two GroEL rings to the inter-ring negative cooperativity [55]. In addition, as they also found, the symmetric complex formed with ADP in one ring and ATP in the other ring was only a transient intermediate and could rapidly break into the asymmetric bullet by releasing GroES from the ADP bound ring [56]. Therefore, they concluded that

i) due to the strong inter-ring negative cooperativity, the symmetric complex with both ring occupied by ATP ('ATP' football) could not be formed, and *ii)* the symmetric complex with one ring occupied by ATP and the other ring by ADP ('ATP/ADP' football) could only transiently exist and be sparsely populated. Consequently, only the asymmetric bullet can be the predominant folding active species and its lifetime was set by the rate of ATP hydrolysis [9, 38, 57].

Unexpectedly, this is not the end of the story. Ten years later, T. Funatsu et.al. pointed out that the 'ATP bullet' formed by mixing D398A, an ATP hydrolysis-deficient GroEL mutant is actually an 'ATP football' with both ring occupied by ATP and GroES [45, 58]. It therefore provides an alternative explanation for what Horwich et.al. had observed, with no need to invoke the abnormally strong inter-ring negative cooperativity: there is simply no room for the binding of a third GroES to 'ATP' football. In addition, Funatsu et.al. also showed that if only one equivalent of GroES was used to form the true 'ATP bullet', it can indeed recruit a second GroES quantitatively and form the football-shaped symmetric particle indicating that the negative cooperativity is not so strong as to prevent symmetric complex formation [58].

In their follow-up studies, by using a FRET based measurement, Funatsu and his colleagues attempted to figure out the conditions under which the symmetric complex formation is favored. Their points can be summarized as follows: *1)* the symmetric complex formation is favored in the presence of ATP but inhibited by ADP [45], and *2)* SP can promote the symmetric complex formation presumably by accelerating ADP release from GroEL [46]. Based on these two key findings, they proposed a two-cycle model that comprises a 'bullet cycle' (in the absence of SP, turning over slowly) and a

'football cycle' (in the presence of SP, turning over rapidly) with SP as the trigger for the transition between the two cycles. This is an excellent and insightful model, but its limitation lies in the fact that it is proposed based on almost exclusively steady-state kinetic data, many important details of the model are missing or not fully supported by their experiments. Not surprisingly, it didn't receive much recognition after its publication. In Chapter 4 and 5, I present a comprehensive pre-steady state analysis on the two cycle model by using different spectroscopic probes for monitoring different aspects of the GroEL functional cycle. My work not only recapitulates the major points reached by Funatsu and his colleagues, but also reveals a novel aspect of GroEL turnover in the SP-refolding related symmetric cycle, the breakage of symmetry problem (BoS), which is dealt with by work presented in Chapter 6 and 7.

1.5 Two different models of GroEL mediated SP refolding

How GroEL facilitate SP refolding is one of the central questions that had been pursued for decades [7, 9-10, 57, 59]. Despite a large body of accumulated experimental data, no clear answer to the question has been reached. The dispute mainly focus on the role played by GroEL in mediating SP refolding: in a passive refolding model, GroEL is depicted as an 'Anfinsen cage' preventing aggregate formation by segregating hydrophobic exposed SP in the enclosed chamber formed underneath GroES [59-60]; while in an active refolding model, in addition to passive aggregation prevention, GroEL is also believed to actively unfold captured SP achieved by the large scale domain movement accompanying ATP and GroES binding (forceful unfolding) [61-63] (Figure 1-3A). The benefit that comes with forceful unfolding of SP for its refolding lies in the fact that most SPs recognized by GroEL populate a kinetically trapped state (local

minimum in Figure 1-3B) where the steep energy barrier prevents these mis-folded SPs from reaching their native states (the global minimum in Figure 1-3B). Being forcefully unfolded by GroEL, SP is 'lifted up' from the local minimum and is given another chance for folding to its native state [10]. This optimized trial-and-error approach for folding of kinetically trapped SPs is phrased as the iterative annealing mechanism [64]. Support for both models exists both experimentally and computationally (for a more comprehensive review on the matter please refer to [10, 57]). Since the role of GroEL in assisted SP folding is not dealt with directly in this dissertation, instead of providing detailed reviews on the subject, I offer an interesting example which illustrates how study of the GroEL functional cycle can help to shed light on resolving the dispute. This is because the GroEL assisted SP refolding is embedded in the chaperonin turnover cycle driven by ATP hydrolysis, therefore, the role played by GroEL, either being passive or active, should be consistent with what actually happens in the ATPase cycle under physiological conditions.

In a 2009 publication, A. Horwich and his colleagues attempted to deny the existence of SP forced unfolding by determining the order of ligand arrival onto the trans-ring of GroEL/ES asymmetric complex [35]. They found that ATP can be recruited to the trans-ring much faster than SP, and therefore they argued that by the time SP reaches the trans-ring, the conformational change that might unfold SP, had already finished. Therefore, any forceful unfolding, if there were any, would be simply physiologically irrelevant. The argument, however, relies heavily on the disputed assumption that ADP releases immediately after ATP hydrolysis so that the asymmetric complex with an empty trans-ring (the 'acceptor state' complex) is the major SP acceptor species. But if ADP is

not readily released, as suggested by [39-41], it will stay on the trans-ring and prevent ATP binding. And as pointed out in [40], SP binding to the trans-ring can accelerate ADP release, so it is quite possible that the actual order of ligand arrival is that SP first, causing ADP to be released, followed by ATP binding and GroES binding. As a result, the forceful unfolding of SP bound to GroEL induced by ATP binding is still possible. And indeed, as suggested by work presented in Chapter 5 and 8, all the important adjustments made by the chaperonins in response to the presence of SP appear to allow optimized SP refolding via the iterative annealing mechanism.

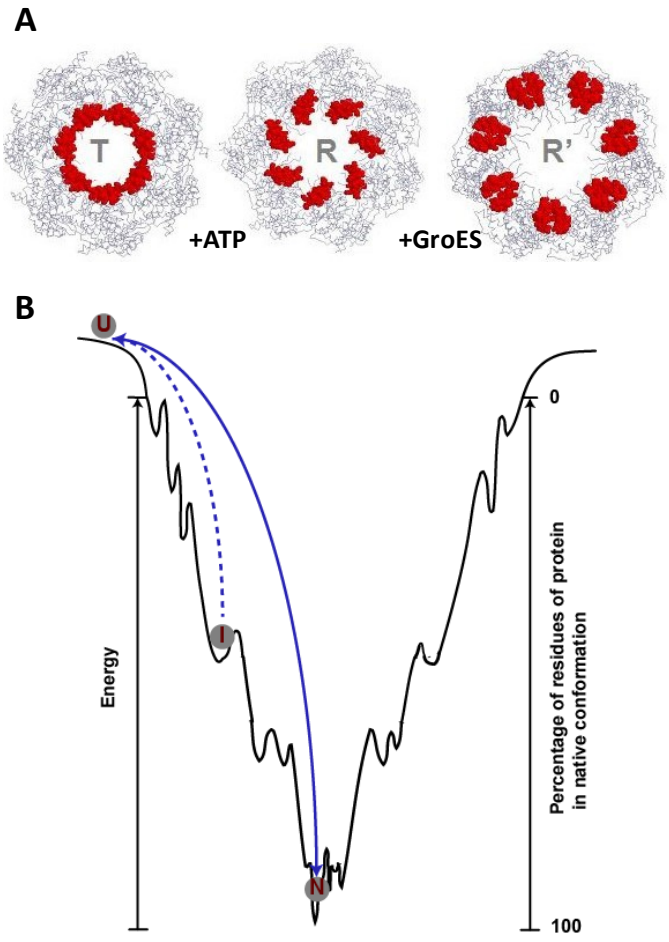

Figure 1-3: GroEL assist SP refolding via iterative annealing optimized forceful unfolding. (A) Movement of SP Binding Sites in the Transition from T to R'. The allosteric transitions that occur upon ATP binding (T to R) and subsequently GroES

binding (R to R') cause the substrate binding sites (red) to move apart from one another. The first transition is thought to actively unfold the substrate protein while the second transition encapsulates it. The figure is reproduced from [32]. **(B)** Illustration of rescuing kinetically trapped SP by forceful unfolding. 'I' stands for kinetically trapped state trapped in local minimum. Upon being forcefully unfolded, it is lifted up to the less structured unfolded state 'U', and after SP being released, the 'U' state partition between the fully native state 'F' in the global minimum and the 'I' state. The figure is reproduced from [10].

1.6 Specific Aims

In summary, the general goal of my work was to develop a unifying model of GroEL functional cycle to account for different experimental observations with specific emphasis on solving these three disputes: the identity of the rate determining step, the role of the symmetric GroEL-$GroES_2$ "football" complex in the overall chaperonin cycle, and the physiological order of arrival of ligands (ATP, SP and GroES) to GroEL trans-ring. The general goal can be approached from the following four specific aims:

***Specific Aim I*:** In order to determine the rate determing step of the whole cycle, it is necessary to measure the kinetics of release of the two ATP hydrolysis products, Pi and ADP, since the whole cycle is driven by binding and hydrolysis of ATP. The release of Pi can be followed by a fluorescently labeled phosphate binding protein (MDCC-PBP [65-66]) and ADP release can be measured by PEP /Pyruvate kinase /NADH /Lactate dehydrogenase coupling enzyme system [67]. Pre-steady state measurements of both products were examined under a wide variety of conditions (different initiation states, different [ATP]s, different [K^+]s and with or without SP), and results are presented in Chapter 3 and Chapter 4.

***Specific Aim II*:** In light of the results from studies of the first specific aim, the role of the symmetric complex in the cycle was re-evaluated and tested. Formation of the symmetric complex was monitored with the well-established FRET pair built into GroEL

(FRET donor) and GroES (FRET acceptor). The kinetics of formation of the symmetric complex and its population change were measured with pre-steady methods under different conditions (mainly, different [K^+] and [SP]). (Chapter 5)

***Specific Aim III*:** The symmetric complex was in general thought to be a static dead-end species. However, from the work presented in both Chapter 4 and 5, symmetric complex formed in the presence of SP represents a highly dynamic state, and it appears not all bound ATP needed to be hydrolyzed to go through one cycle of SP capture, encapsulation and release for one of the two GroEL rings. The way that the symmetric complex breaks into the asymmetric complex as ATP hydrolysis occurs (BoS) was studied from two aspects: *1)* with help from my colleague Nicolas Corsepius on mathematical modeling, I manage to describe how stochastic ATP hydrolysis between the two GroEL rings results in BoS (Chapter 6); *2)* a key inter-ring communication site was identified and the corresponding mutant was studied thoroughly to reveal the physical chemical basis for BoS (Chapter 7).

Specific aim IV: As the predominant species in the presence of SP, the dynamic symmetric complex plays a vital role in assisting SP refolding. Work presented in Chapter 8 probes such role from three major perspectives and demonstrates that *1)* both rings of the symmetric complex are available for SP encapsulation making GroEL a parallel processing machine; *2)* ADP occupied trans-ring of the resting state complex ([^{cis}GroEL$_7$-ADP$_7$-GroES$_7$]-[^{trans}GroEL$_7$-ADP$_7$]) is not only the physiological SP acceptor state but also indispensible in efficient SP encapsulation; *3)* the benefits for the chaperonins operating in the dynamic symmetric complex is studied and its relevance in cell survival from heat stress is also discussed. A FRET based quenching system was

implemented for study of the first two aspects consisting of QSY-7 (the quencher) labeled SPs and fluorescein labeled GroES.

Chapter 2: General Methods and Experimental Procedures

2.1 A Note on Protein Concentrations

All GroEL and GroES protein concentrations in this dissertation are for monomers. In rare occasions, the protomer concentrations are used for clarity or comparative purpose, and they will be designated with a subscript ($GroEL_{14}$ or $GroES_7$) or signaled by plain terms (tetradecamer or heptamer).

2.2 Purification of $GroEL^{wt}$, $GroES^{wt}$, and $GroES^{his}$

These three proteins were purified according to the published protocols ([69,32] for $GroEL^{wt}$, [71] for $GroES^{wt}$, and [32] for $GroES^{his}$).

2.3 Coupled Enzyme ATPase Assay

The ATPase activity of chaperonin was measured by a coupled enzyme assay which transfers phosphate from phosphoenolpyruvate (PEP) by pyruvate kinase (PK) to ADP to regenerate ATP and oxidizes NADH by lactate dehydrogenase (LDH) at the same time [67], as shown in Scheme 2-1. The last step can be measured spectroscopically by monitoring the absorbance change at 340nm over the time course of reaction. Assay buffer is composed of 50mM Tris-OAc (Acetate) pH 7.5, 10mM $Mg(OAc)_2$, 100mM KOAc, 0.4mM PEP, 0.2mM NADH, 5 units PK and 5 units LDH. Typically, 2μM GroEL was used along with various [ATP]s. 3μM GroES could also be included in the middle of measurement if needed. The assays were performed and the data were processed in essentially the same as described in [31-32] except that a Cary100 Bio UV-visible spectrophotometer coupled with a Cary temperature controller was used which has a much superior signal stability and higher signal to noise ratio.

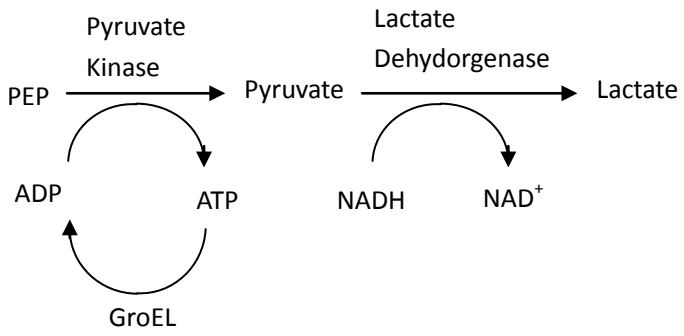

Scheme 2-1: Coupled Enzyme ATPase Assay.

2.4 Preparing Unfolded Substrate Proteins

The unfolded protein is a very important allosteric effector of GroEL ATPase activity and thus instrumental for the study of the mechanism by which GroEL functions. There are many kinds of substrate proteins that can be found in literature and among them one was used the most in this thesis: reduced α-lactalbumin (α-LA) from bovine milk (*Sigma-Aldrich*). To unfold it, a concentrated aliquot of such protein was diluted into cold water containing 2mM DTT to a final concentration of less than 5mg/ml, then the solution was combined with equal volume of 12mM HCl and allowed to denature for at least one and half hour on ice. Afterward, the denatured protein sample was extensively dialyzed against 10mM Tris pH=7.5 and concentrated to about 200uM by using centriplus YM-5 centrifugal filter devices. The final concentrations of protein were measured spectroscopically with extinction coefficient of $28400 M^{-1}cm^{-1}$ for α-LA (*Expasy*, on-line protein primary structure analysis software). Denatured α-LA could be stably stored in -80^{o}C freezer in small aliquots and remained in denatured state in the presence of DTT (reducing environment) and absence of Ca^{2+} [73].

2.5 Bradford Assay to determine protein concentration

Most of the protein concentrations reported in this dissertation were determined by measuring absorption at 280nm and calculated with corresponding extinction coefficients. But protein concentrations under the following conditions were determined by Bradford assay instead: the aliquots taken from stop flow measurement with protein concentration too low to be accurately determined otherwise, and labeled protein samples with serious dye absorption interference at 280nm. The reagent used in this assay, Coomassie Brilliant Blue G-250, can non-covalently bind to aromatic amino acids and arginine of protein sample and change absorption at 595nm. Because different proteins have different amino acid composition, to accurately measure target protein concentration, standard curve used to calibrate the measurement should be generated with the same kind of protein. For a typical measurement, 20µl protein sample with concentration ranging from 2 to 20µM was mixed with 1ml Bradford reagent and incubated at 37^{o}C for 15min before taking the absorption at 595nm. The absorption was converted to concentration by using a linear standard curve generated in a similar manner with protein samples of known concentration.

2.6 Stopped-flow Fluorescence Measurements and preparation of initiation state for pre-steady state kinetic measurements

All pre-steady state kinetic measurements were performed in an Applied Photophysics SX18MV-R stopped-flow apparatus. The instrument was configured with a 20µl flow cell with a dimension of 1mm×2mm×1cm. For fluorescence measurements, the 2mm path length was used, and for absorption measurements, 1cm path length was used. A cutoff filter was installed between the flow cell and the fluorescence detector to cut off

strong incident light while permit fluorescence light entering the detector. The monochronometer entry and exit slits were each set to 2mm, which corresponds to a band pass of 9.3 nm. The syringes and flow cell were kept at a constant temperature of 37^{o}C using a circulating water bath. The shot volume was set to approximately 110μl, consuming 55μl from each syringe for each shot. For all measurements, oversampling was used to reduce the amount of noise in the signal. This is a feature where the instrument takes data every 40μsec, and then averages several consecutive readings to give a total of 1000 data points. To also reduce noise, several traces were averaged to obtain the final trace shown in the following chapters. To stabilize the baseline, the feature 'auto-adjustment' was also activated to allow baseline adjustment between consecutive traces which were averaged to give the final trace. Other than these common instrument setups, parameters such as excitation wavelength, PMT voltage, cut-off filter wavelength varies as for the purpose and subject of the measurement, and specific details are given in the corresponding chapters.

There are three commonly used initiation states in which the *GroE* system can be synchronized for pre-steady state measurements shown in this dissertation. They are the apo GroEL state (un-complexed mixture of GroEL and GroES), the acceptor state [^{cis}GroEL-ADP-GroES][^{trans}GroEL] (the asymmetric GroEL/ES complex with an empty trans-ring, the square brackets signify the two heptameric rings of GroEL), and the resting state [^{cis}GroEL-ADP-GroES][^{trans}GroEL-ADP] (the acceptor state plus ADP bound to or in equilibrium with the trans-ring). The latter two can be prepared in the following way: 40 μM GroEL and 60 μM GroES in 50 mM Tris-OAc, pH 7.5, 10 mM $Mg(OAc)_2$, 100 mM KOAc, 1 mM DTT, were mixed with 300 μM ATP/500 μM ADP.

This was allowed to incubate for 30 minutes if ATP was used or 10min if ADP used at room temperature. The solution was then desalted on a PD-10 column equilibrated with 50 mM Tris-OAc, pH 7.5, 10 mM $Mg(OAc)_2$, 100 mM KOAc (or any other $[K^+]$ as stated), and 1 mM DTT in order to remove excess nucleotide in solution and any ADP bound to the trans ring, which is freely exchangeable. The acceptor complex thus made can be used for pre-steady state measurements as it were, or alternatively ADP can be added back to make resting state complex either almost entirely populated (at high [ADP] such as 50 μM) or in equilibrium with acceptor state (at lower [ADP]). The standard buffer solution for all stopped-flow measurements is: 50 mM Tris-OAc, pH 7.5, 10 mM $Mg(OAc)_2$, 100 mM KOAc (or any other $[K^+]$ as stated), 1 mM DTT, and whenever different concentrations of $[K^+]$ were used, Na^+ was used to balance the ionic strength such that $([K^+] + [Na^+]) = 0.1M$.

2.7 Computer software

All the protein structures shown in this thesis were generated with PyMOL (Delano Scientific). Unless otherwise stated, all data plot graphs were accomplished with Excel 2007 (Microsoft Co.). Data fitting was done with Prism 5 (GraphPad Software Inc).

Chapter 3: Pre-steady state kinetic study of GroEL ATPase activity by Pi release measurement

3.1 Introduction

Like any machine that converts energy to work, GroEL, the so-called molecular machine, is propelled by the most common form of energy available in cell, ATP, to assist refolding of its client protein substrate (SP) [10-11]. The whole process, termed the GroEL ATPase cycle, is a multi-stepped cycle through which GroEL uses the energy released from ATP binding and hydrolysis to mediate SP refolding. Due to its utmost importance, it has been intensively studies for decades. However, due to the complex nature of GroEL ATPase cycle, i.e., two ringed structure, nested cooperativity, and complex interplay between different allosteric effectors (also see Section 1.3 of Chapter 1), standard enzymatic kinetic methods such as steady-state ATPase assay, inhibition pattern study, do not yield a clear coherent model to account for the complex kinetic behavior of GroEL under different conditions.

Compared with steady-state methods, pre-steady state kinetics is more powerful because instead of dealing all at once with an ensemble of different enzymatic intermediates along the catalytic cycle, pre-steady state methods allow dissection of the complex cycle into individual step(s) by initiating the kinetic measurement at a synchronized state [74]. However, performing pre-steady state kinetic measurement is not as straight forward as that of steady-state kinetics. In order to follow the rapid conversion between different enzymatic species before steady-state was reached, a rapid-mixing instrument is needed such a stopped-flow or quenched-flow device. In addition, depending on the sensitivity and type of the assay, i.e., continuous (stopped flow) *VS*

discontinuous (quenched flow), more enzyme material may be consumed for each measurement since it is common practice to average multiple traces to improve signal to noise ratio. Last but not the least, the mathematics is more involved for processing pre-steady data than steady state in that without the steady-state assumption, the differential term *d[ES]/dt* cannot be set to zero and therefore the differential equation $d[E_iS]/dt=f([E_iS]*k_i)$ has to be solved usually in the form of ordinary differential equation groups (ODEs) [75]. Other than a few simple examples such as single turnover assay and burst kinetics, many complex ODEs do not have a simple analytical solution and thus have to be solved numerically by mathematic software tools such as Matlab.

Due to these difficulties, throughout the literature, only a few examples of pre-steady studies on GroEL ATPase activity can be found, and frustratingly enough, results from these studies often contradict each other. One key question that is in dispute is the identity of the rate-determining step (RDS) of the GroEL ATPase cycle. By using a rapid gel filtration based assay, H.S. Rye and his colleague found that the release of ADP proceeded with a half time of 20sec, and they also reported the burst release of Pi from GroEL/ES asymmetric complex which can be suppressed almost entirely by pre-incubating the complex with ADP. Based on their experimental results, they concluded that ADP release must be slower than ATP hydrolysis and thus must be the RDS [41]. However, Horwich *et.at.* used the coupled enzyme method (Pyruvate kinase/Lactate hedyrogenase) to measure the rate of ADP release and came to a very different conclusion stating that it was ATP hydrolysis not ADP release that made the RDS [36].

This thesis critically exams both of these works. The reasons are as follows: for [41], the spin column method applied to measure ADP release may be too slow to follow

this process and may even be the source of error introduced into their measured values as correctly pointed out by [36]: under the same conditions (10mM K^+ and in the presence of SP), the whole hemicycle only takes about 10sec which is much shorter than the measured half time of ADP release (20sec) by this method. The coupled enzyme assay used by Horwich et.al. [36] can follow the release of ADP continuously and is more reliable than the gel-filtration method, however, the amount of coupling enzyme used in [36] is insufficient to follow the ADP release under the conditions applied which is evident from the rate constants they measured, $0.15s^{-1}$ for the release of ADP from GroEL/ES asymmetric complex, whereas almost half of that time is due to ADP turnover by the coupling enzymes itself ($0.3s^{-1}$). Another problem shared by both studies is that they performed their measurements under very low [K^+] (5 to 10mM). However, it is estimated that the in-vivo [K^+] is up to 100-200mM [80]. As shown in a previous publication from our group, increasing [K^+] can significantly slow down the overall turnover rate of the *GroE* system which can be attributed to enhanced affinity for ADP. Indeed, when we performed the ADP release measurement in the same way as [36], we've found that the higher the [K^+] applied, the slower the rate at which ADP is released (Figure 4-3 Chapter 4).

A relatively straightforward way to tell if ATP hydrolysis (or the conformational change that leads to ATP hydrolysis) or ADP release (or the related conformational change) is the RDS is to measure the rate of both and compare which is the slower one. However, it is no easy task as evident from the dispute mentioned above arisen from attempt to make such measurement which is likely due to the complex nature of GroEL catalyzed ATP hydrolysis as review in Chapter 1. Nevertheless, given the importance of

identifying the correct RDS for understanding the *GroE* functional cycle and the contradictory results yielded so far, it is warranted to conduct a comprehensive study on the *GroE* ATPase activity with carefully designed pre-steady state kinetic methods in order to clarify this important aspect of the chaperonin system.

There are two products of ATP hydrolysis: inorganic phosphate (Pi) and ADP. Studies presented in this chapter focus on measuring the release of the former while the latter is presented in the next chapter. Like many other proteins that posses ATPase activity, GroEL release Pi as soon as the cleavage of the γ-phosphate bond [76-77], and therefore, hydrolysis of ATP can be followed by Pi released into the solution. In a previous study from our group [39], Pi release was measured by a fluorescent dye labeled phosphate binding protein developed in Dr. Martin Webb's lab [65]. This is a much better way to monitor Pi release accurately and in real time than either the paper chromatography based or the malachite green based discontinuous assay [78]. The environment-sensitive dye MDCC was attached to a mutant form of the protein (PBP^{A197C}) at the opening of the Pi binding cleft. The Pi binding induced conformational change closes the cleft, and as a result, the fluorescence emission undergoes a large enhancement (~7 fold) [79]. Because the apparent affinity for Pi was found to be around 0.1μM, even 1μM MDCC labeled PBP (PBP-MDCC) is enough to report the presence of Pi quantitatively and in real time (apparent rate constant ~200 s^{-1} at 25°C) [65].

3.2 Methods specific to Chapter 3

3.2.1 Purification and labeling of Phosphate Binding Protein PBP^{A197C} was purified by following the procedure established in our lab by Dr. John Grason [32].

3.2.2 Pre-steady state ATP hydrolysis measured with PBP-MDCC These measurements were performed according to a modified version of a previously described method [39]. 10μM labeled PBP-MDCC was used throughout, all the measurements were conducted at 37°C, and asymmetric complexes containing 1μM GroEL subunits were employed. Compounds such as ATP, ADP, and phosphoenolpyruvate (PEP) were treated with the 'Pi mop' to lower background [Pi]. The fluorescence change of PBP-MDCC was calibrated against known concentrations of Pi standard by mixing the two in the stopped-flow device. As shown in Figure 3-1A, the kinetic traces are slightly different from those previously reported (e.g. the minor overshoot at 10-50ms). To make sure it is not due to PBP protein itself, I repeated the kinetic assay in the same way as reported in [66] for measurement of Pi binding to PBP. The overshoot is absent under such condition (Figure 3-1C) and the apparent binding constant agrees with the reported value in the range of error. Therefore, we attribute these differences to the higher temperature (37°C versus 20°C) and higher ionic strength that we employed. Under our conditions, the system reaches equilibrium at ~60ms after mixing, and therefore, the final level of the fluorescence trace was plotted against known [Pi] to calculate the PBP response factor from the slope of the line (Figure 3-1B). In a typical stopped-flow measurement, 1μM of the asymmetric complex prepared as described in Section 2.9 was included in one syringe while in the other syringe were 500μM ATP and 10μM PBP-MDCC. The fluorescence enhancement was converted to Pi released in μM by divided by the PBP response factor described above. So long as the same batch of PBP-MDCC was used and PMT voltage kept constant (usually 300V), the same PBP response factor can be used for independent measurements.

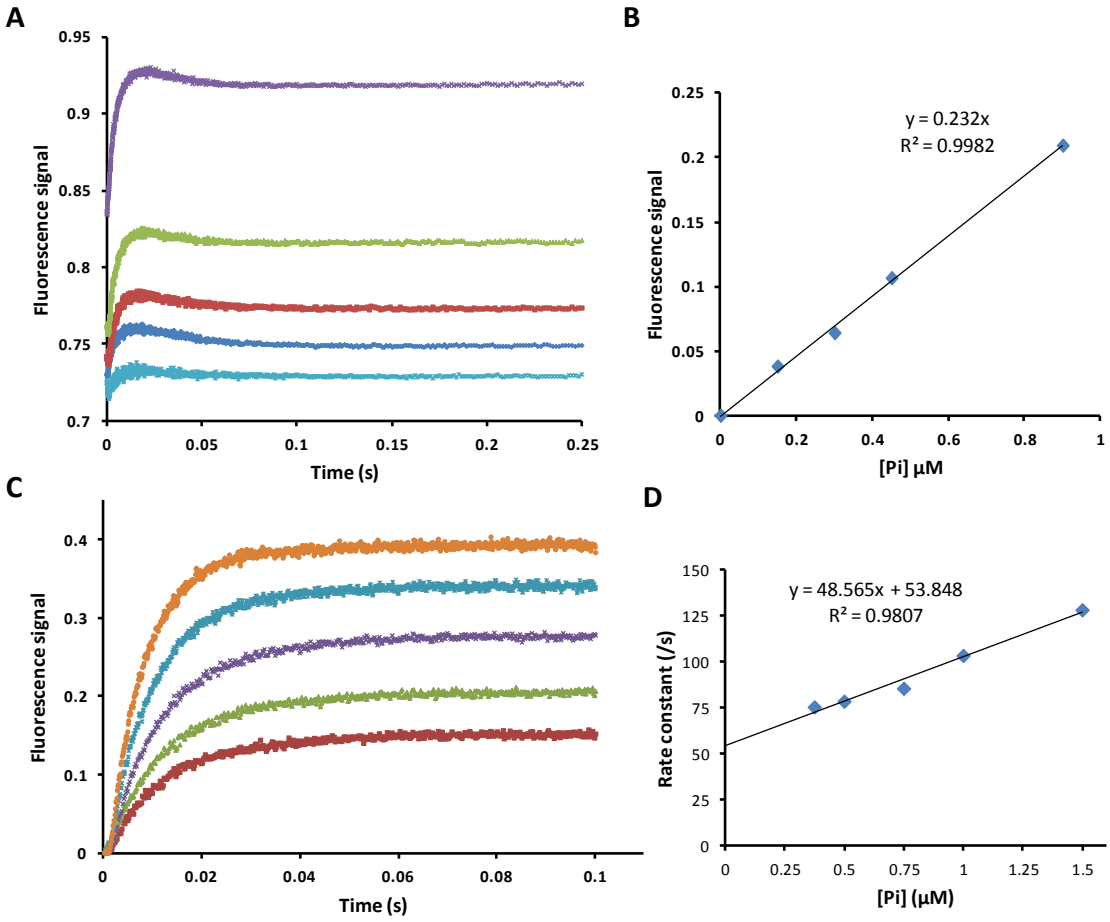

Figure 3-1: Calibrating the PBP-MDCC florescence signal in response to Pi binding. **(A)** 10µM PBP-MDCC was mixed with Pi at concentrations of 0µM, 0.15µM, 0.30µM, 0.45µM and 0.90µM. The calibration was done under the same condition as the stopped-flow measurement. **(B)** The change of fluorescence emission is a linear function of [Pi]. The back ground trace at 0µM [Pi] was subtracted from the rest of the traces shown in A. **(C)** The same measurement as shown in A was repeat under the conditions employed as in [66], i.e., 10mM TrisHCl, pH=7.6, 0.1µM PBP at 20°C. The traces take the same shape as previously reported [66]. **(D)** The kinetic traces shown in C were fitted to a single exponential equation to extract the rate constant of the transition which was plotted against the [Pi]. The rate under such conditions varies linearly with [Pi] as previously reported though the y-intercept is higher than the reported value due to a higher background [Pi] present in this study.

3.2.3 Computational analysis of the kinetics of ATP hydrolysis by GroEL

Consider the simplest case of enzyme reaction scheme as follows:

$$E \underset{k_2}{\overset{k_1[S]}{\rightleftharpoons}} ES \xrightarrow{k_{cat}} E+P$$

in which E, S, P stand for enzyme, substrate and product. The time dependent change of [ES] under pseudo first order conditions can be expressed as

$$\frac{d[ES]}{dt} = [E](k_1[S] - k_2) - [ES] \cdot k_{cat}$$

with steady-state assumption, *d[ES]/dt=0*, and thus the time dependent differential term drop out of the equation and makes solving the math of steady state kinetics fairly straightforward. But as for pre-steady state, the differential term remains, and to get the integrated expression to describe the evolution of pre-steady state, one has to solve the ordinary differential equations (ODEs).

A simple analytical solution to ODEs can be obtained from one step and some form of two step and three step kinetic schemes, which help to connect the microscopic rate constant with the measurable relaxation rate and amplitude obtained by fitting the kinetic trajectory with multi-exponential termed equations such as the burst kinetics shown below:

$$E \underset{k_{-1}}{\overset{k_1[S]}{\rightleftharpoons}} ES \underset{P_1}{\overset{k_2}{\rightarrow}} EP_2 \underset{[P_2]k_{-3}}{\overset{k_3}{\rightleftharpoons}} E+P_2$$

The first product release, the process commonly monitored experimentally, can be expressed as:

$$[P_1] = Amp(1 - e^{-k_{burst}*t}) + k_{steady-state} * t$$

under saturating [S] and binding step rapid equilibrium assumption, the exponential amplitude (*Amp*), the burst rate (k_{burst}) and the steady-state rate ($k_{steady\text{-}state}$) can be expressed in terms of microscopic rate constants as:

$$Amp = \left(\frac{k_2}{k_2 + k_3}\right)^2 * E_{total},$$

$$k_{burst} = k_2 + k_3, \text{and} \quad k_{steady-state} = \frac{k_2 k_3}{k_2 + k_3}$$

However, when it comes to even more complex kinetic schemes, a straightforward analytical solution may not be found and one has to solve the ODEs numerically and adjust the parameter values to achieve the best fit to the experimental data points. This can be done conveniently by using math software such as Matlab.

The pre-steady state release of Pi by GroEL was previously found to follow burst kinetics [39]. However, further study described in this dissertation revealed additional complexity, that is, there are four phases resolvable from the trajectory of Pi release: in addition to the burst and steady-state phase, a rapid lag phase precedes these two phases while a slow delay phase follows the burst phase before it goes into steady-state. Because the four phases are well separated, the rate constants obtained by fitting with Equation 3.1 (Page 33), i.e. by performing a simple exponential phase analysis, were assigned to individual steps of GroEL functional cycle especially for the burst phase and the delay phase (Scheme 3-1 and Figure 3-3). The same Pi release data were also subject to the more mathematically rigorous ODE analysis by my colleague Nicolas Corsepius, and a similar analysis is also included in Appendix II of this dissertation. Such ODE analysis reveals the existence of an additional step that is absent from the minimal kinetic scheme used to describe the four phase transition of Pi release trajectory, but the kinetics

of the other three steps match the rate constants of the three exponential phases respectively. Based on ADP release measurement shown in Figure 4-3 of the next chapter, this additional step is attributed to conformational change preceding ADP release, and is discussed in greater detail there.

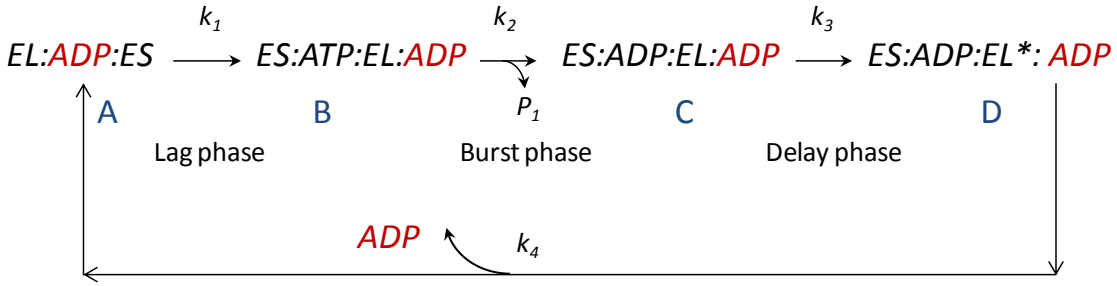

Scheme 3-1: Minimal four step model to describe the four phases of Pi release trace. In the scheme, only one GroEL ring is shown for simplicity.

3.3 Results

The following study of the asymmetric chaperonin cycle (Figure 3-2) involves two initiation species: the resting state [^{cis}GroEL-ADP-GroES][^{trans}GroEL-ADP], to which the system reverts whenever there is no SP nor enough ATP to drive a further cycle, and the acceptor state [^{cis}GroEL-ADP-GroES][^{trans}GroEL], which is poised to accept ATP so as to initiate further cycles. Both states are sufficiently stable that the entire population of GroEL molecules can be synchronized in either state (see Section 2.9 for the preparation of the resting state and the acceptor state complexes).

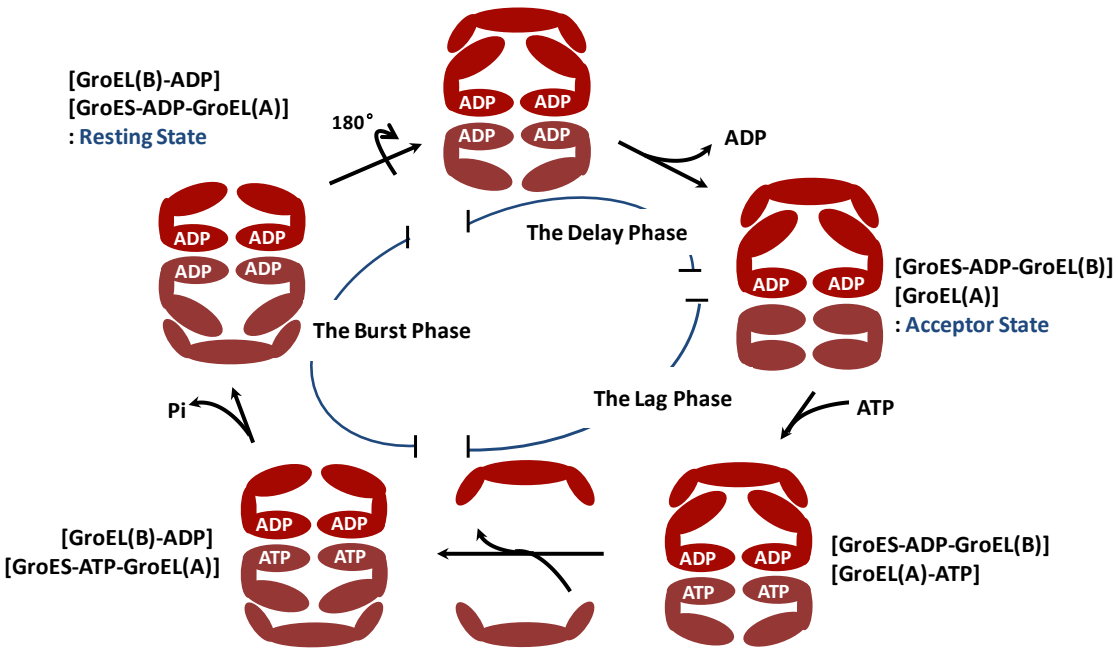

Figure 3-2: The asymmetric GroEL ATPase cycle in the absence of SP. The whole cycle is divided into three parts corresponding to the three exponential phases revealed by Pi release in pre-steady state kinetic measurements (Figure 3-3).

3.3.1 Overview of pre-steady state GroEL ATP hydrolysis followed by Pi release

For the study of the kinetics of ATP hydrolysis in the absence of SP, the reaction was initiated by adding ATP to the *trans* ring of the acceptor state GroEL ring A (Figure 3-2); a complex trajectory of Pi release resulted, monitored in real time by the fluorescent phosphate binding protein (Figure 3-3). Visual inspection alone reveals that there are at least three phases preceding the linear steady-state, (i) a "lag" phase of ~ 100ms, (ii) a "burst" phase corresponding to the hydrolysis of ATP by GroEL ring A (Figure 3-2) and (iii) a "delay" phase that will be shown corresponds to the rate-determining release of ADP from the nascent *trans* ring, GroEL ring B (Figure 3-2). The trajectory of Pi release was, as judged by random residuals (Figure 3-3 lower panel), satisfactorily fitted to the sum of three exponential terms describing the pre-steady state lag, burst and delay phases plus a linear term describing the steady-state rate of Pi release *{[Pi] /[GroEL subunits]* =

$\sum_{i=1}^{3}[-(-1)^i \cdot A_i \cdot exp\,(-k_i \cdot t)] + P \cdot t + B$ *(Equation. 3.1)}*. The delay phase in previous work [39] is not as evident as it is here. The reason may lie in the slightly different conditions applied by these two studies: *1)* the experiments of the previous work were conducted at 30°C rather than 37°C used here, and thus the slow delay phase may extend beyond the time range that was shown in [39]. *2)* In [39] only 6µM of PBP-MDCC was used to follow ATP hydrolysis by 2µM GroEL/ES complex, while 10µM PBP-MDCC was used for 1µM GroEL/ES complex in this study. Therefore, the absence of delay phase in [39] may be also due to insufficient amount of PBP-MDCC over-saturated by released Pi which leads to non-linear response of PBP fluorescence.

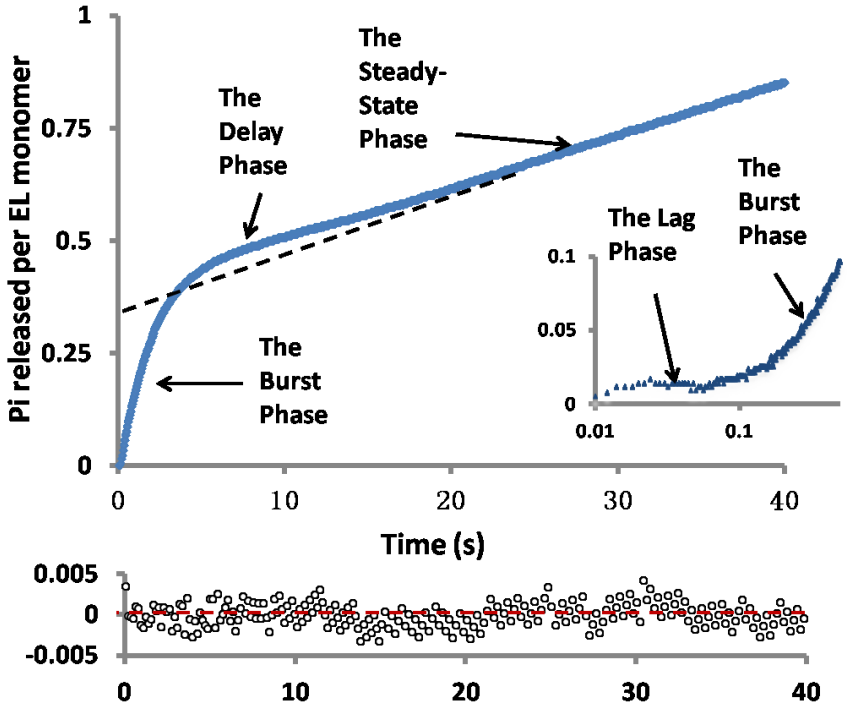

Figure 3-3: The release of Pi upon adding ATP to the *trans* ring of the acceptor state complex [^{cis}GroEL-ADP-GroES][^{trans}GroEL], monitored in real time by the changes in the fluorescence of the MDCC-labeled Pi binding protein. Dashed line, an extension of linear steady-state, highlighting the existence of the third exponential phase (the delay phase) before the system enters the linear steady-state. *Inset*: The early events (lag phase) following mixing (log time scale). Lower panel shows the residuals generated from

fitting the kinetic data to three exponential plus a linear term (Equation 3-1). y-axis of residual plot expanded twenty times that of the data plot.

3.3.2 The pre-steady-state kinetics of Pi release (starting with the acceptor state)

Lag Phase*:* Less than ~0.05 mol of Pi/ mol of GroEL sub-units were released during the first 100ms of the lag phase (Figure 3-3 inset), and most of that can be attributed to trace quantities of contaminating Pi in one or more of the reagents. Note however, that under our experimental conditions about 60ms are required for the phosphate binding protein to fully equilibrate with Pi (Figure 3-1A). Previous studies ([39-40]) have shown that the hydrolysis of ATP (the burst phase) is preceded by several rapid events (Figure 3-1). The binding of Mg^{2+}•ATP to the *trans* ring A of the acceptor state triggers the release of GroES from the *cis* ring B and permits the binding of GroES to ring A, together with several allosteric conformational changes in both rings that accompany these transitions. The kinetics of the lag phase are indifferent to $[K^+]$ > 10mM, [ATP] > 50μM and the presence of a 100-fold molar excess of unfolded α-lactalbumin (data not shown).

Burst and Delay Phases: At 100mM K^+ and 0.5mM ATP, the amplitude of the burst was a linear function of the concentration of GroEL sub-units (0.49 Pi per subunit, R^2=0.9957) (Figure 3-4) indicating that one ring (ring A of Figure 3-2) turns over once during the burst phase.

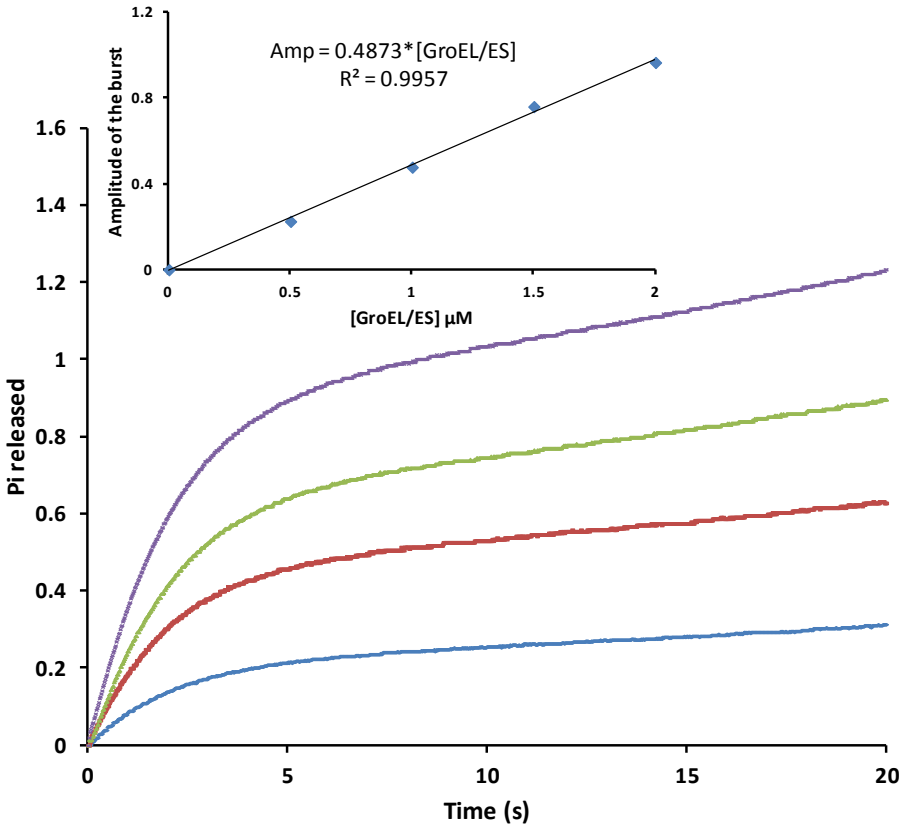

Figure 3-4: The stoichiometry of Pi released during the burst phase. Experiments of the sort shown in Figure 3-3 were conducted at 100mM [K^+] and 0.5mM [ATP] by using the 0.5 (blue), 1.0(red), 1.5(green), 2.0µM (purple) acceptor state subunits. The kinetic trajectory were fitted with Equation 3-1 in the same way as that of Figure 3-3 and the amplitude of the burst phase was plotted against the GroEL subunit concentration as shown in the inset.

Influence of [K^+]: next, I explored the effects of varying the concentration of the potassium ion on the amplitudes and rates of the burst and delay phases. Previous work of our lab shown [39-40] that, within the concentration range (30-100mM) both the amplitude and the rate of the burst phase were independent of [K^+]. As shown in Figure 3-5, the analysis was extended to the concentration range (5-200mM), the latter being the physiological [K^+] in *E. coli* [80]. As before, the amplitude and kinetics of the burst phase were largely independent of [K^+] (Figure 3-5 Table). This was to be expected on structural grounds. The conformational change that accompanies the binding of GroES

brings about the closure of the nucleotide-binding site and commits ATP to hydrolysis [14, 44].

$[K^+]$	Amp of burst (subunit^{-1})	Rate of burst (s^{-1})	Rate of delay (s^{-1})
10mM	0.2879±0.0007	0.615±0.003	N.A.
100mM	0.495±0.005	0.514±0.005	0.145±0.009
200mM	0.512±0.002	0.518±0.002	0.091±0.009

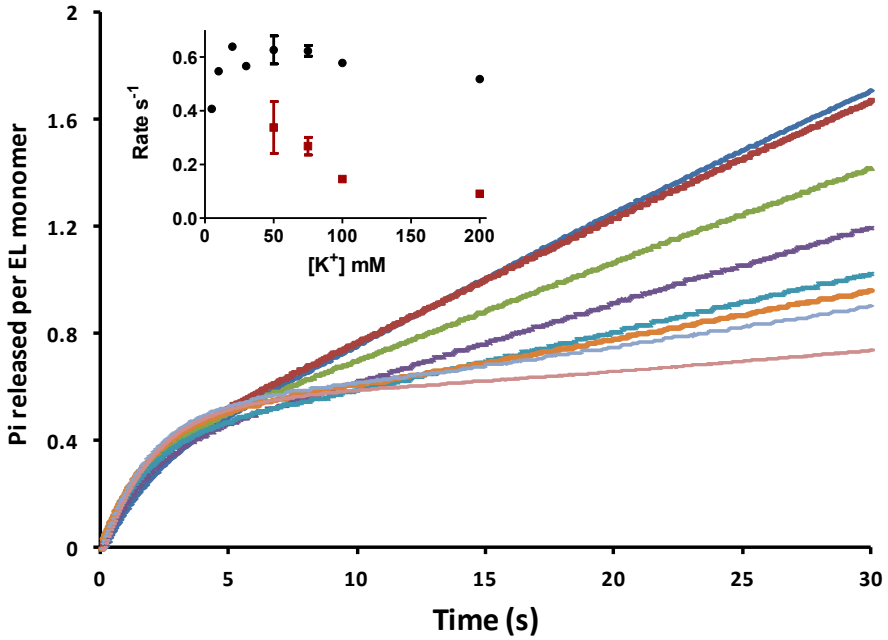

Figure 3-5: The influence of $[K^+]$ on the pre-steady state kinetics of ATP hydrolysis. From top to bottom the $[K^+]$ applied are: 5mM (dark blue), 10mM (red), 20mM (green), 30mM (purple), 50mM (light blue), 75mM (orange), 100mM (corn flower blue), 200mM (pink). The reaction was initiated by adding 0.5mM ATP to a solution of the acceptor state complex (2μM in GroEL subunits) as in Figure 3-3. The 10mM, 100mM, and 200mM K^+ traces are each of average of 25 trajectories and the results of fitting to Equation 3-1 are presented in the table above the data plot. The rest traces are average of 5. *Inset*: The rates of the burst (black dots) and delay (red) phases as a function of $[K^+]$ at 0.5mM ATP.

Closer inspection of the delay phase, especially an analysis of the residuals, provided additional insight. At $[K^+]$ >10mM the trajectory of Pi release required a third exponential term, $Amp_3(e^{-k3t}-1)$ corresponding to the delay phase, to achieve a satisfactory fit to the experimental data (Appendix I, Figure A-1 A&B). However, at or below 0.01M K^+ a satisfactory fit to the experimental data was achieved without this term. Previous

work in our lab has shown that the principal effect of K^+ is to enhance the affinity of the system for the product ADP. Thus, at physiological [K^+] (~200mM) [80], the release of ADP becomes the rate-determining step in the asymmetric cycle of ATP hydrolysis. This is consistent with the observation made here that the rate of the delay phase is the smallest of the three pre-steady state phases (Figure 3-5 Table), which makes it easily discernible from the other phases. It only requires that the rate constant for the delay phase approach or exceed the rate constant of the burst phase, such as appears to be the case at 10mM [K^+], for the delay phase to become indistinguishable (Figure 3-5 insert, and residual plot shown in A-1 A&B of Appendix I).

Influence of [ATP]: The same conclusion can be drawn from a different perspective via manipulating the kinetics of the burst phase by lowering [ATP], while keeping the kinetics of the delay phase unaffected. As the kinetics of the burst phase approach those of the delay phase (e.g. at approximately [ATP] = 15μM) it becomes possible to achieve a satisfactory fit with two exponential terms rather than three (Figure3-6 insert, and residual plot shown in A-1 C-E of Appendix I).

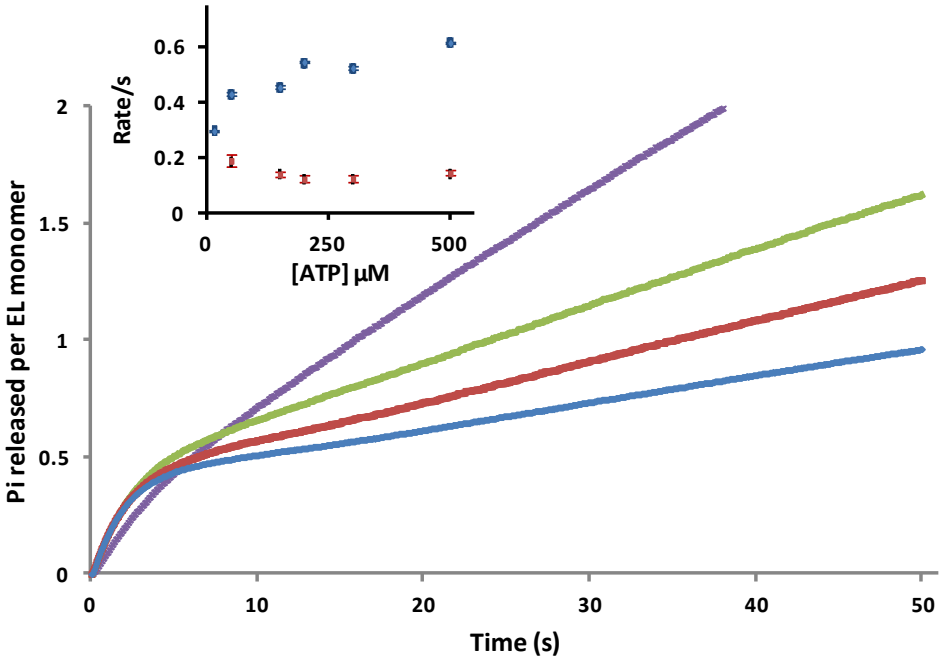

Figure 3-6: The influence of [ATP] on the pre-steady state kinetics of ATP hydrolysis. The Pi release measurements were conducted under 0.1M [K^+]. Color code: purple, 15µM [ATP]; green, 50µM [ATP]; red 150µM [ATP]; and blue 500µM [ATP]. ATP regenerating system (5unit/ml PK plus 0.4mM phosphoenolpyruvate) was included to keep the [ATP] constant. Average of 20 trajectories. *Inset*: The rates of the burst (blue) and delay (red) phases as a function of [ATP] at 100mM K^+.

Effects of [SP]: The trajectories of Pi release as a function of [α-LA] are shown in Figure 3-7. Small concentrations of SP ([α-LA]: [$^{trans}GroEL_7$]<4), sufficient to stimulate the steady-state hydrolysis of ATP, did not influence the kinetics of the burst phase of Pi release (Figure 3-7A; insert). At saturating SP concentrations ([α-LA]: [$^{trans}GroEL_7$]=100], the trajectory of the burst phase is subsumed by the linear steady state (Figure 3-7B purple). However, by employing BeF_3 that forms an inhibitory, active-site complex with ADP, it became possible to show that the burst phase of Pi release was not affected even at saturating SP (Figure 3-7B). The stimulatory effect of SP upon the steady-state rate of ATP hydrolysis must therefore (by default) be found in events taking place during the delay phase.

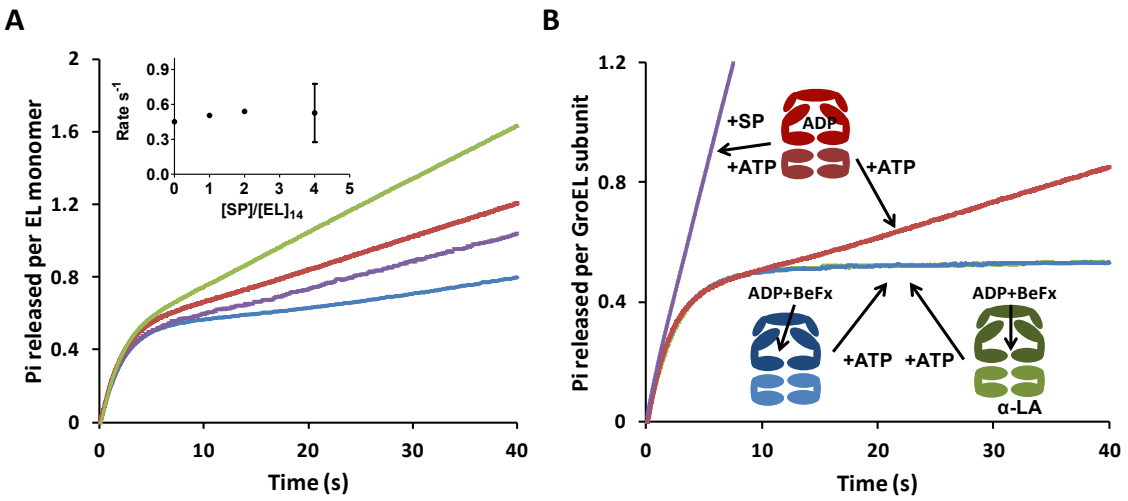

Figure 3-7: The influence of SP on the kinetics of Pi release. The reactions were started by addition of ATP to the acceptor state complex. **(A)** [^{trans}GroEL$_7$]=0.07μM, [α-LA]=green, 0.28μM; red, 0.14μM; purple, 0.07μM; blue, 0μM. For all traces, [K^+]=200mM. *Insert*: the rate of the burst phase is independent of [SP]. **(B)** Measurements initiated with acceptor state made under saturating [SP]: purple and red, acceptor state complex; green (overlapping with blue), 1mM BeF_3 pre-incubated acceptor state; blue, 1mM BeF_3 and 7.1μM α–LA (100×[GroEL]$_{14}$) pre-incubated acceptor state. The trajectories of Pi release in the presence of BeF_3 overlap regardless of the presence or absence of α–LA.

3.3.3 Asymmetric complex affinity for ADP As one of the two ATP hydrolysis products and an important allosteric effecter, ADP can exert a profound influence on the asymmetric chaperonin cycle. It has been shown previously that occupancy of the *trans*-ring by ADP decelerates (by ~10^4 fold) both the dissociation of GroES from the GroEL *cis*-ring (ring B in Figure 3-2) and recruitment of another GroES on the *trans*-ring (Ring A) [39-40]. It is also known that pre-incubating the acceptor state asymmetric complex with ADP (~30μM) can reduce the size of the burst of Pi release almost to zero [39]. Both phenomena can be attributed to the slow release of ADP from ring A that precedes and prevents ATP binding to the same ring. As a result, all events that are initiated by ATP binding to ring A are delayed, such as recruitment of a new GroES and the turnover of ATP capped in the nascent *cis*-ring (ring A). The experimental evidence presented

here, obtained by systematically investigating the influence of [ADP] on the pre-steady state kinetics of ATP hydrolysis, demonstrates that ADP binding to the *trans*-ring of the asymmetric complex is not only tight but also cooperative.

Based on the knowledge that high [ADP] can completely suppress the burst of Pi release from the asymmetric complex [39], the study here extends to intermediate [ADP]s. As [ADP] pre-incubated with the acceptor-state complex increased, the amplitude of the subsequent ATP-induced burst phase decreased (Figure 3-8). Binding of ADP to the *trans* ring shifts the equilibrium toward the formation of the resting state complex, which is unable to bind or hydrolyze ATP. Consequently the size of the burst measured in the presence of pre-incubated ADP directly reflects the equilibrium distribution between the resting and acceptor states (Figure 3-2). In this way, the dissociation constant for binding of ADP to the *trans*-ring can be accurately determined (Figure 3-8 right). Measurements of the sort shown in the left of Figure 3-8 were also repeated at three additional [K^+] (Figure 3-8 Table). As [K^+] increased from 1mM to 200mM, the dissociation constant of ADP was reduced from 29±1μM to 5.3±0.2μM. This is consistent with our understanding that the major role played by K^+ is to enhance nucleotide affinity for GroEL.

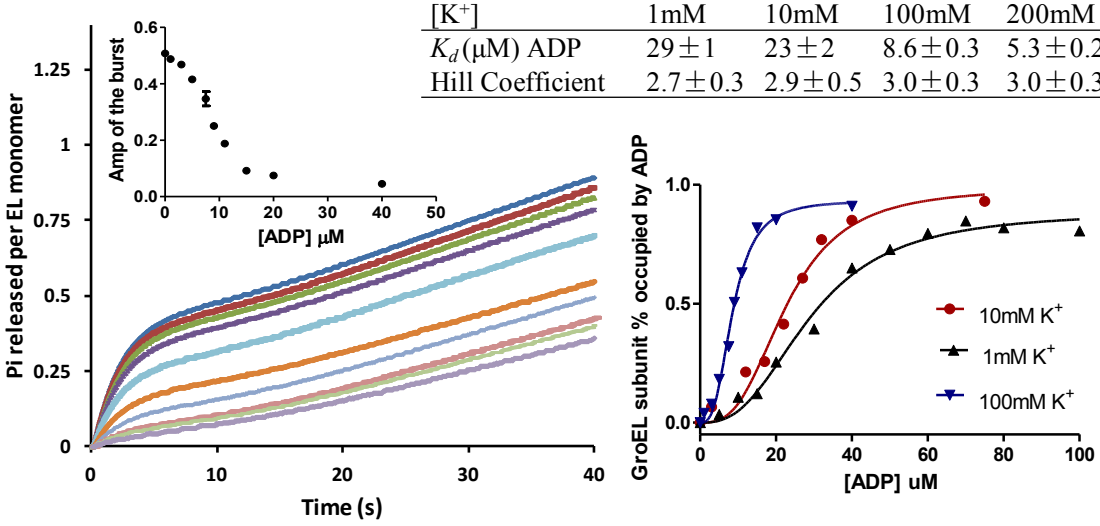

[K+]	1mM	10mM	100mM	200mM
K_d (μM) ADP	29±1	23±2	8.6±0.3	5.3±0.2
Hill Coefficient	2.7±0.3	2.9±0.5	3.0±0.3	3.0±0.3

Figure 3-8: The influence of ADP on pre-steady state Pi release from the asymmetric complex. **Left:** ADP was pre-incubated with the acceptor state complex before ATP was introduced. All the measurements were conducted at 100mM [K^+]. [ADP] applied from top to bottom: 0μM, 1μM, 3μM, 5μM, 7.5μM, 9μM, 11μM, 15μM, 20μM, 40μM. *Inset*: The fitted amplitudes of the burst phase of kinetic traces shown in the left were plotted against [ADP]. Error bars were generated by fitting the trajectories with Equation 3-1. **Lower right:** The amplitudes of the sort shown in the inset on the left acquired under different [K^+]s as indicated were converted to the percentage of *trans*-ring occupied by ADP. Then each set of data was fitted with the Hill equation: $y=B_{max}*[ADP]^h/([ADP]^h+K_d^h)$, in which h is Hill coefficient, K_d is dissociation constant of ADP, and B_{max} is a scalar coefficient with its value close to 1. The results of the fitting were presented in the table above the graph.

Although the binding of ADP to apo-GroEL has previously been reported to be non-cooperative [81], in the study shown here, the binding of ADP was found to be cooperative and the Hill coefficient, irrespective of [K^+], was determined to be ~3, a value very close to that for ATP [37] (Figure 3-8 Table). Cooperative binding of ADP, together with the greatly enhanced affinity for it, indicates that ADP is not merely a hydrolysis product but also plays a very important role as an allosteric effecter in the GroEL functional cycle.

3.3.4 The pre-steady-state kinetics of Pi release (starting with the resting state)

To prepare the resting state complex for this series of experiments, the acceptor state was

first pre-incubated with 50μM ADP so as to substantially populate the *trans* ring (ring B Figure 3-2), together with varying [K^+] and [SP] (unfolded α-LA). The reaction was initiated by mixing 1:1 with 1.0mM ATP. Consistent with the phase assignment presented above (ADP release from the nascent *trans* ring), the delay phase was largely unchanged by initiating with the resting state versus the acceptor state. However, starting with the resting state, the burst phase was almost completely suppressed while the delay phase became predominant (Figure 3-9), permitting a more detailed analysis of the latter phase.

***Influence of [K^+]*:** The kinetics of Pi release as a function of the pre-incubation [K^+] are shown in Figure 3-9A. The data are well fitted by two exponential phases: a small burst (amplitude < 0.1) phase due to incomplete occupancy of the *trans* ring with ADP, and the delay phase plus a linear steady state term (Appendix I Figure A-2 A-D). The rate of the delay phase was accelerated as the pre-incubation [K^+] decreased (Figure 3-9A inset), and approaches the rate of the burst phase, as we expected since this has the effect of lowing the affinity of the *trans* ring for ADP. The steady state rate also increased as the pre-incubation [K^+] decreased, as expected since in the absence of substrate protein, the rate determining step is the dissociation of ADP from the *trans* ring.

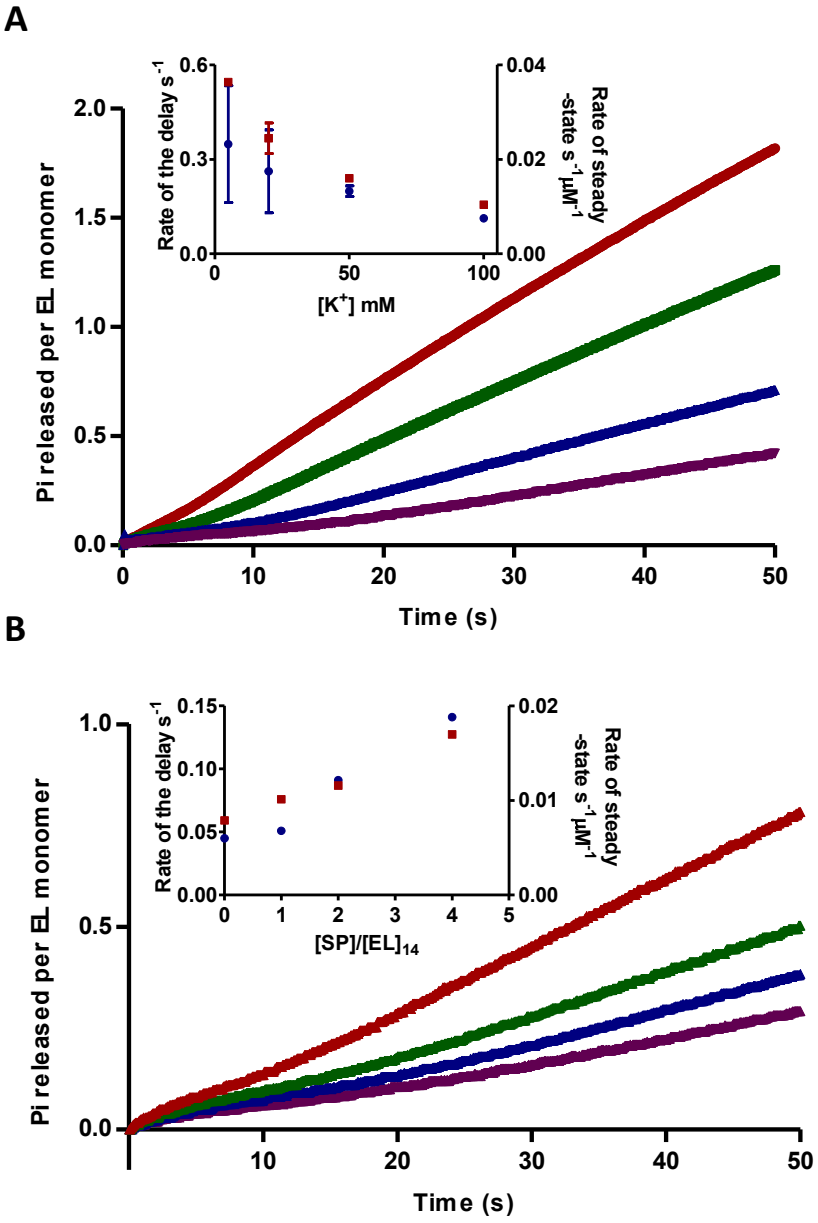

Figure 3-9: Pi release measurements initiated with the resting state complex (the asymmetric complex pre-incubated with 50μM ADP) at varying [K^+] (A) or [SP] (B). (A) From top to bottom: red, 5mM K^+; green, 20mM K^+; blue, 50mM K^+; purple, 100mM K^+. *Inset*: overlay plot of the rate of the delay phase (blue, left y-axis) and steady-state rate (red, right left y-axis) against [K^+]. **(B)** From top to bottom [α-LA]/[GroEL/ES]$_{14}$: red, 4; green, 2; blue, 1; purple, 0. For all traces, [K^+]=200mM. The initial mini burst (Amp<0.1) of Pi release corresponding to the small fraction of *trans*-ring that is not occupied by ADP. *Inset*: overlay plot of the rate of the delay phase (blue, left y-axis) and steady-state rate (red, right y-axis) against [SP]/[EL]$_{14}$.

***Influence of [SP]*:** The kinetics of Pi release as a function of the pre-incubation [α-LA] are shown in Fig. 3-9B. The data are well fitted by two exponential phases: a small burst phase of amplitude <0.1 and the delay phase plus a linear steady state term (Appendix I Figure A-2 E-H). The rate of the delay phase and the steady state rate were accelerated as the pre-incubation [SP] increased (Fig. 3-9B *inset*), as expected since, as will be shown in Chapter4 and 5, the presence of SP catalyzes ADP/ATP exchange on the *trans* ring, a necessary condition for initiating a new cycle of ATP hydrolysis.

3.4 Discussion

All the studies presented in this chapter were conducted without SP or under low [SP]. Under such conditions, the kinetics of Pi release are described by 4 phases: a "lag", a "burst", a "delay", and the steady-state ATP hydrolysis. The amplitude of the burst phase is found to be linearly proportional to [GroEL] with a ratio close to 0.5 Pi per GroEL subunit and thus was assigned to be the single turnover of ATP encapsulated in ring A of Figure 3-2. The fact that neither $[K^+]$ (>10mM) nor presence of SP have much influence on both the amplitude and the rate of this exponential phase is consistent with our understanding that binding of GroES commits the 7 ATP bound in the *cis* ring to hydrolysis (ring A of Figure 3-2). On the other hand, the kinetics of the delay phase is heavily influenced by both $[K^+]$ and [SP]: lower $[K^+]$ and higher [SP] can accelerate the delay phase and eventually make it indistinguishable from the burst phase. The trend of influence exerted by these two allosteric effectors on the delay phase can also be observed by initiating the measurements from the resting state GroEL/ES complex to eliminate influence from the burst phase. Therefore, the delay phase was assigned as the release of ADP from ring B (Figure 3-2). The ODE analysis presented in Appendix

indicates the release of ADP may not be a single step but instead a combination of two steps: a conformational change that leads to release of ADP possibly the R to T allosteric transition and the actual release of ADP from the trans-ring in T state. The same point is also demonstrated in Figure 4-3 of the next chapter as well as in my colleague Nicolas Corsepius' PhD dissertation [66]. Nevertheless, a solid conclusion can be drawn from both types of analysis: the kinetics of ADP release are much slower than that of ATP hydrolysis and thus in the absence of SP and at physiological concentrations of [K^+] (100-200mM), ADP release must be the RDS of the whole cycle.

The dissociation constant of ADP from apo GroEL was previously determined to be ~100μM (at 10mM K^+) and the binding was found to be non-cooperative [81], which was believed to be applicable for the trans-ring (ring B) of the asymmetric complex as well [57]. This is one of the several pieces of evidence used to support the claim that ADP is released instantaneously after ejection of GroES and SP from ring A (Figure 3-2) [35, 38, 57]. However, in a previously published work from our group, the affinity of the GroEL/ES asymmetric to ADP complex was determined to be ~2μM [40]. Though the binding pattern was not explicitly stated, the data points clearly cannot be fitted with a non-cooperative binding model. The results presented here unambiguously demonstrate that the asymmetric complex can bind ADP not only with high affinity (~8.6μM at 100mM K^+) but also cooperatively (Hill coefficient ~3). The results obtained at different [K^+] also recapitulate the point that has been inferred from steady-state ATPase studies [39] and structural analysis [14]: potassium can enhance the affinity of GroEL for nucleotide. Last but not the least, the apparent transition from non-cooperative binding of ADP to apo GroEL to cooperative binding to the *trans* ring of asymmetric complex may

reflect the fact that more work needs to be done to change between ADP-bound and non-bound conformations by the asymmetric complex than the apo state, since cooperative binding is generally viewed as a way to release binding energy in a more concerted fashion in order to do more work. However, testing the above assumption is beyond the scope of this dissertation.

Chapter 4: Pre-steady state kinetic study of GroEL ATPase activity by ADP release measurement

4.1 Introduction

A number of previous studies have implicated ADP in playing a very important role in modulating GroEL ATPase activity, but most of them are indirect studies based either GroEL conformationally induced fluorescence change or variation of the steady-state ATPase activity. Among those few that directly monitor ADP release, unfortunately, conclusions reached by two of them contradict each other [36, 41] as already reviewed in Chapter 1. The results of Pi release study presented in the last chapter strongly indicate that ADP release is much slower than ATP hydrolysis in the absence of SP. In order to unambiguously characterize this important step, it is also necessary to measure the ADP release directly.

To this aim, two slightly different methods of measuring ADP release were employed. In one, an ATP hydrolysis mutant $GroEL^{D398A}$ was used where the catalytically important aspartic acid that forms hydrogen bond to the proton of hydrolytic H_2O at the active site was mutated to alanine [56]. Only ~0.1% of the activity remained (contrary to previously reported 2% as will be further explained in Chapter 6). The benefits of using this mutant are that *i)* it was used before for the same end, i.e. measuring ADP release by Horwich et.al.[36]. However, in that study, the $[K^+]$ was much lower than physiology and there was not enough coupling enzymes applied to fully couple the release of ADP to oxidation of NADH. I corrected these two flaws by including enough coupling enzymes (15 times more than [36]) and conducting the measurement under physiologically relevant $[K^+]$. In addition, using $GroEL^{D398A}$ with a low level steady-state

turnover allows measurement of ADP release under near single turnover conditions making analyzing kinetic data much more straight forward.

However, only limited [NADH] can be applied in such assay. This is because the oxidation of NADH is followed by its fluorescence change, and the highest [NADH] can be applied in such measurement is limited by inner filter effects, i.e. absorption at 340nm where the NADH florescence was excited should not exceed 0.1 otherwise the light would not be uniformly absorbed along the light path which leads to non-linear response of the signal [82]. The shortest light path of our stopped-flow flow cell is 0.2cm and given the absorption coefficient of NADH to be 6.22 $mM^{-1}cm^{-1}$, 80μM is the highest [NADH] that can be used. This is enough for a single turnover experiment such as the one performed with D398A but not for a turnover experiment with the $GroEL^{wt}$ in the presence of SP where the NADH would be rapidly consumed. As a result, for measurements under turning over conditions, to permit the use of higher [NADH] (~0.2mM), absorption instead of fluorescence emission was followed in the stopped-flow device with a light path close to 1cm.

In the same way, the influence of SP on ADP release can also be studied. It is well known that SP can significantly accelerates steady-state ATP hydrolysis [10, 37]. If ADP release is the RDS, the effect of SP on ATP steady-state hydrolysis should be largely attributed to the SP accelerated ADP release. Indeed, this is reflected from the disappearance of the delay phase of the Pi release trajectory presented in Figure 3-7 of Chapter 3. In addition, in one of our previous studies [40], it is reported that introducing SP can tremendously accelerate both release of *cis*-bound GroES from the resting state GroEL/ES complex and recruitment of new GroES from the solution, which was also

attributed to SP-accelerated ADP release. The work presented in this chapter, as a result, was intended to show directly how SP can affect the GroEL functional cycle by accelerating ADP release.

4.2 Methods specific to chapter 4

4.2.1 Protein purification and experimental materials The GroEL ATP hydrolysis mutant $GroEL^{D398A}$ was purified essentially in the same way as $GroEL^{wt}$ but the plasmid containing the mutant was provided by Dr. H.S.Rye. The coupling enzymes Pyruvate kinase and Lactate dehydrogenase were purchased from Roche applied science in the form of ammonium sulfate suspension. The enzymes used for ADP release measurements were freshly prepared in the same day of experiment as follows: ammonium sulfate precipitate was spin down and resuspended in 10mM Tris-OAc, pH=7.6 and 10mM $Mg(OAc)_2$ and put through PD-10 equilibrated with the same buffer to remove residual $(NH_4)_2SO_4$. The gel-filtrated enzymes were concentrated to about 15mg/ml (~2500unit/ml) and were not left overnight nor frozen since the denatured form of those enzymes can act as SP for GroEL and complicate the measurement.

4.2.2 Pre-steady state ADP release measured from $GroEL^{D398A}$ These measurements were made by coupling the release of ADP from GroEL to the oxidation of NADH via the classic pyruvate kinase/ lactate dehydrogenase system (Scheme 2-1 of Chapter 2). While we typically employ ~5 unit/ml of each of the coupling enzymes in the steady-state analysis of ATP hydrolysis by GroEL, we used ~50 units/ml each to measure the pre-steady state release of ADP. The design of experiment is similar to that of [36] by using $GroEL^{D398A}$ and form the acceptor state complex as describe in Section 2.9 but incubating the asymmetric complex with ATP for 3 hours to allow complete hydrolysis

of bound ATP before gel-filtrating it through PD10. The acceptor state complex made in such a way contains 10μM $GroEL^{D398A}$ subunit and was loaded into one syringe. In the other syringe, 100 units/ml each of the coupling enzymes and their substrates (0.8mM PEP and 0.16mM NADH) were included along with 1mM ATP. The stopped flow measurements were initiated by mixing the content of the two syringes at 37°C. Fluorescence of NADH was excited at 340nm and its emission above 420nm was collected. As in the case of Pi release measured by PBP-MDCC, the NADH fluorescence change also need to be calibrated against known [ADP] to convert it to [ADP] change. As shown in Figure 4-1, complete turnover of ADP takes about 1sec in the presence of 200mM K^+ which is much faster than that applied in [36]. However, due to the dependence of pyruvate kinase on potassium, we do observe a dramatic drop of turnover efficiency at $[K^+]$ below 20mM and so ADP release at lower $[K^+]$ was not studied. Whenever lower $[K^+]$ was used, NaOAc was used to balance the $[K^+]+[Na^+]=200$mM.

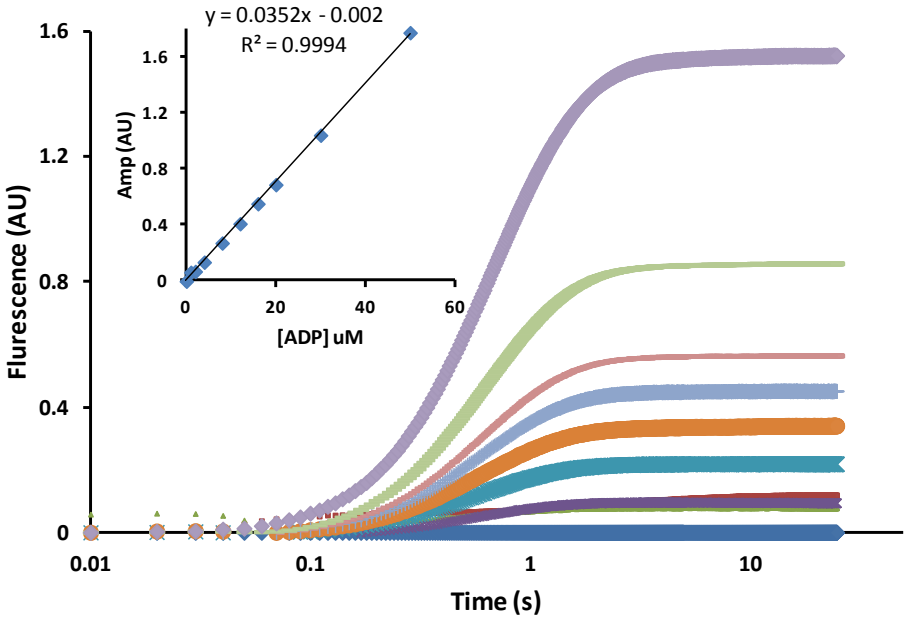

Figure 4-1: Calibrating the NADH fluorescence signal. The calibration was done under the standard conditions (50mM TrisOAc, 10mM $Mg(OAc)_2$, 200mM KOAc) by mixing 0.4mM PEP, 0.08mM NADH plus 50unit/ml each of the coupling enzymes with ADP of varying concentrations as indicated from top to bottom: 50μM, 30μM, 20μM, 16μM, 12μM, 8μM, 4μM (purple), 2μM (green), 1μM (red), 0μM. The plot was generated by subtracting the background trace (0μM ADP) by each one of the traces so that all the trajectories start from 0 and the signal increases as NADH get oxidized. The kinetic traces obtained in this way were fitted with a single exponential equation to extract the amplitude of the fluorescence change and plotted against [ADP] applied. The slope of the linear regression is the response factor of NADH fluorescence emission.

4.2.3 Pre-steady state ADP release from turning over chaperonin system These measurements were made under essentially the same conditions as NADH fluorescence measurement except with a higher [NADH] for absorption measurement. The stopped-flow was reconnected to operate under absorption mode with a flow cell light path of ~1cm. However, I could not use the well accepted extinction coefficient of NADH of a value of 6.22 $mM^{-1}cm^{-1}$ for two reasons: *1)* the photomultiplier tube (PMT) was used to follow the absorption change instead of a two-beamed system, *2)* and the flow cell dimension doesn't account for the thickness of the cell wall. It is, therefore, necessary to calibrate the NADH absorption signal to determine the 'working' extinction coefficient on this instrument. The calibration is shown in Figure 4-2 and the working extinction coefficient was determined to be 4.6 $mM^{-1}cm^{-1}$. Indeed, it is smaller than the extinction coefficient determined from well-calibrated spectrophotometer.

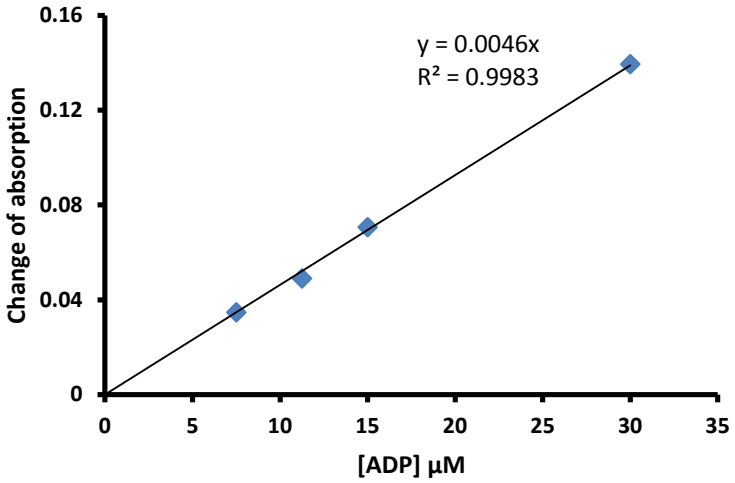

Figure 4-2: Determination of the working extinction coefficient of NADH. The calibration was done in a similar fashion as that of Figure 4.1 except NADH absorption at 340nm was monitored rather than fluorescence. The apparent extinction coefficient from this set of data is 4.6 $mM^{-1}cm^{-1}$ as from the slope of the linear fit.

In addition, since ADP release is expected to proceed faster in the presence of SP than in its absence, more coupling enzymes are needed to reduce the response time to couple ADP release to NADH oxidation. 500 unit/ml each of the coupling enzymes were used on this end reducing the response time to ~100msec. Maintaining a reasonable signal to noise ratio is also a concern with switching from a sensitive assay (like fluorescence) to a less sensitive one (absorption in this case). Base on the response factor of NADH fluorescence (35.2 $mM^{-1}cm^{-1}$) and the working extinction coefficient of NADH (4.6 $mM^{-1}cm^{-1}$) there is about 7 times drop of sensitivity, however, due to limitation on preparing synchronized single GroEL/ES acceptor complex, as will be discussed in more detail, a compromise was made to raise the GroEL subunit concentration to 20µM (final concentration). Such high concentration of protein materials requires a different way of generating acceptor state asymmetric complex from what was described in Section 2.9. 120 µM GroEL and 180 µM GroES in 50 mM Tris-OAc, pH 7.5, 10 mM $Mg(OAc)_2$, 100

mM KOAc, 1 mM DTT, were incubated with 250 μM ATP for 15min. The free and ADP bound to the trans-ring were removed by putting the protein solution through PD-10 equilibrated with the same buffer composition but [K^+] was reduced to 1mM to lower the asymmetric complex affinity for ADP. The flow-through of the column were then concentrated up to the desired asymmetric concentration before loading to the stopped-flow syringe. Protein solution with higher concentration than the one listed above should be avoided because the carry-over of ADP in the void volume of PD-10 becomes intolerable.

4.3 Results

4.3.1 A single round of ADP release from GroEL^{D398A} acceptor state complex

The asymmetric GroEL^{D398A} complex at the acceptor state was challenged by excess ATP and GroES to expose the *cis*-bound ADP (ring B in cartoon illustration in Figure 4-3), and the ADP release into solution was coupled to NADH oxidation and reported by NADH fluorescence change (Figure 4-3A).

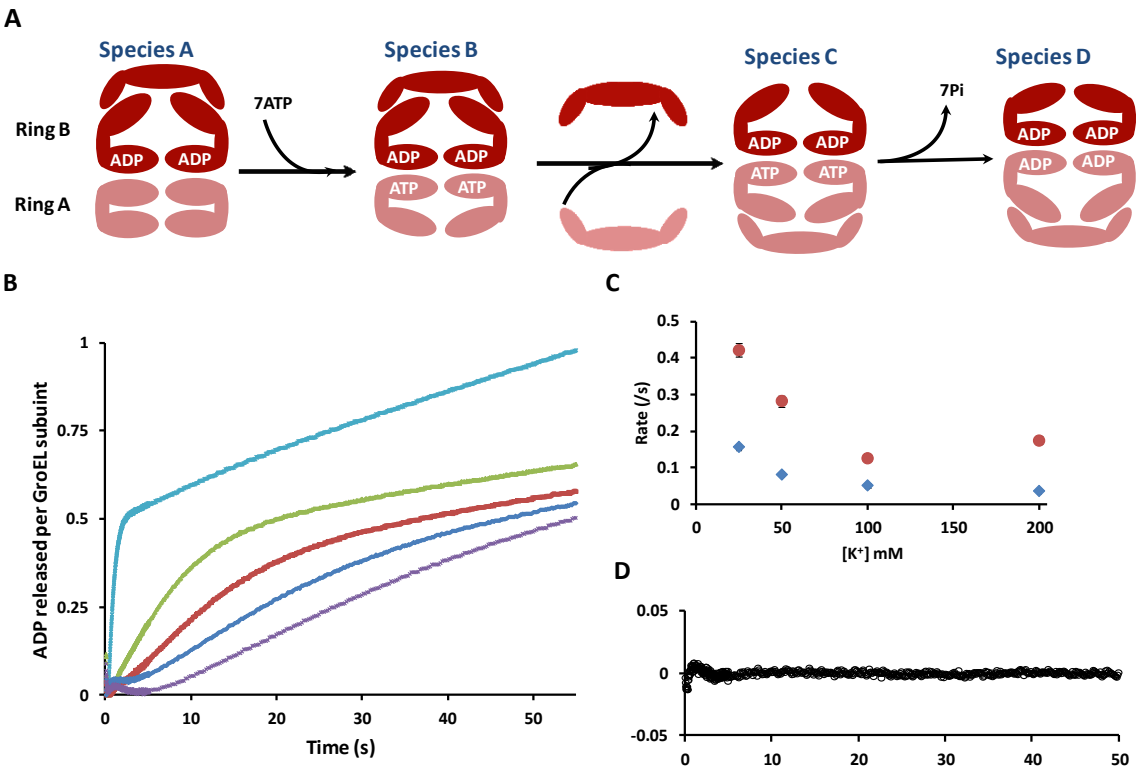

Figure 4-3: ADP release from the GroEL^{D398A} asymmetric complex. The measurements were performed as described in Section 4.2.2 with varying [K^+]. **(A)** Cartoon illustrates the events that lead to the measured kinetic events embodied in ADP release trajectories, that is, the measurements were initiated with acceptor state complex (Species A) but Species D is the actual starting point of ADP release that is reflected in B**)** The kinetic trajectories are identified as purple, 200mM K^+; blue, 100mM K^+, red, 50mM K^+; green, 25mM K^+; and light blue, 100mM K^+ plus 7.1μM denatured α-LA (SP). The y-axis was converted to ADP released per GroEL subunit from the NADH fluorescence change by using the NADH fluorescence response factor determined as described in Figure 4-1. All five traces were fitted with Equation 4-1, and the residual plot of the blue trace at 100mM K^+ is shown in D as an example. **(C)** The apparent rate constants for the stalling phase (blue dots) and ADP exponential release phase (red dots) were plotted. Error bars reflect the uncertainty of the model fitting. **(D)** The residual plot of the blue trace at 100mM K^+ shown in B. All five traces show systematic deviation from the fitting model at early time points.

Visual inspection reveals at least three phases for all ADP release trajectories: an initial 'stalling' phase where little detectable ADP was actually released, followed by an exponential ADP release phase with an amplitude close to 0.5 ADP per GroEL subunit corresponding to turnover of one out of the two rings, and finally, the system comes into

a linear steady-state phase. All the kinetic traces were fitted in such way with Equation 4-1 ($[ADP]/[EL\ subunits] = \sum_{i=1}^{2}[-(-1)^i \cdot A_i \cdot exp(-k_i \cdot t)] + P \cdot t + B$). However, residual analysis reveals non random deviation from the fitting model (though the amplitude of the deviation is only around 5% of the entire transition of ADP release trace shown in Figure 4-3B), which is most likely due to perturbation of the signal either from the stopped-flow system or due to the fact that solution of high protein concentration was used. Since most of the useful kinetic information was extracted from data points collected after the initial stage, the fitting results can still yield credible information regarding how the ADP was released. Another unexpected feature of these kinetic traces is that the rate of the steady-state of ADP release does not approach zero and appears to correlate with $[K^+]$, however, as is shown later in Chapter 6, it can be largely attributed to the presence of small amount of endogenously expressed $GroEL^{wt}_{14}$ produced from the chromosomal copy of $GroEL^{wt}$ gene before IPTG induction.

Despite the slight deviation from the model, this set of data reveals some very interesting features of ADP release from GroEL/ES complex. First and foremost, at $[K^+] \geq$ 100mM, the rate constants of both the stalling phase and ADP exponential release phase are much smaller than the ATP hydrolysis rate (~$0.5s^{-1}$ by PBP measurement) which corroborates the conclusion drawn from Pi release study of the last chapter that ADP release is the RDS of GroEL functional cycle. What's more, consistent with our understanding of the role played by potassium to enhance the GroEL affinity for nucleotides, the ADP release was slowed down approximately three fold from 200mM to 25mM $[K^+]$ as in Figure 4-3B. In addition, by comparing the blue and light blue trace in Figure 4-3A, it is obvious that introducing SP can dramatically accelerate ADP release to

such extent that the amount of coupling enzyme utilized here is not sufficient to fully couple the process to NADH oxidation, well expected based on our understanding that SP can accelerate the turnover of GroEL functional cycle.

The existence of the initial stalling phase preceding the exponential ADP release is also very intriguing in that, its presence is consistent with my colleague Nicolas Corsepius' ODE analysis of the Pi release trajectory (a similar analysis is also included in the Appendix II Figure A-3) and the value of its rate constant (~$0.2s^{-1}$) resembles that of the delay phase (~$0.15s^{-1}$) and the predicted conformational change step (~$0.22s^{-1}$) by ODE analysis of Pi release data, but its very nature is elusive from such computational analysis. Here, it is clearly shown that during the stalling phase there is barely any ADP release detected and thus this phase is most likely due to some conformational change that allows ADP to be released. However, such conformational change cannot be simply attributed to the ATP induced ring inversion of the asymmetric complex (from Species A to C in Figure 4-3A cartoon) because as indicated by Pi release measurements, the combination of these three steps, corresponding to the lag phase, proceeds at a rate much faster than that of the stalling phase (~$15s^{-1}$ *VS* 0.1-$0.45s^{-1}$).

According to my colleague Xue Fei's structural analysis [21], the opening of the nucleotide binding pocket formed in the inter-face of the intermediate domain and equatorial domain varies significantly from T to R and R' state with T the largest opening, R in between, and R' the smallest. Such trend correlates with their respective affinities for ADP with the T state being the lowest followed by R and R'. Therefore, the conformational change underlying the stalling phase can be either R' to R transition or R to T transition. Due to lack of structural and molecular dynamic (MD) characterization of

the GroEL conformational change after departure of GroES, however, it is difficult to pinpoint the exact cause underlying the stalling phase.

4.3.2 Monitoring ADP release in the presence of SP (α-LA) Studies on both the kinetics of Pi release and ADP release lead to the inescapable conclusion that ADP release step is the RDS at physiological [K^+] and in the absence of SP. In the following study, ADP release was directly monitored in the presence of SP in two distinct but related fashions. In this section, I presented the study on the equilibrium established between free ADP and ADP bound by the asymmetric complex [^{cis}GroEL-ADP-GroES][^{trans}GroEL-ADP]. Such equilibrium was characterized by a phenomenon termed 'missing amplitude', equivalent to the concentration of trans-ring bound ADP, which allows us to study binding of ADP by the asymmetric GroEL/ES complex both in the presence and absence of SP under (or close to) equilibrium conditions. In next section, I study the kinetics of ADP release from nascent trans-ring (ring B in Figure 4.3A) which is essentially the experiments shown in Figure 4.3 but done with GroEL^{wt} instead of GroEL^{D398A}. A wealth of kinetic information can therefore be extracted from these kind of experiments and would be discussed in more details in the discussion section of this chapter. For studies presented in both sections, to modulate ADP release in the presence of SP, a model SP, α-LA, was used which has the advantage that it exist in a stable mis-folded state that will neither aggregate nor fold back to its native conformation provided reducing environment and no Ca^{2+} present, and therefore its concentration remains constant despite multiple turnovers by chaperonins.

Measurements of ADP release in this and next section were performed with a still higher amount of coupling enzyme (500 unit/ml per each enzyme) to follow faster

ADP departure and with a higher [NADH] (0.15mM) to couple more released ADP. The absorption, rather than fluorescence change of NADH was therefore, monitored to generate data shown in both sections. Under such conditions, the coupling capacity was raised approximately 10 fold and the response time reduced to ~100ms (purple trace in Figure 4-4B).

As shown in Figure 4-4, due to slow release of ADP from GroEL trans-ring, the catalysis of ADP by the coupling enzymes finishes long before reestablishment of new equilibrium. Therefore, the amount of free ADP present at time zero can be accurately determined by extrapolating the slow linear phase back to y-axis. In the absence of SP, there is only about 5μM free ADP (green trace Figure 4-4 A) and the other half, the missing amplitude, must be tightly bound by the trans-ring.

On the other hand, the missing amplitude disappeared after saturating amount of SP (～14μM α-LA) was introduced to the system (either by pre-incubating with asymmetric complex or introducing upon mixing Figure 4-4A, red traces). And when extrapolating the kinetic trace back to time zero, a value close to 10μM ADP can be obtained, meaning that all the ADP titrated into the asymmetric complex was released by the end of the reaction time of the coupling system (~100ms) demonstrating the powerful effect on ADP release exerted by SP. In addition, the missing amplitude was found to be influenced not only by [SP] but also by [K^+]. Reducing [K^+] from 200mM to 20mM reduced the size of the missing amplitude from ~6μM to ~2μM (Figure 4-4B) consistent with our understanding that potassium can enhance GroEL affinity for ADP.

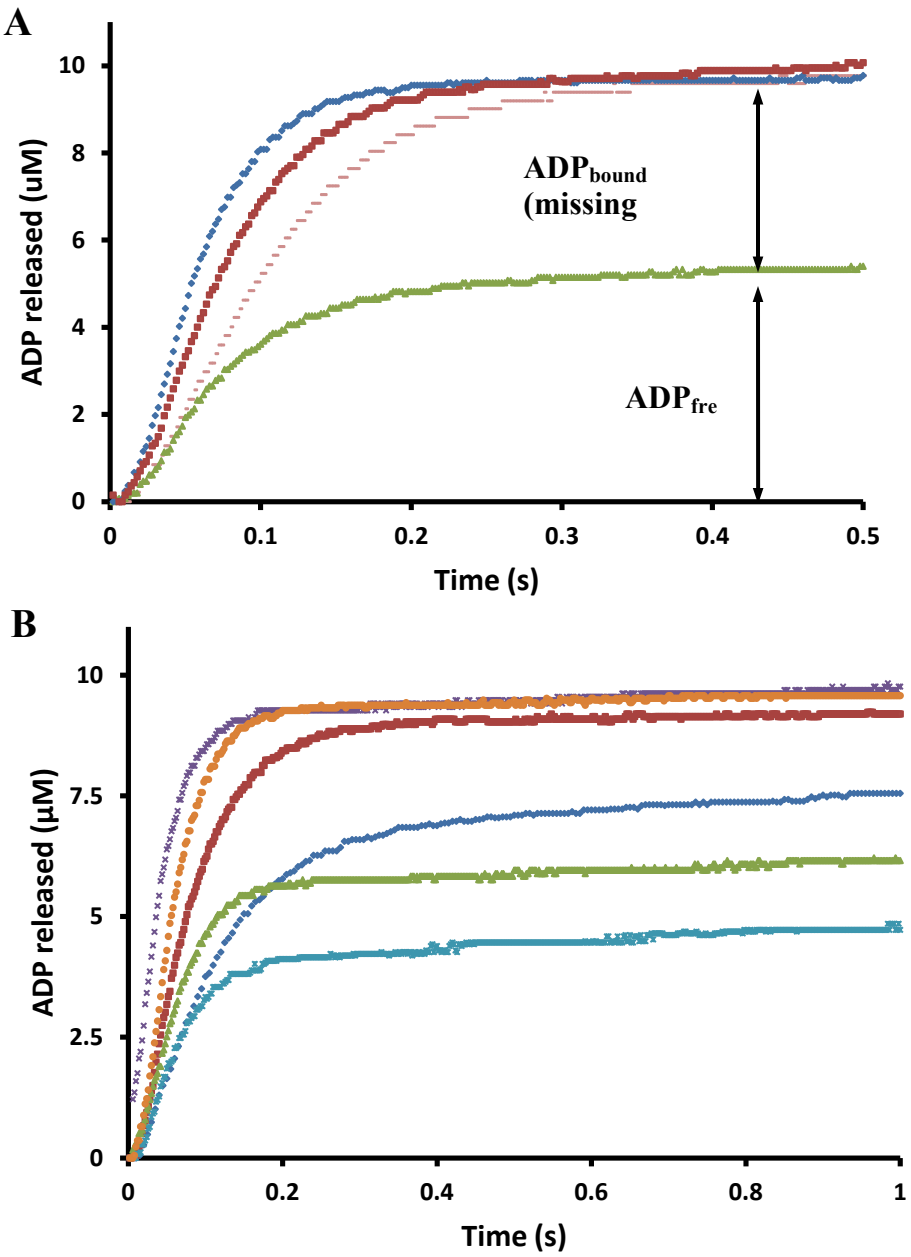

Figure 4-4: ADP in equilibrium with the *trans* ring of the asymmetric complex. (A) 20μM acceptor state asymmetric complex was incubated with 10μM ADP (final concentration) prior to mixing with coupling enzymes in the stopped-flow. The blue trace shows turnover of 10μM free ADP by the coupling system; the green one was taken without added SP; the red traces were taken in the presence of SP (α-LA) either with pre-incubation (dark red) or being introduced upon mixing with the coupling system (light red). The amplitude difference between the green and the blue trace is the missing amplitude representing the bound ADP by the GroEL trans-ring. **(B)** similar experimental setup as the set shown in A except varying amount of [K^+] was applied and identified as: dark blue, 20mM [K^+]; green, 100mM [K^+]; and cyan, 200mM [K^+]. 10μM ADP alone was also mixed with the coupling enzymes in the absence of the asymmetric complex at

the same set of [K^+]s to check if the catalytic capacity of the coupling enzymes was affected. The resulted traces are: red, 20mM [K^+]; orange, 100mM [K^+]; purple, 200mM [K^+]. ADP release measurement below 20mM [K^+] was not performed because the catalytic capacity of the coupling enzymes was substantially compromised.

4.3.3 SP induces a shift of the rate-determining step After GroES dissociates from the cis-ring (ring B in Figure 4-3 cartoon), the bound ADP can only be slowly released in the absence of SP at physiological [K^+], a conclusion that can be drawn from the presence of the slow delay phase of Pi release trajectory as well as the rate directly measured of ADP release from the $GroEL^{D398A}$ asymmetric complex. Here, the same ADP release measurement was performed with the $GroEL^{wt}$ asymmetric complex after challenging the acceptor state asymmetric complex with ATP (Figure 4-5).

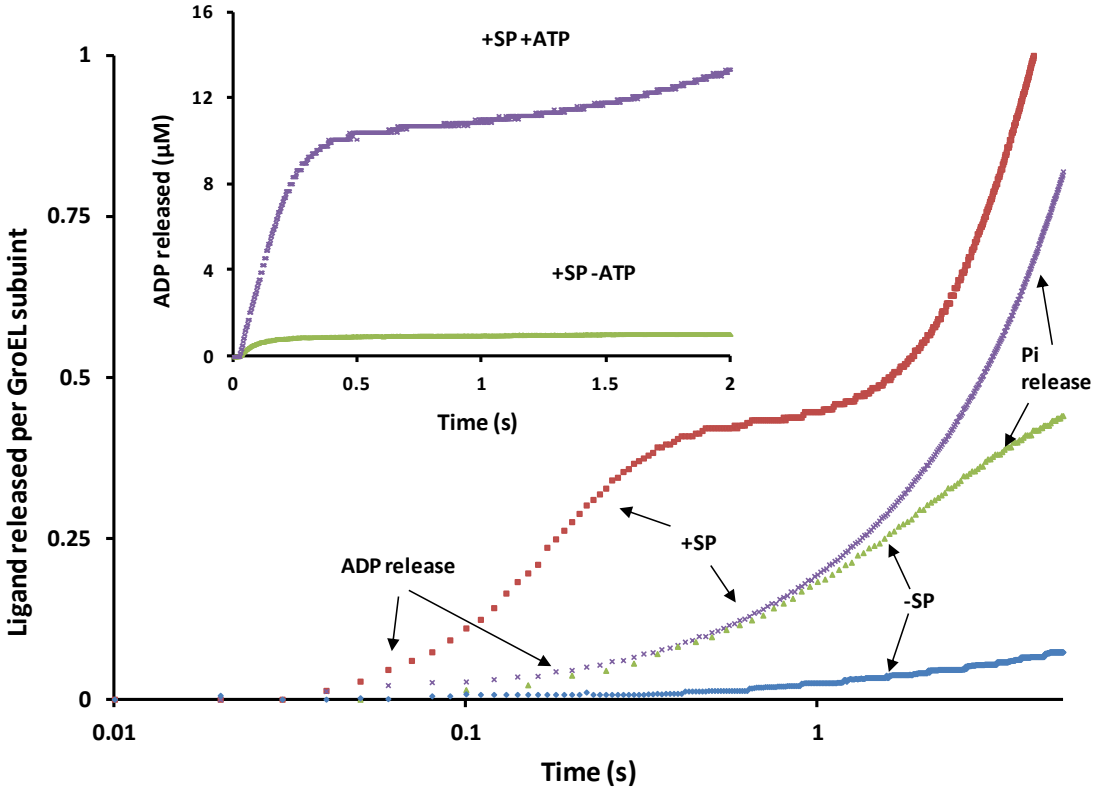

Figure 4-5: A change in the rate-determining step of the GroEL ATPase cycle is induced by SP. All measurements were started with acceptor state complex and performed with 100mM [K^+] and 0.5mM ATP with different concentrations of acceptor state complex: 30μM for ADP release, 1μM for Pi release. The kinetic traces were plotted on a logarithmic time scale. The trajectories of ADP release (blue) and ATP hydrolysis

(green) were combined with no SP present and with SP (10.7μM α–LA) present (red for ADP release and purple for Pi release). The left y-axis was normalized to moles of ligand released per mole of GroEL subunit on which the Pi release and ADP release data were plotted. The kinetics of ADP release in the presence of SP can be resolved into four phases: a "lag, a "surge" of ADP release with amplitude equal to 0.5 ADP per subunit, a "pause" during which symmetrical "football" particles are formed, followed by steady state ATP hydrolysis. *Inset*: Both traces were obtained from ADP release experiments similar to those shown in the main body of the figure, started with 20μM asymmetric complex at acceptor state under 0.1M [K^+]. The difference is: the purple trace was obtained by challenging acceptor asymmetric complex with saturating SP and ATP, while for the green trace the complex was only challenged with SP. The data were plotted on a linear time scale to make the small burst observed at the beginning of the green trace of ADP released clear. This small burst (～0.5μM ADP) cannot come from the nascent trans-ring since the asymmetric complex was only challenged with SP but no with ATP. Therefore it must be due to the trace amount of ADP that could not be removed by gel-filtration in preparation of the acceptor asymmetric complex.

The $GroEL^{wt}$ acceptor complex was carefully prepared by gel-filtration to remove ADP bound to the trans-ring as described in Section 4.2.3. In the absence of SP, the kinetics of ADP release is rather simple and comprises a minor burst phase, during which less than 0.05 moles of ADP per mole of subunit was released, and a linear steady state phase. The initial burst release of ADP can be attributed to trans-bound ADP carried over from gel-filtration (Figure 4-5 Inset green). The ADP release trace was plotted side by side with Pi release obtained under similar conditions (Figure 4-5 the green and the blue traces). A clear contrast is immediately visible: after the first round of ATP hydrolysis completed (~5sec), only approximately 15% of ADP can be detected in solution. The contrast between the kinetics of Pi release and ADP release processes recapitulates the finding that in the absence of SP, ATP hydrolysis in the nascent cis-ring (ring A, Figure 4-3) precedes ADP release from the opposite ring (ring B).

On the other hand, the kinetics of ADP release was dramatically altered by the presence of saturating amount of SP (Figure 4-5 red and purple traces): A brief lag phase due to the limited catalytic capacity of the coupling enzyme, then a rapid 'surge' of ADP

release with its kinetics partially restrained by the turnover of the coupling enzymes (lasted for ~0.5s as in Figure 4-5 red trace), and then a pause phase with little ADP released (lasted for ~2s) before the system went into steady state. We found the rapid 'surge' release of ADP was not from the initial *trans* ring of the asymmetric complex (ring A in Figure 4-3 cartoon) because if ATP was omitted in the measurement, such rapid surge of ADP release was almost entirely gone (Figure 4-5 inset green trace). Nor did it come from the hydrolysis of ATP that was rapidly mixed with the asymmetric complex since during this 0.5s of surge of ADP release, very little ATP was observed to be hydrolyzed (Figure 4-5 purple trace). Therefore, the only possible source of the 'ADP surge' is the ADP initially locked in the *cis* ring (ring B in Figure 4-3 cartoon) when the asymmetric complex was prepared. To test such assumption, I repeated experiments of the kind at varying site concentrations, ranging from 5μM to 40μM, and found the size of this rapid ADP release was a linear function of one half of the GroEL site concentration corresponding to one of the two rings of GroEL (Figure 4-6).

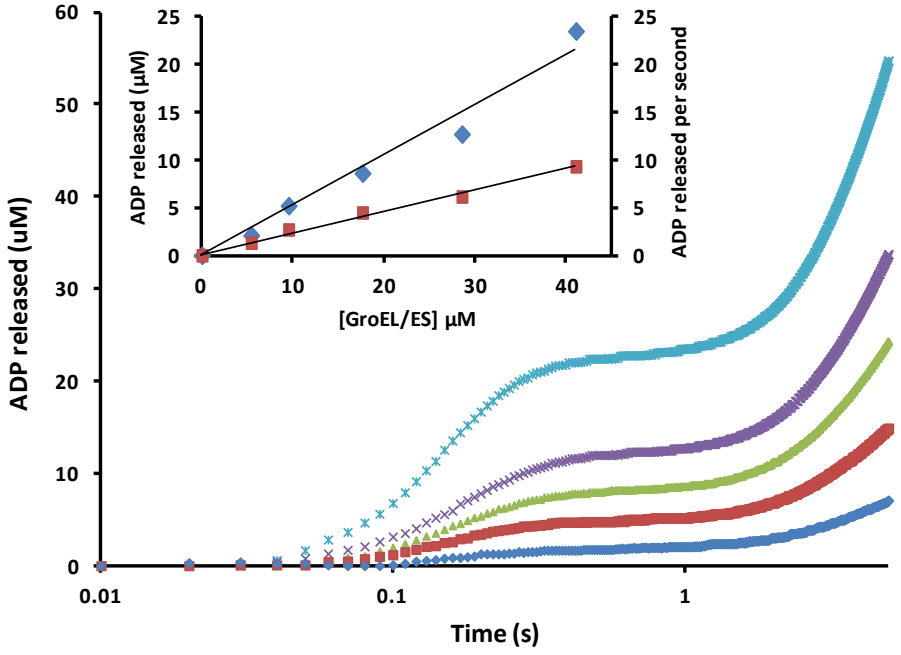

Figure 4-6: The size of the 'ADP surge' is proportional to the GroEL *trans* subunit concentration. All the ADP release trajectories were obtained with experiments performed under the same condition with that of Figure 4-5 except varying [subunit] of GroEL was used to form the acceptor state asymmetric complex. The traces are identified from top to bottom as: cyan, 41μM subunit; purple, 29μM; green, 18μM; red, 9.5μM; and blue, 5.5μM. *Inset*: linear correlation between [subunit] and the size of the burst (blue dots) and steady state rate (unit in s^{-1}, red dots) respectively. Fitted results are: slope=0.5261 ADP per subunit and R^2=0.9727 for the former, and slope=0.2291 $s^{-1}\cdot subunit^{-1}$ and R^2=0.9891 for the latter.

This rapid ADP release mediated by SP presents us with a very intriguing situation. By comparing the ADP release trajectory (red with SP, blue without) to that of Pi release (purple with SP, green without) in the presence and absence of SP (Figure 4-5), one can easily identify the obvious shift of rate-determining step from being ADP release (without SP) to ATP hydrolysis (with SP). By the time ADP release from the newly formed trans-ring finished (～0.5s, in the presence of SP), the majority of ATP (～80%) capsulated in the cis-ring remained unhydrolyzed. It is reasonable to postulate that such shift of rate determining step is responsible for the extra Pi released during the initial ATP turnover time period (up to 6s) in the presence of SP (Figure 4-5, compare the purple trace with the green trace). These extra hydrolyzed ATP must come from the vacant trans-ring (Ring B) from which previously bound ADP was rapidly exchanged off. This means that the two rings must be able to turnover simultaneously, a mode of work very different from the one predicted by the two-stroke motor model [42].

4.4 Discussion

The pre-steady state studies on GroEL the ATPase cycle presented so far on both ATP hydrolysis and ADP release reveals a very important regulation mechanism utilized by the chaperonins: GroEL/ES complex releases ADP at dramatically different rates modulated by SP binding, a key to appreciate the elegant design of this molecular

machine by nature. In the absence of SP, both the presence of the delay phase in Pi release data and slow release of ADP directly measured in this chapter demonstrate that ADP release lags far behind ATP hydrolysis which makes it the RDS of the whole cycle. On the other hand, the presence of SP dramatically accelerates the ADP release while does not exert any measurable influence on the intrinsic rate of ATP hydrolysis (Figure 3-7). The net result is that ADP release over-takes ATP hydrolysis, which makes the latter the new rate-determining step. Understanding such delicate design lends us great insights into the mechanism by which chaperonins couple the mediated SP refolding with its complex ATPase cycle.

On one hand, targeting ligand release for regulation rather than catalysis seems to be quite common among many important allosterically regulated enzymes, such as Kinesin [83], and the α subunit of G protein [84]. The logic behind it, specifically for chaperonins, is that it makes regulation more efficient and tunable by controlling ADP release rather than ATP hydrolysis to set the overall pace of the functional cycle. In order to function under harsh stressed conditions, chaperonins need a robust rigid protein fold especially around the active site to guarantee reliable catalysis which makes catalysis not a likely target for regulation. When the ligand binding/release is targeted for regulation, GroEL is capable of populating among different allosteric states (T, R, R') induced by ligand binding/dissociation. These allosteric states come with different degree of nucleotide binding pocket opening and thus different affinity for ADP. In this way, the rate of the system turnover can be conveniently regulated by changing the rate at which ADP is released. Without SP, slow release of ADP guarantees that no valuable energy currency ATP would be wasted in futile cycle. SP binding to the apical domain of the

trans-ring locks the trans-ring conformation at the T state [40, 85] which dramatically accelerates release of ADP from its binding pocket and thus allows the chaperonin molecular machine to respond to stressed conditions in a timely manner and to function at its maximum rate, set by its intrinsic ATPase activity instead of ADP release.

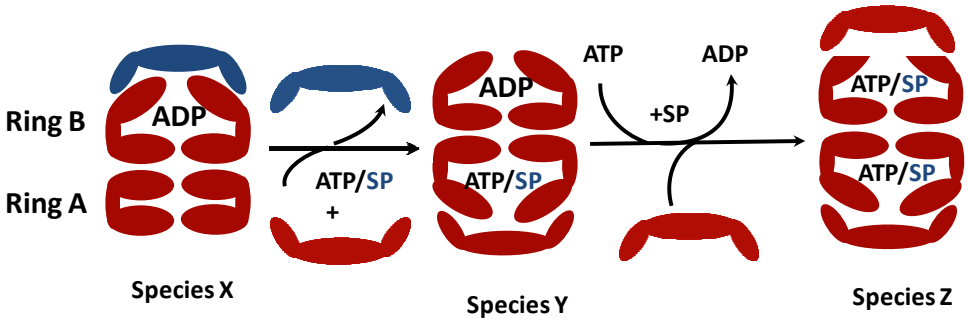

Figure 4-7: cartoon illustration describes how accelerated ADP release results in formation of the symmetric complex. The key for the formation of the symmetric complex is that ADP release from Ring B is finished before ATP in Ring A gets hydrolyzed.

On the other hand, according to basic kinetic rules, a shift of RDS is always accompanied by a change of predominant species provided that the two RDS candidates do not branch out from the same enzymatic species. In light of the source of the 'ADP surge' in Figure 4-5 and 4-6, i.e. the ADP bound in the initial *cis* ring (Ring B in Figure 4-7), it is reasonable to propose the following sequence of events depicted in Figure 4-7: by the time all ADP were exchanged off from the nascent trans-ring (old *cis* ring, Ring B Figure 4-7) promoted by SP, which corresponds to the end of the surge phase, ATP encapsulated in the newly formed *cis* ring (Ring A) remains largely un-hydrolyzed. Therefore, this 'ATP bullet' with an open empty trans-ring (Species Y) is capable of forming the symmetric complex [$GroES_7$-$GroEL_{14}$-$GroES_7$] (Species Z) is provided sufficient [ATP] and [GroES] present. This deduction is made based on the following: *1)* work done by H.S. Rye et.al. [55-56] indicates that the *cis*-bound GroES will not be

released until ATP is bound in the same ring being hydrolyzed to ADP; *2)* Funatsu *et.al* [58] have shown that *cis*-bound ATP doesn't prevent ATP from occupying the *trans* ring and therefore formation of the symmetric complex in the presence of ATP is entirely possible. In my next chapter, I will present my work with a FRET based system to follow the complex formation between GroEL and GroES which reveals the detailed mechanism by which chaperonins shuttle between two distinct but related cycles to optimize refolding of SPs.

Chapter 5: FRET study on the chaperonin complex formation in GroEL functional cycle

5.1 Introduction

Though it is universally accepted that ATP and GroES are obligatory in GroEL optimized SP refolding, the nature of the GroEL/ES complex formed in such functional cycle remains disputed. Two types of GroEL/ES complexes have been observed: the asymmetric $GroEL_{14}$:$GroES_7$ 'bullet' complex and the symmetric $GroES_7$:$GroEL_{14}$:$GroES_7$ 'football' complex. Experimental evidence can be found in literature in support for existence of both complexes [43-46, 48-53, 56], and different models of the GroEL functional cycle have been proposed based on either complex as the predominant functional species [9-10, 38, 57] as reviewed in details in Section 1.4 and 1.5. Despite the frustration and confusion involved, identifying the correct GroEL/ES complex responsible for SP refolding is essential in understanding how GroEL couples ATP binding/hydrolysis and association with GroES to its core biological function, i.e., assisting SP refolding. In this chapter, I present studies on the formation of both types of GroEL/ES complex by a robust FRET technique. These studies allow identification of preferable conditions for the formation of both types of complex respectively. And in combination with the insights learned from ligand release studies presented in the previous two chapters, an altogether new view of GroEL functional cycle was developed and presented here, crystallized in the form of a two cycle model: *i)* in the absence of SP, ADP release is the rate-determining step (RDS) of the whole cycle and consequently, the asymmetric GroEL-GroES1, 'bullet' which precedes this step, is the pre-dominant species; *ii)* in the presence of SP, the release of ADP is greatly accelerated while the

intrinsic ATPase activity of GroEL remained unaffected, consequently ATP hydrolysis becomes the RDS and the symmetric GroEL-GroES2, 'football' becomes the predominant species. Its significance in providing constraints on the possible mechanism *via* which GroEL optimize its denatured SP was also discussed.

5.2 Methods specific to Chapter 5

5.2.1 Protein purification and labeling The protein mutants used for constructing FRET pair to study GroEL/ES complex formation are $GroEL^{E315C}$ and $GroES^{C98}$. For both, a cysteine was introduced to a solvent exposed position close to the binding interface of the two proteins with a distance between the Cα of the two cysteines ~36Å [86]. Plasmids containing the two mutations were created by Dr. John Grason, and purification of the two mutant proteins follows essentially the same protocol as for the wild-type protein except a higher DTT (2mM) should be used to keep the reactive cysteine reduced.

Purified $GroEL^{E315C}$ was labeled with IAEDANS (5-((((2-iodoacetyl)amino)ethyl)amino) naphthalene- 1-sulfonic acid) as FRET donor, and $GroES^{98C}$ with fluorescein-5-maleimide (both from Life technology) as FRET acceptor. The Föster distance (R_0) of this FRET pair is 46Å [86]. Stock solutions of both fluorescent dyes were made in DMSO to a final concentration of 10-15mM. Mutant proteins were reduced with 5 mM DTT for 10 minutes at room temperature immediately prior to labeling. The DTT was then removed by gel filtration on a PD-10 column equilibrated with 10 mM TrisHCl, pH7.5, 10 mM $MgCl_2$.

$GroEL^{E315C}$ was labeled at a concentration of 350μM by using the same concentration of IAEDANS dye. The reaction was allowed to proceed in darkness at

room temperature for 45 minutes. Unreacted dyes were quenched with 6 mM DTT, and removed by PD-10 gel-filtration. The extent of labeling was determined spectroscopically by determining protein and labeled dye concentrations at 280 nm and 336 nm, respectively ($\varepsilon_{280,\ GroEL}$=9600 $M^{-1}cm^{-1}$ and $\varepsilon_{336,\ IAEDANS}$ =5400 $M^{-1}cm^{-1}$). The protein absorption at 280nm should be adjusted to take account of the dye absorption at the same wavelength, that is, $Abs_{(protein\ adjusted)} = Abs_{280} - 0.16 * Abs_{336}$. Conditions applied here resulted in attaching approximately 4-5 dyes per GroEL ring. Labeled GroEL will hereafter be referred to as $GroEL^{IAEDANS}$.

$GroES^{98C}$ was labeled at a concentration of 120μM by using the same concentration of F5M over ES monomers. The reaction was carried out in the dark for 10 minutes at room temperature and then quenched with 5 mM DTT. Excess label was removed by PD-10 equilibrated with 10 mM TrisHCl, pH 7.5. Because the label interferes with the UV spectra at 280 nm, protein concentration was determined by Bradford assay. The label concentration was determined by checking the absorbance at 491 nm (ε=74,500 $M^{-1}cm^{-1}$). The extent of labeling under these conditions was 2-3 dye per GroES ring. Labeled GroES will hereafter be referred to as $GroES^{F5M}$. An example steady-state FRET spectrum is shown in Figure 5-1 demonstrating that upon GroEL/ES complex formation, both the donor and acceptor signal are altered with the former quenched and the latter enhanced simultaneously, and the extent of fluorescence signal change can be used to identify formation of either the asymmetric bullet complex or the symmetric football complex.

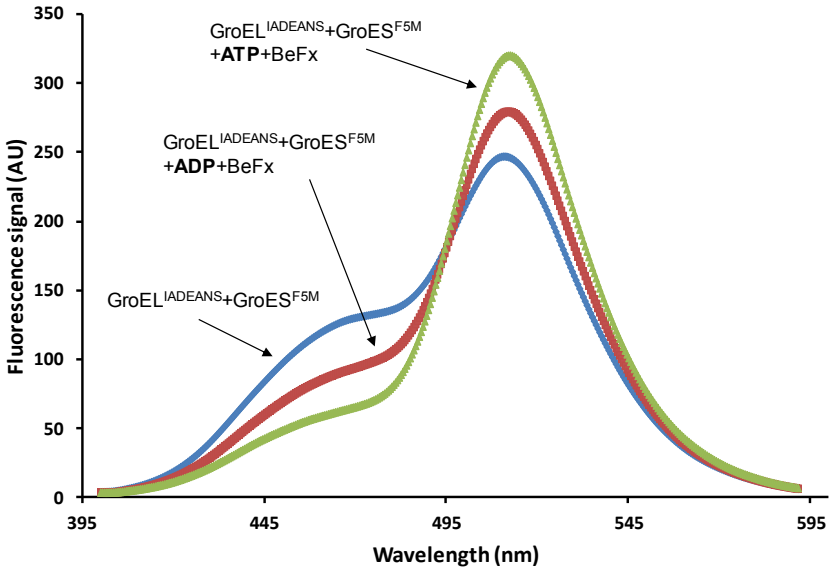

Figure 5-1: An example steady-state FRET measurement showing formation of football (green trace) and bullet (red trace) under conditions specified in the plot. The blue trace is the initial fluorescence signal before any GroEL/ES complex formed. All three traces were generated with an apo mixture of 2μM $GroEL^{IAEDANS}$ and 3μM $GroES^{F5M}$. The solution was excited at 336nm (donor absorption peak) with a band width of 15nm and fluorescence emission between 400nm and 590nm was collected with an emission band width of 20nm.

5.2.2 Stopped-flow FRET measurements All measurements of the sort were performed in essentially the same way as described in Section 2.9 except for the following modifications: FRET donor excited at 336nm, emission spectrum beyond 530nm was collected by implementing a cut-off filter at that wavelength, and the GroEL and GroES subunit concentration applied were 2μM and 5μM respectively. Since the cut-off filter was used, only the FRET acceptor signal change can be followed with our stopped-flow device. The FRET signal in the stopped-flow was, therefore, calibrated in the way shown in Figure 5-2 based on the fact that in the presence of ATP+BeF_3, $GroEL_{14}$ can recruit two $GroES_7$ and form the symmetric football complex whereas in the presence of ADP+BeF_3, $GroEL_{14}$ can only bind one $GroES_7$ and form the asymmetric bullet complex [87]. This is exactly what is observed in experiments shown in Figure 5-2:

the magnitude of fluorescence enhancement in the presence of ATP+BeF_3 is twice that of ADP+BeF_3, therefore, the FRET acceptor fluorescence change can be converted to number of GroES associated with GroEL which is also supported by negatively stained electron micrograph presented in [13].

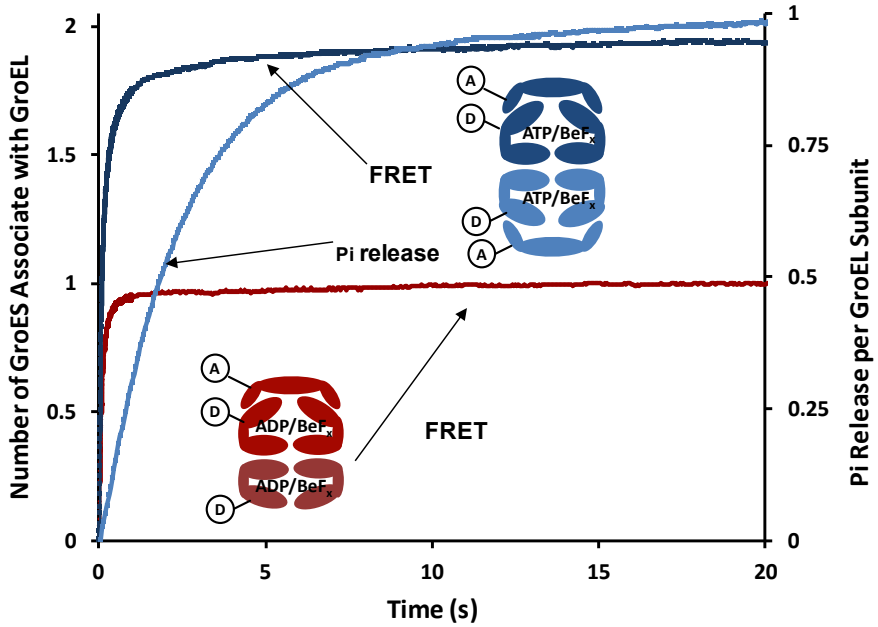

Figure 5-2: Stopped-flow calibration of the FRET-based system. It is for monitoring the formation of the symmetric complex and the asymmetric complex formed in the presence of ATP+BeF_3 (blue traces) and ADP+BeF_3 (red trace) respectively. For all three kinetic trajectories, the measurements were started by mixing apo-$GroEL^{IAEDANS}$ and $GroES^{F5M}$ and the development of FRET signal (red and dark blue traces) or Pi released from ATP hydrolysis (light blue traces) were monitored. The magnitude of fluorescence change in the presence of ATP+BeF_3 is twice that of ADP+BeF_3 in accordance with the fact that symmetric complex and asymmetric complex were formed under these two different conditions [87]. The left y-axis can, therefore, be converted to the average number of GroES associated with GroEL. Pi release trace was analyzed in the same way as that of Chapter 3 and was included here to show that all 14 bound ATP can be hydrolyzed upon football formation.

5.3 Results

5.3.1 SP induced rapid ADP release promotes formation of the symmetric complex The observations made in Figure 5-2 provide a convenient basis for calibrating a FRET based system for monitoring in real time the population of the symmetric

"football" and the asymmetric "bullet" particles. It is demonstrated that upon mixing FRET donor $GroEL^{IAEDANS}$, FRET acceptor $GroES^{F5M}$, ATP and BeF_3, the formation of the symmetric "footballs" was accompanied by the hydrolysis of exactly one ATP per GroEL subunit.

On the other hand, upon mixing $GroEL^{IAEDANS}$, $GroES^{F5M}$, ADP and BeF_3, the formation of the asymmetric "bullets" occurred. As shown in Figure 6-3 of the next chapter, the ATPase deficient GroEL mutant ($GroEL^{D398A}$) forms footballs upon mixing with GroES and ATP (no BeF_3) showing that the binding and not the hydrolysis of ATP is necessary for the formation of the symmetrical particles, confirming a previous result [58]. Both of these results demonstrate that both rings of GroEL can bind and hydrolyze ATP simultaneously, contrary to the claim that 'when one ring has seven ATPs, the other ring does not bind ATP [38, 55]'.

Next, the number of GroES associated with GroEL in the presence or absence of SP was measured with FRET. The obtained FRET trajectories, combined with ligand release (Pi and ADP) traces taken under the same condition already shown in Figure 4-5, were plotted in Figure 5-3. In the absence of SP, on average there is one GroES associated with GroEL (Figure 5-3A) indicating the asymmetric bullet complex predominates under such condition. This is to be expected on kinetic grounds: ADP release is the RDS in the absence of SP, which causes large amount of accumulation of the asymmetric resting state complex, immediately preceding this slow step; and the symmetric complex formation is effectively inhibited due to the fact that ADP release is much slower than ATP hydrolysis ($0.1s^{-1}$ *VS* $0.5s^{-1}$).

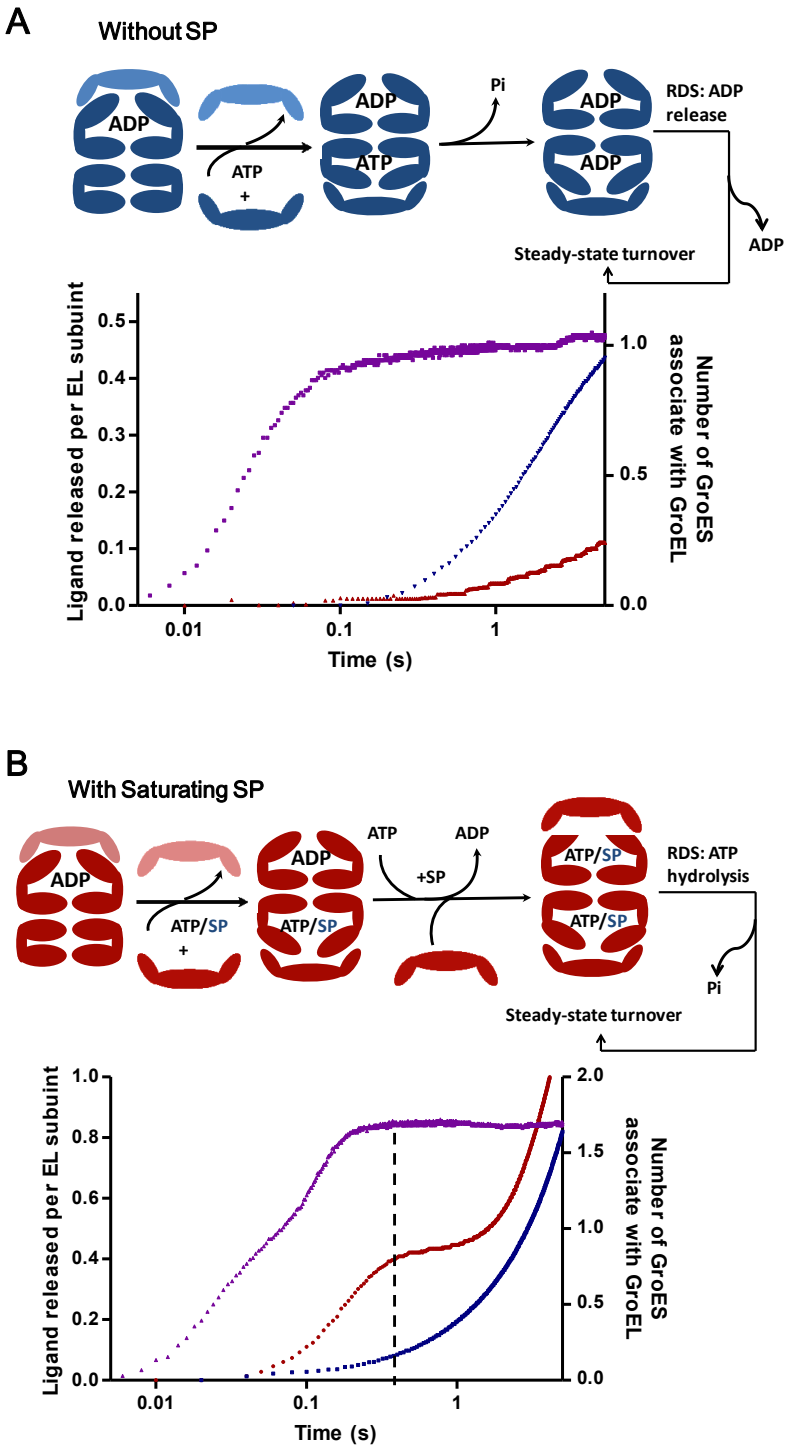

Figure 5-3: SP induced change in the rate-determining step and shift of dominant kinetic species of the GroEL ATPase cycle. All measurements were started with the acceptor state complex and performed with 100mM [K^+] and 0.5mM ATP with different concentrations of the acceptor state complex: 30μM for ADP release (red traces), 1μM for Pi release (blue traces), 2μM for FRET measurements (purple trace). The kinetic

trajectories of ADP release, ATP hydrolysis (both duplicated from Figure 4-5), and FRET were combined with no SP present in **(A)** or with SP (10.7μM α–LA) present in **(B)**. The left y-axis was normalized to moles of ligand released per mole of GroEL subunit on which the Pi release and ADP release data were plotted. It is clear from the figure that in the absence of SP, the ADP release is the RDS and thus the asymmetric resting state complex is the predominant species with ~1 $GroES_7$ per $GroEL_{14}$ on average; while in the presence of SP, the RDS becomes the hydrolysis of ATP from the symmetric complex which is the predominant species. The cartoon illustrations show the shift of predominant species from the asymmetric to the symmetric complex caused by the change of rate-determining step (RDS) that in turn is caused by SP acceleration of ADP release. Light color stands for Non-FRET $GroES^{wt}$ while dark color for FRET labeled $GroES^{F5M}$.

On the other hand, the average number of GroES associated with GroEL increases to two in the presence of saturating [SP] shown in Figure 5-3B indicating the symmetric football complex becomes the predominant species. This is due to the change induced by SP on GroEL functional cycle: the empty nascent trans-ring that was created by SP-accelerated ADP release can accept new ATP and GroES, and in the meanwhile, the ATP bound in the opposite ring remains largely unhydrolyzed (the dashed line in Figure 5-3B indicates by the time initial round of ADP release finished, <20% of ATP were hydrolyzed). As a result, it gives rise to the symmetric complex with both rings mostly occupied by ATP which yields the corresponding FRET trace (purple) in Figure 5-3B. Notice however, that the kinetics of football formation seems slightly faster than the surge of ADP release. This may reflect the fact that the kinetics of the 'ADP surge' (initially introduced in Figure 4-5 of Chapter 4) is largely limited by the turnover of the coupling enzyme system rather than reflects the real ADP release rate, a point that was made in the last chapter.

5.3.2 Measuring the true rate of SP-catalyzed ADP release The PK/LDH coupled enzyme method yielded only a semi-quantitative measurement of the effect of SP on the release of ADP. However, this is the key to understand the SP induced symmetric

complex formation as discussed above. Therefore, here, the changes in the accompanying FRET signal was exploited to make a more reliable estimate of the rate of SP induced ADP release (Figure 5-4A). The asymmetric acceptor complex was first prepared using $GroES^{wt}$ and $GroEL^{IAEDANS}$. When this was mixed with ATP, SP, and $GroES^{F5M}$, formation of the symmetric FRET $GroEL^{IAEDANS}$:$(GroES^{F5M})_2$ complexes ensued in two distinct stages (Figure 5-4A purple). In the first stage, without a discernible lag, ATP and $GroES^{F5M}$ rapidly add to the *trans* ring of the acceptor complex, displacing the $GroES^{wt}$ from the *cis* ring leaving ADP behind on the nascent *trans* ring (reactions k_1 and k_2 of Figure 5-4B). Next, following SP induced ADP/ATP exchange (reaction k_3 of Figure 5-4B) a second $GroES^{F5M}$ adds to create an ensemble of predominantly symmetric "football" particles (practically a repetition of reactions k_1 and k_2 of Figure 5-4B). Note that these events are complete within ~200ms, i.e. before hardly any of the 14 ATP has been hydrolyzed. Note also that whereas in the first stage ATP adds to the *trans* ring of the asymmetric complex containing ADP in the *cis* ring, in the second stage ATP adds to the *trans* ring of the asymmetric complex containing ATP in the *cis* ring.

The same protocol was repeated after first populating the *trans* ring of the asymmetric complex with 50μM ADP (Figure 5-4A red and cyan). In the absence of SP, upon introducing ATP, essentially no change in the FRET signal occurred on this time scale (Figure 5-4A cyan), as expected from the slow release of ADP which effectively delays any event that follows it. In the presence of SP, two phases were evident (Figure 5-4A red): a lag phase of ~60ms occurred preceding the development of the FRET signal (see also insert to Figure 5-4A). Note that this lag phase was independent of [SP] in the range 3 to 14μM α-lactalbumin (insert in Figure 5-4A). Due to the fact that the kinetics

of all the processes described in the cartoon illustration in Figure 5-4B are not well resolved from each other, the interpretation of the apparent rate constants obtained by fitting the trajectories with exponential equations becomes dubious. Therefore, the trajectories (red and purple) were globally analyzed by ODE using the mechanism outlined in Figure 4-5B in much of a similar way as that of Chapter 3. Note that in this scheme the only difference between starting with the resting state complex (+ADP) and the acceptor state complex (-ADP) is the addition of a second term k_3, describing the SP-induced ADP/ATP exchange from the resting state complex. The two trajectories are thus described by (k_3+k_1+k_2+k_3+k_1+k_2) and (k_1+k_2+k_3+k_1+k_2). Global simulation of both trajectories (black lines in Figure 5-4A) yields values for each of these rate constants: k_1 (the 2nd order rate constant for the binding of ATP to the trans ring) = (7±1)x 10^5 $M^{-1}s^{-1}$, k_2 (the 2nd order rate constant for the binding of FRET-GroES to the trans ring) = (4.1±0.6) x 10^7 $M^{-1}s^{-1}$ and k_3 (the SP saturated first order rate constant for ADP dissociation) = 13.0±0.2 s^{-1}. The values for k_1 and k_2 are similar to those previously reported [35, 40, 55, 85].

The microscopic rate constant k_3, obtained with saturating [SP], therefore represents the rate at which SP induced ADP release which may likely include two microscopic steps that cannot be resolved by our measurement: the SP induced opening of nucleotide binding pocket characterized by R to T transition, and the release of ADP from its binding site at T state. Nevertheless, the process(es) characterized by k_3 is at least 100 times faster than that obtained in the absence of SP characterized by the kinetics of the delay phase of Pi release (~0.1s^{-1}) or the actual ADP release (~0.05s^{-1}). This is a clear demonstration of the enormous influence exerted by SP on GroEL ATPase cycle and lays

the kinetic foundation based on which we understand the SP induced shift of predominant species of GroEL functional cycle.

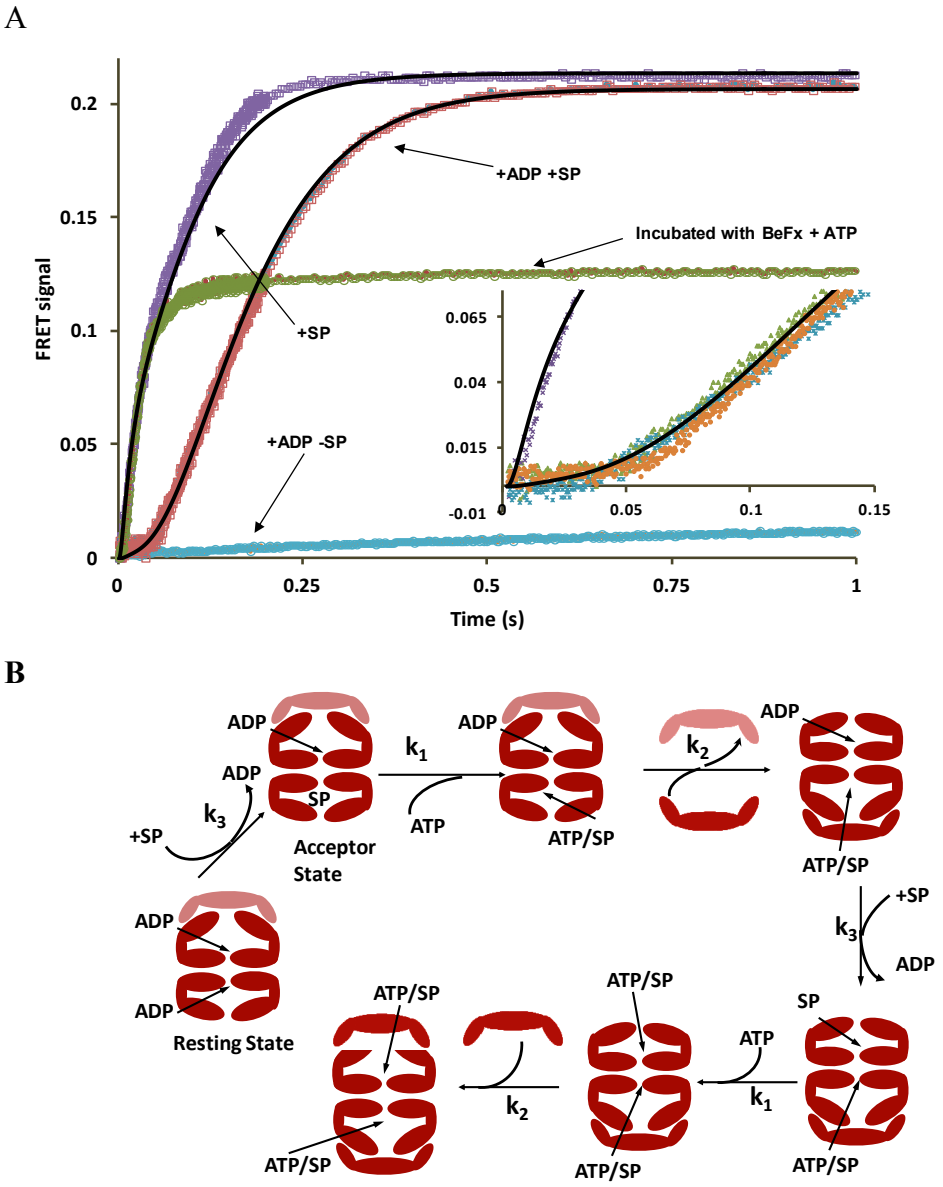

Figure 5-4: The dramatic acceleration of ADP release from the *trans* ring of GroEL by SP was followed by FRET measurements. (A) These measurements were initiated with asymmetric complex containing non-FRET GroES^{wt} in the acceptor state (purple) or resting state (red and cyan), created by pre-incubating the acceptor state with 50μM ADP. The purple and red trajectories were generated in the presence of SP (7.1μM) (introduced upon mixing), while the cyan trajectory was obtained in the absence of SP. A calibration trace was also included by challenging the BeF_3 preincubated acceptor complex (GroEL^{IAEDANS}/GroES^{F5M}) with ATP, showing the addition of one FRET GroES^{F5M} onto FRET GroEL^{IAEDANS}. The two traces with SP can be simulated globally with the kinetic

model depicted in B using a single set of microscopic rate constants; k_1 (the 2nd order rate constant for the binding of ATP to the trans ring) = 7±1 x 10^5 $M^{-1}s^{-1}$, k_2 (the 2nd order rate constant for the binding of FRET-GroES to the trans ring) = 4.1±0.6 x 10^7 $M^{-1}s^{-1}$ and k_3 (the SP saturated first order rate constant for ADP dissociation) = 13.0±0.2 s^{-1}. *Insert*: The initial lag phase of the resting state trajectories at three different [SP]s; 3.5μM (blue), 7.1μM (red), 14.2μM (green). **(B)** The kinetic model used to fit the trajectories. $GroES^{wt}$ is light red. Dark red GroEL and GroES depict FRET donor and FRET acceptor respectively.

5.3.3 Kinetic properties of football complex formed in the absence and presence of SP As demonstrated in experiments shown in Figure 5-3 and 5-4, football complex formation is promoted by the SP accelerated ADP release. Furthermore, the steady-state rate measured by both Pi and ADP release shows significant acceleration in the presence of SP indicating the football thus formed turnover dynamically, contrary to what was previously believed. In this section, I present studies that directly characterize this important property of the football complex and its implication in the possible mechanism by which GroEL mediate its SP refolding.

The series of experiments that are shown in Figure 5-5 and 5-6 were obtained by initiating the measurements with apo $GroEL^{IAEDANS}$, with which $GroES^{F5M}$ and ATP were mixed. Though it has been pointed out that under normal in-vivo circumstances, GroEL always associates with one or two GroES and this apo-state doesn't exist, initiating measurements from this state lends us important insights that is otherwise inaccessible.

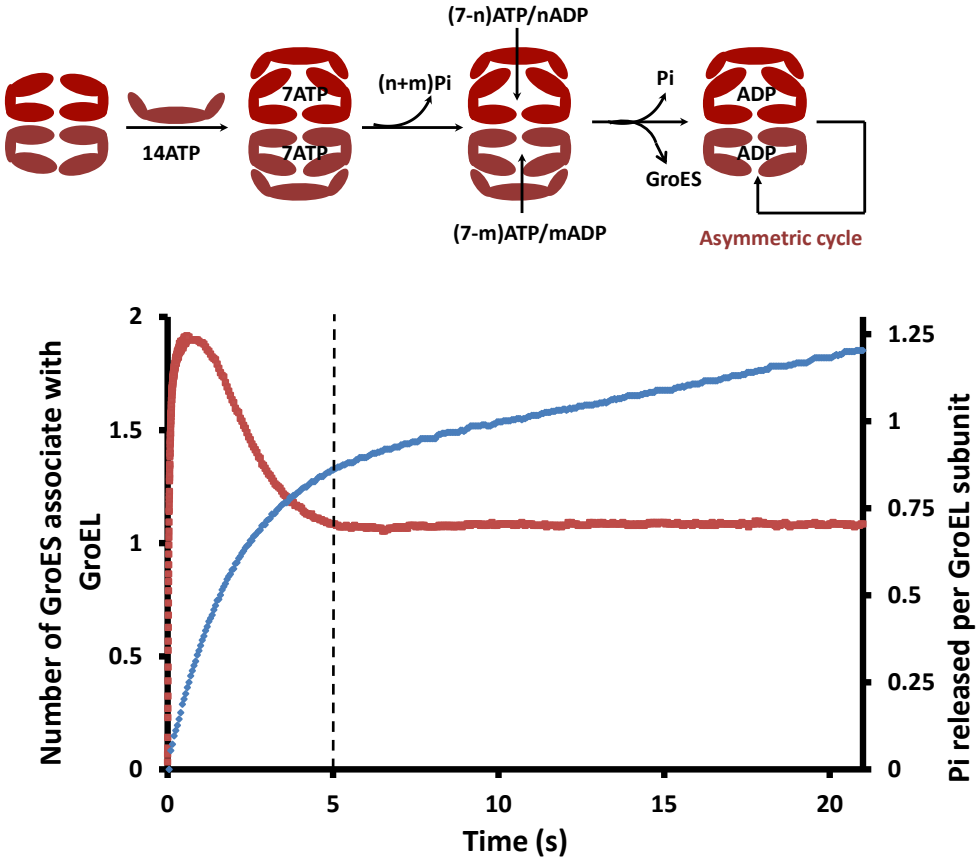

Figure 5-5: Formation and decay of GroEL:GroES$_2$ complexes in the absence of SP. Formation of the symmetric GroEL:GroES$_2$ and the asymmetric GroEL:GroES$_1$ complexes measured by FRET (red) overlaid with Pi release trace (blue). Both experiments were started with a mixture of 2μM apo-GroEL^{IAEDANS} and 5μM GroES^{F5M} at 100mM K^+, which was rapidly mixed with 0.5mM ATP (final) in a stopped-flow apparatus. Pi release was measured with 1μM GroEL and 2.5μM GroES respectively, as previously described. The FRET signal (left axis) was converted to number of GroES associate with GroEL based on calibration of the sort shown in Figure 5-2 while the Pi release data (right axis) was converted to Pi released per GroEL subunit. The cartoon above the graph depicts the formation and fate of the GroEL:GroES$_2$ symmetric complex in such measurement.

***In the absence of SP*:** In Figure 5-5, the red FRET trajectory shows that upon mixing apo-GroEL^{IAEDANS}, GroES^{F5M} and ATP in the absence of SP, an ensemble of particles, substantially enriched with the symmetric GroEL: GroES$_2$ was formed within one second. During that time, from the accompanying blue Pi release trace, only ~3 of the 14 ATPs have undergone hydrolysis. It is clear that both GroEL rings are simultaneously populated with ATP, which can be deduced based on the size of the Pi release burst (~1

Pi per GroEL subunit) and formation of the symmetric complex. This is consistent with our understanding that there is no mechanistic constrain between the two GroEL rings that prevents simultaneous occupation of both rings with GroES, contrary to the previously accepted proposal. In the absence of SP, in the next 3-4 sec after >90% football complex formed, the symmetric complex reverted back to largely asymmetric complex as reflected by the drop of the average number of GroES associated with GroEL from ~2 to ~1. This relaxation is completed when one cycle of ATP hydrolysis has occurred with a rate constant of ~$0.5s^{-1}$ (dashed line in Figure 5-5). Although these asymmetric particles persist for tens of minutes [55-56], they are dynamic, as revealed by the continuing steady-state hydrolysis of ATP (blue trace Figure 5-5), and such dynamic property can be clearly demonstrated by a GroES 'washout' experiment shown in Figure 5-7A. Here the asymmetric complex was formed by mixing $GroEL^{IAEDANS}$ and $GroES^{F5M}$ with ATP in the absence of SP allowing them to turnover to roll over the 'hilltop' to the plateau stage as in the FRET trace of Figure 5-5. The turning-over particles at this stage, almost entirely asymmetric in nature, were next loaded into the stopped-flow device at 37°C. After turning over for 2min., the asymmetric complex was challenged with a 10-fold molar excess of non-FRET $GroES^{wt}$, which would effectively prevent re-association of $GroES^{F5M}$ after being released. The FRET signal decayed, as $GroES^{wt}$ displaced the $GroES^{F5M}$, with an exponential phase accounting for ~92% of total signal change characterized by a rate of $0.126s^{-1}$. This rate is very close to that of the rate-determining step under such condition, namely, the dissociation of ADP from the *trans* ring at ~0.1 s^{-1}.

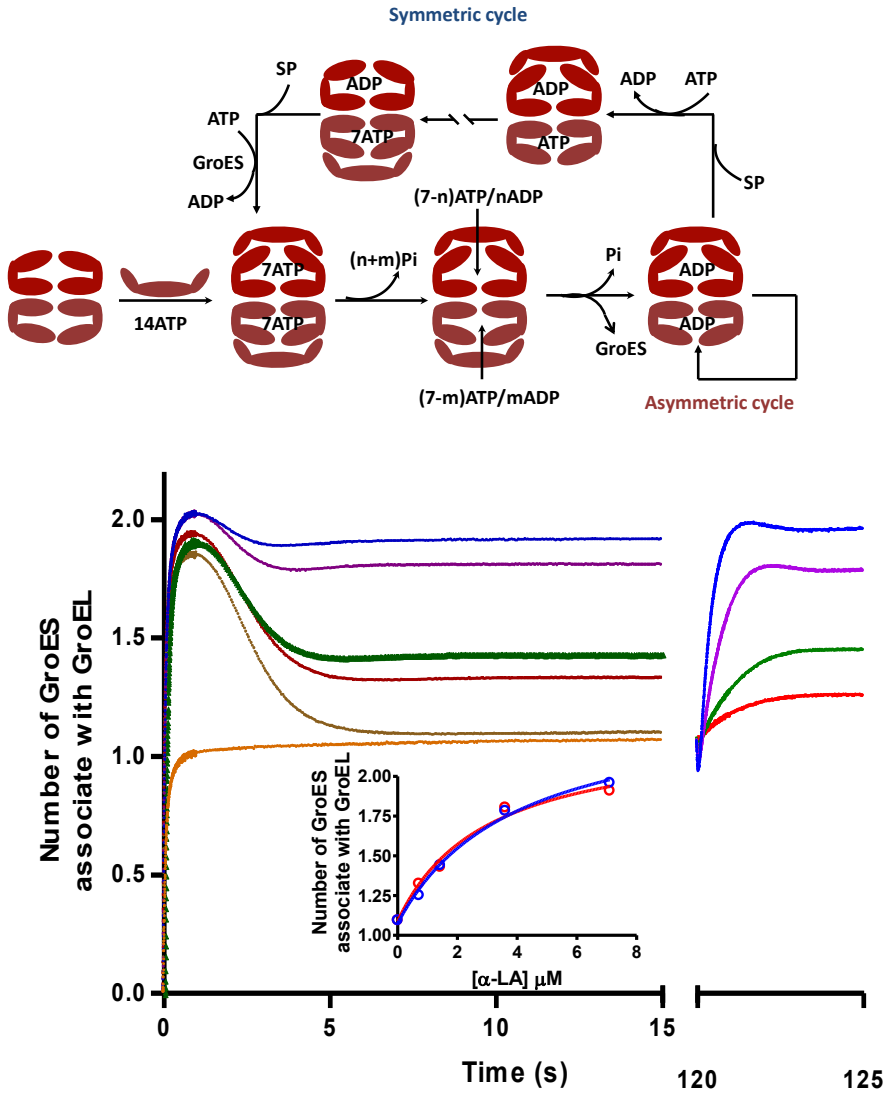

Figure 5-6: Kinetic partitioning of GroEL/ES complex into the symmetric cycle mediated by SP. Two sets of experiments are presented: the darker colored traces (left) were generated with reactions initiated as in Figure 5-5 by mixing 2μM apo-GroEL^{IAEDANS}, 5μM GroES^{F5M} mixture with 0.5mM ATP (final) plus the indicated concentrations of SP (denatured α-LA). The lighter colored set of traces (right) was acquired by introducing the indicated concentration of SP into an actively turning-over system comprising 2μM GroEL^{IAEDANS}, 5μM GroES^{F5M}, 0.5mM ATP plus an ATP regenerating system (0.4mM phosphoenol pyruvate (PEP), 5unit/ml pyruvate kinase), 2 min after the experiment was initiated. Concentrations of SP applied in both cases: 0μM (brown trace), 0.71μM (red), 1.42μM (green), 3.6μM (violet), 7.1μM (blue). The orange trace was acquired by mixing GroEL^{IAEDANS} and GroES^{F5M} mixture with 0.5mM ADP and 1mM BeF_3 to generate a base line showing the signal level of the asymmetric complex upon which the second set of 'SP jump' trajectories were based. *Inset*: the level of the symmetric GroEL:GroES$_2$ complex was plotted against the concentration of α-lactalbumin(α-LA). Two different sets of experiments with different starting states were combined and plotted together: red, apo-GroEL+GroES mixture; blue, asynchronous

GroEL:$GroES_1$ complexes turning over via the asymmetric cycle. Solid lines represent fitting with the simple single site binding model with the apparent K_d as 3±1μM (red) and 4±1μM (blue). The cartoon above the figure illustrates the kinetic partitioning of GroEL:GroES complexes between the symmetric and asymmetric cycles under the influence of SP.

***In the presence of SP**:* When the same experiment was conducted in the presence of varying concentrations of SP (unfolded α-lactalbumin) an altogether different scenario developed (Figure 5-6). As in the absence of SP, the symmetrical particles formed within one second of mixing. What transpired thereafter depended on the concentration of SP. With a saturation concentration of SP (blue in the left plot of Figure 5-6), only a little breakage of football symmetric complex to asymmetric complex was evident, even as ATP hydrolysis occurred; the population of the symmetric GroEL:$GroES_2$ particles persisted for tens of minutes provided an ATP-regenerating system was present [13]. At intermediate concentrations of SP, the system relaxed to a steady state mixture of symmetric and asymmetric particles (purple, green, and red in the left part of Figure 5-6).

The football complex state can also be reached from a largely asymmetric population provided enough SP was introduced, demonstrated by a set of 'SP jump' experiments and shown in the right portion of Figure 5-6. Here apo $GroEL^{IAEDANS}$ was first mixed with $GroES^{F5M}$ and ATP (plus an ATP regenerating system) in the absence of SP, and the system was permitted to relax to asymmetric particles. Two minutes afterwards, the asymmetric particles were then challenged with SP at the same concentrations as used in the right portion of Figure 5-6. The system reaches a new equilibrium position within a second or two. The equilibrium position depends on the concentration of SP. At saturating concentrations the ensemble consists predominantly of the symmetric particles, while at intermediate concentrations equilibrium between

mixtures of both the asymmetric and the symmetric particles are established. As shown in the inset of the same figure, the equilibrium position is the same regardless of whether it is approached from the symmetric particles (with SP present initially) or from the asymmetric particles (with SP added after 2 min).

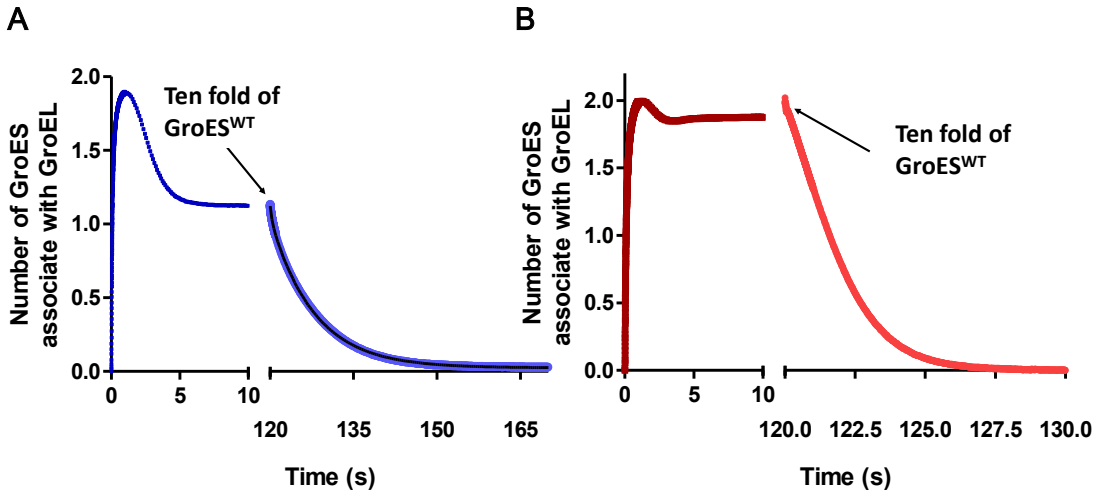

Figure 5-7: Dynamics of the GroEL:GroES$_1$ asymmetric and the GroEL:ES$_2$ symmetric complexes under turnover conditions. (A) GroES "wash out" from the asymmetric GroEL:GroES$_1$ complex. The plot combines two related FRET measurements. Both measurements include 2μM apo-GroEL^{IAEDANS} and 3μM GroES^{F5M} mixture. The trajectory on the left (dark blue) was initiated by mixing with 0.5mM ATP and a similar transient was resulted as in Figure 5-5 and Figure 5-6. The right trajectory (light blue) was generated as follows: after addition of 0.5mM ATP, the system was left turning over for 2min (marked by the arrow) before 30μM GroES^{wt} (dark blue) was added, displacing the FRET GroES^{F5M} and thus showing the kinetics of the turnover of the asymmetric complex. An ATP regenerating system (0.4mM PEP plus 10units/ml pyruvate kinase) was included in both measurements. The GroES 'wash-off' trace can be fitted with double exponential equations ($y = \sum_{i=1}^{2}[-(-1)^i \cdot A_i \cdot exp\,(-k_i \cdot t)] + B$, solid black line) yielding two rate constants: 2.49±0.06s^{-1} ($Amp \sim 7\%$) and 0.1265±0.0003s^{-1}($Amp \sim 93\%$). The latter is very close to the rate constant for the dissociation of ADP *trans* ring from the resting state asymmetric complex, while the former can be attributed to a small fraction of asymmetric complex in the acceptor state (no ADP release required before ATP-induced dissociation of the cis-bound GroES). **(B)** GroES "wash out" from the symmetric GroEL:GroES$_2$ complex. Similar to A, two plots were combined: dark red trace on the left was obtained by mixing apo-GroEL^{IAEDANS} and GroES^{F5M} with 0.5mM ATP in the presence of saturating SP (7.1μM α-LA); while the light red trace on the right was initiated with a turning over system in the presence of 7.1μM α-LA, in which the symmetric complex is the predominant species. 2min later, 10 fold GroES^{wt} (indicated by the arrow) was added, displacing the FRET GroES^{F5M} and thus showing the kinetics of the turnover of the symmetric complex. An ATP

regenerating system (0.4mM PEP plus 10units/ml pyruvate kinase) was also included in both measurements. No exponential fitting was shown however, due to the unacceptable large non-random residuals generated. The kinetics of symmetric complex turnover was evaluated from its approximate half time which is ~1.5s and is approximately 5 times faster than that of the asymmetric complex turnover.

The fact that symmetric complex can be approached from both sides indicates that these particles must be highly dynamic. In order to probe this dynamic aspect of symmetric particles, I performed the GroES 'washout' experiment in the presence of SP. The symmetric complex was first created by mixing $GroEL^{IAEDANS}$, $GroES^{F5M}$ and ATP (plus a regenerating system) in the presence of a saturating concentration of SP. Two minutes later a ten-fold molar excess of $GroES^{wt}$ was introduced to follow the dissociation of the $GroES^{F5M}$ from both rings of $GroEL^{IAEDANS}$ (Figure 5-7B). The reaction leading to the dissociation of the $GroES^{F5M}$ from both rings of GroEL proceeded with a half time of ~1.5s, even though the population of the symmetric particles was maintained throughout.

5.4 Discussion

The studies presented in this chapter focus mainly on GroEL/ES complex formation in the GroEL functional cycle and lend great insight to us into the mechanism by which chaperonin function: SP plays a key role in coordinating steps in the cycle while the ADP release is the target for regulation. It is clear from Figure 5-3 that in the absence of SP, ADP release is the rate-determining step (RDS) of the whole cycle and consequently, the asymmetric GroEL-$GroES_1$,"bullet" which precedes this step, is the pre-dominant species. On the other hand, in the presence of SP, the release of ADP is greatly accelerated while the intrinsic ATPase activity of GroEL remained unaffected. Consequently ATP hydrolysis becomes the RDS and the symmetric GroEL-$GroES_2$

,"football" the predominant species. The latter point was further supported by our observation that both rings of GroEL can be occupied by ATP simultaneously as the size of the Pi burst produced by mixing apo GroEL+GroES and ATP equals to one Pi per GroEL subunit (Figure 5-2 and Figure 5-5).

Additional FRET measurements further illuminate the dynamic nature of the football symmetric particle formed in the presence of SP. Among them, the most arguable evidence for the involvement of the symmetric complex under normal turnover conditions is the series of experiments shown in Figure 5-5 and 5-6 which were initiated by mixing apo-GroEL, GroES and ATP. Rapid ATP binding to both GroEL rings brings about association with two GroES and formation of football at the very beginning of the measurement, then as ATP hydrolysis occurs the symmetric complex fall apart to the asymmetric bullet by releasing one of the two bound GroES. The football can be reformed if SP was introduced into this largely asymmetric complex state, and the amount of football that can be formed by such 'SP jump' reaches the same level if SP was included at the very beginning of the measurement (apo GroEL and GroES state) (Figure 5-6 inset). This is a clear indication that football and bullet coexist in a pseudo-equilibrium under normal turnover conditions and the partition between the two state is highly dependent on the [SP]. The pathway by which football turnover is also revealed by experiments of the sort: the symmetric football has to break into asymmetric bullet as enough ATP has been hydrolyzed to allow release of encapsulated SP and exchange of ADP with ATP promoted by another SP from solution (we phrase this whole process as 'nucleotide exchange catalyzed by SP'), which in turn brings about football restoration.

Both symmetric and asymmetric complex can turnover, but at different rate limited by different RDS and thus via different kinetic pathways (Figure 5-7). The turnover rate of the asymmetric complex as measured by exchanging off the FRET $GroES^{F5M}$ is comparable with the rate of ADP release, consistent with our understanding that ADP release is RDS in the absence of SP. On the other hand, the turnover of the symmetric complex measured in the a similar fashion was found to be of similar value as that of ATP hydrolysis rate (apparent half time ~1.5s) indicating the turnover of the symmetric complex is largely limited by ATP hydrolysis.

All the experimental evidence we have garnered so far points to a two-cycle model shown in Figure 5-8 which was initially proposed by [46] and further enriched and refined by work shown in this dissertation and our two recent publications [12-13]. In this model, in a SP dependent manner, GroEL shuttle between two distinct but related cycles with different RDSs. In the absence of SP, GroEL turnover in an asymmetric cycle as the predominant species is an asymmetric GroEL:$GroES_2$ complex. In this cycle, GroEL functions in a similar way as previously described as a 'two-stroke' motor with each ring turnover sequentially. This is imposed by the slow release of ADP which can *i)* effectively prevent both rings from being occupied by ATP simultaneously at any step of the asymmetric cycle and thus prevent the formation of symmetric complex to any detectable extent, and *ii)* minimize futile ATP hydrolysis when no biological function is required for chaperonin to fulfill. Nevertheless, the resting state bullet complex (in black rectangle in asymmetric cycle in Figure 5-7) can still turnover (half time ~7 sec) which is largely limited by the slow release of ADP as probed by measuring the $GroES^{F5M}$ exchange off rate (Figure 5-6A).

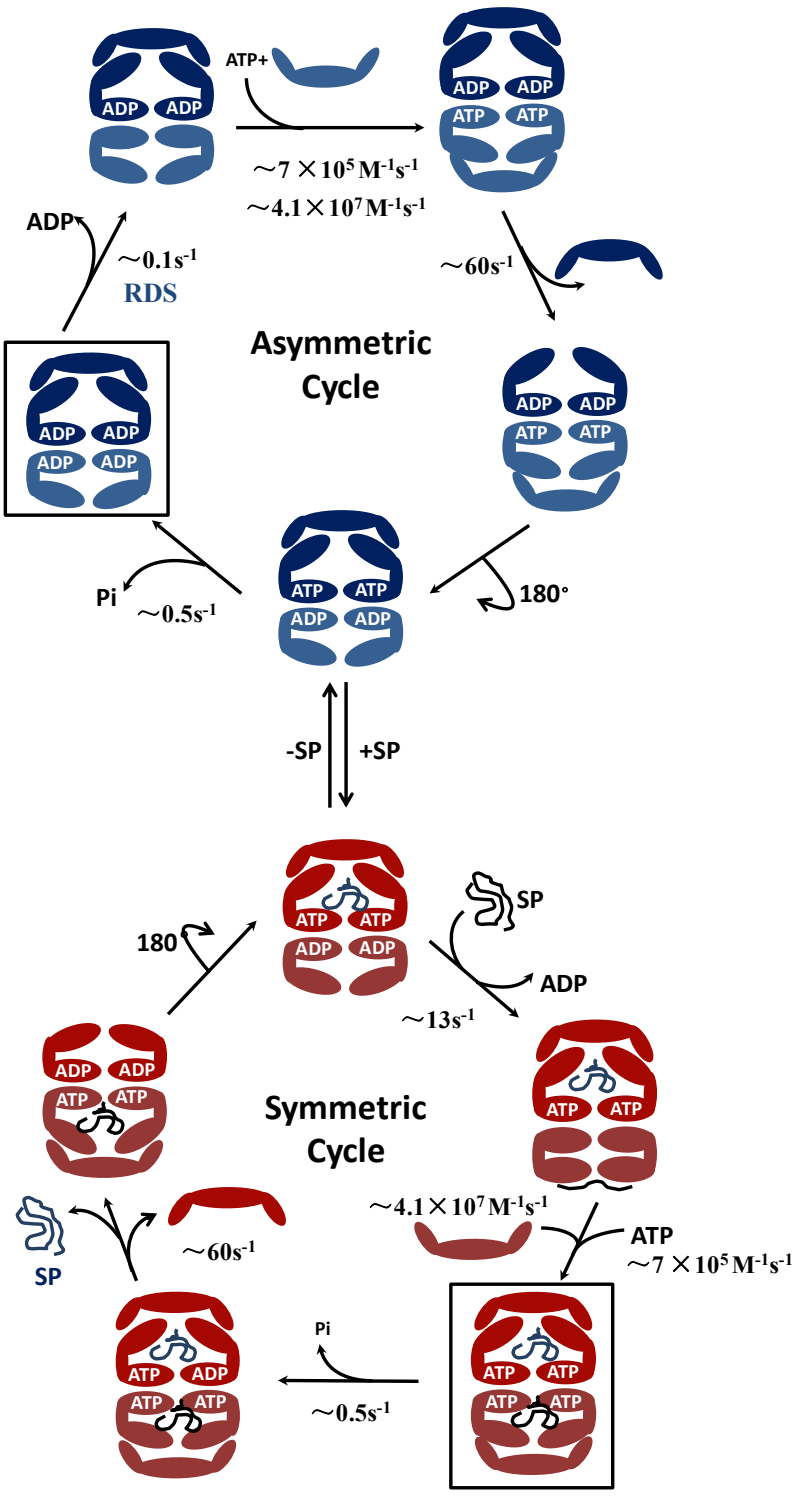

Figure 5-8: The two catalytic cycles (asymmetric and symmetric) of the GroEL-GroES nanomachine. The asymmetric cycle (blue) operates in the absence of SP; its rate-determining step (~0.1s^{-1}) is the dissociation of ADP from the nascent *trans* ring of the resting state complex. This rate is ~4-fold slower than the rate of ATP hydrolysis (~0.5 s^{-1} determined from the burst phase of Pi release). Because the rate-determining

step is preceded by the asymmetric "bullet" GroEL-$GroES_1$ complex this species predominates in solution. Symmetric "football" GroEL-$GroES_2$ complexes are formed only transiently in the asymmetric cycle. The symmetric cycle (red) operates in the presence of SP; its rate-determining step (~0.5 s^{-1}) is the hydrolysis of ATP as before. The rate of dissociation of ADP is accelerated ~100 fold in the presence of SP to a rate ~13 s^{-1}. Since the rate-determining step is preceded by the symmetric "football" GroEL-$GroES_2$ complex this species predominates in solution.

On the other hand, this resting state complex is primed for accepting SP if provided. This is evident from the series of 'SP jump' experiment shown in Figure 5-6 where the equilibrium was shifted from predominantly asymmetric complex to symmetric complex upon introduction of SP. Such remarkable transition is achieved by SP mediated nucleotide exchange, i.e., upon SP binding to the open trans-ring of asymmetric resting complex, ADP was rapidly replaced by ATP from solution which in turn brings about formation of football after two hemicycles of turning over (Figure 5-4 cartoon). Once in the symmetric cycle, the GroEL functions as a parallel machine with both rings turning over simultaneously in terms of binding and hydrolysis of ATP, recruiting GroES, and encapsulating SP. In a similar fashion of measurement (Figure 5-6B), the symmetric complex is found to be much more dynamic than the asymmetric complex, consistent with the previous observation that SP can tremendously accelerate GroEL functional cycle. In addition, this rate measured as GroES mean residence time on GroEL (half time ~1.5s) also represents the mean encapsulation time of SP inside GroEL/ES chamber [13] consistent with our understanding that GroES release is followed immediately by SP ejection from GroEL ring.

Though hitherto presented studies haven't directly dealt with the role played by GroEL in mediated SP refolding, they allow us to evaluate 'what should happen' in GroEL optimized SP refolding process consistent with the way GroEL turnover revealed

in this chapter. As reviewed in Section 1.5 of Chapter 1, there are two different views on GroEL assisted SP refolding, a passive model and an active refolding model. Currently the former is the most widely accepted mechanism of chaperonin assisted SP folding [38, 57] and it is based upon analysis of the chaperonin ATPase cycle performed mainly with a single-ring version of GroEL that doesn't turnover [102] or in the absence of SP [44]. In this scenario, the encapsulation of a single SP molecule by the chaperonin nano-machine creates a sequestered space, the so-called Anfinsen cage that is viewed as a space of infinite SP dilution in which SP folding to the native state can occur unimpeded by self-association events that would otherwise lead to aggregation. It is measured experimentally that for such in-vitro folding process to occur, it requires SP encapsulation in the cage for up to 10 to 20min depending on different SPs used. However, as clearly demonstrated in this chapter, such prolonged encapsulation simply would not occur physiologically, as the half time of SP encapsulation in the symmetric cycle is only 1.5sec.

Based on our experimental observation, the adjustments that was made by the *GroE* system in response to the presence of SP appears to be shortened duration of each hemi-cycle while the number of hemi-cycles at a given time is significantly increased with both faster turnover rate and turnover patterns (two rings simultaneously rather than alternatively). The active folding model as reviewed in Section 1.5, is often tied to the iterative annealing model which envisions GroEL as an iterative refolding machine. Via each round of SP capture, active unfolding induced by ATP binding, encapsulation, and release, the mis-folded kinetically trapped SP was brought up to the top of their folding funnel and granted another chance to reach their native conformation (Figure 1.2 Chapter

1). This model provides excellent explanation for the adjustments made by chaperonins in response to the presence of SP: binding of SP to the trans ring of the resting state complex accelerates ADP release dramatically, permitting *i)* rapid release of ADP which allows the GroEL nano-machine to turnover at its maximal rate, set by its intrinsic ATPase activity; and *ii)* the change of the RDS which alters the nature of predominant species from an inert asymmetric resting state complex to a highly dynamic symmetric complex that can accommodate refolding of two SPs simultaneously. Therefore, in this manner, GroEL is able to maximize the number of trials of refolding SP can go through and thus to achieve optimized SP refolding via its functional cycle which is ultimately driven by ATP hydrolysis.

Chapter 6: ATP hydrolysis causes the symmetric complex to break into the asymmetric complex (BoS)

6.1 Introduction

In the asymmetric cycle, GroEL turns over in a very well defined manner [12, 40]. Starting with the predominant resting state complex, the trans-ring of the complex slowly releases ADP, product of previous hemicycle of ATP hydrolysis, and makes the nucleotide binding sites available for ATP. The binding of ATP to the trans-ring brings about association with free GroES from the solution and at the same time triggers departure of cis-bound GroES and, along with it, the previously encapsulated SP if there were any. The trapped ATP in the nascent cis-ring is committed to hydrolysis and thus completes a hemicycle by returning the whole system back to the starting point, the resting state.

As demonstrated by work presented in the last chapter and elsewhere [12-13, 45-46], unlike a two-stroke motor machine in the asymmetric cycle, the two rings of GroEL in the symmetric cycle in the presence of SP function simultaneously and process SP refolding and ATP hydrolysis in a parallel manner: ATP bound to the two GroEL rings is hydrolyzed simultaneously, and release of one or the other bound GroES is rapid and indistinguishable from each other. Though the formation of such complex has been extensively explored in the last chapter, the mechanism by which the symmetric complex can turnover to allow GroEL to function as a parallel processing machine is not obvious. Since both GroEL rings of the complex are capped by GroES molecules, it might prevent ADP/ATP exchange and release of encapsulated SP, steps necessary to bring the system into the next cycle.

Finding an answer to this question is necessary but challenging. As discussed in Chapter 1 and the last chapter, it is via the GroEL functional cycle that optimized SP re-folding is achieved by chaperonins, and the manner by which GroEL turnover in its functional cycle underlies the possible mechanism that can be utilized by GroEL to mediate its SP refolding. In addition, the way the symmetric complex proceeds to the next cycle directly relates to how encapsulated SP is ejected into the solution at the end of each cycle and recaptured at the beginning of the next cycle. Based on the experimental evidence presented in the last chapter, specifically in Figure 5-5 and 5-7, turnover of the symmetric complex is realized by first reverting to the asymmetric complex, and then SP catalyzed nucleotide exchange results in release of the second GroES and exchange of the encapsulated contents. Since the breakage of the symmetric complex (Figure 5-5) and exchange of GroES (Figure 5-7) proceed with a similar rate with that of ATP hydrolysis, it is reasonable to assume that ATP hydrolysis causes the symmetric complex to break into asymmetric complex (this is a breakage of symmetry problem (BoS)). However as more experimental evidence is acquired on this matter, its complexity gradually unfolds: work presented in this chapter reveals that not just any hydrolytic event leads to GroES release but instead sufficient number of ATP has to be hydrolyzed to initiate BoS which may also be mediated by some level of inter-ring allosteric communication. The possible manner by which sufficient ATP hydrolysis leads to BoS was also explored which is rephrased as how nucleotide binding state of the two GroEL rings (represented by the expression *nATP/mATP*, in which *n* and *m* are number of ATP remains unhydrolyzed in each ring respectively, with $n,m \in [0,7]$) capable of BoS is developed that leads to asymmetry in interaction with GroES. In the next chapter, the physical and structural

basis is discussed as for the way BoS occurs described in this chapter. The discussion is based on my work on a very intriguing mutant K105A which almost entirely devoid of any negative cooperativity and of any sign of inter-ring communication.

6.2 Methods specific to Chapter 6

6.2.1 Measuring Pi release from GroEL^{D398A} as related in the previous chapter, GroEL^{D398A} hydrolyzes ATP much slower than the wild-type and a single round of ATP turnover takes up to hours to finish. Since the coumarin dye used to label PBP is vulnerable to photo-bleaching, it is clearly not suitable to monitor such slow Pi release process with PBP-MDCC as has been done for GroEL^{wt}. An alternative method was employed as a result by coupling Pi release to phosphorolysis of 2-amino-6-mercapto-7-methylpurine ribonucleoside (MESG) [88], a guanosine analog (Figure 6-1). The lysis reaction was catalyzed by bacterial purine-nucleoside phosphorylase (PNPase) and can be monitored by absorption change at 360nm, allowing the Pi release process to be easily followed by spectrophotometric method.

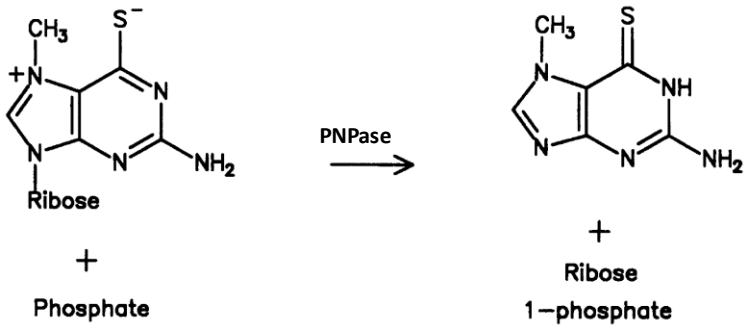

Figure 6-1: the purine-nucleoside phosphorylase (PNPase) catalyzed phosphorolysis reaction that allows Pi release to be followed by absorption change at 360nm [88].

The response factor of the process is the extinction coefficient difference between the phosphorolysis product (2-amino-6mercapto-7-methylpurine) and the reactant

(MESG) at 360nm and was determined to be 11,000 $M^{-1}cm^{-1}$ at pH=7.6, a value very close to previously reported [88]. A typical $GroEL^{D398A}$ Pi release measurement was carried out with 30μM mutant subunit under standard buffer conditions (50mM TrisOAc, pH=7.6, 10mM $Mg(OAc)_2$, 100mM KOAc) plus 200μM MESG and 1unit/ml PNPase to couple Pi release to absorptions change at 360nm. Since $GroEL^{D398A}$ hydrolyze ATP at a much slower rate than ADP release, under normal turnover conditions, no burst kinetics would be observed. Therefore, to measure its intrinsic ATPase activity, the measurement was performed under single turnover conditions by introducing an ATP depleting system (10unit Hexokinase and 10mM Glucose) after the symmetric complex was formed in the presence of GroES (45μM) and 500μM ATP. Data collection was initiated immediately after addition of Hexokinase/Glucose and the delay time is approximately 60sec which was accounted in data analysis.

6.2.2 Determination of the minimum number of ATP required to be hydrolyzed in one ring for GroES to be released as the breakage of the symmetric complex is intimately related to ATP hydrolysis, this set of experiments was intended to provide a quantitative view on how BoS occurs in the special case of *7ATP/nATP* (ATP hydrolysis only occurs in one ring while the other ring always has a full occupancy of ATP as BoS occurs).

A schematic description is shown in Figure 6-4 concerning how experiments of the kind were performed. The 'ATP bullet', i.e. the asymmetric complex of IAEDANS labeled $GroEL^{D398A}$ (50μM) was formed with a limiting amount of $GroES^{F5M}$ ($GroES_7$:$GroEL^{D398A}{}_{14}$=1) and ATP (25-30μM). Thus formed 'ATP bullet' was rapidly loaded into the stopped-flow instrument before ATP started to hydrolyze. At different

time points, the asymmetric complex was challenged with large excess of ATP and $GroES^{wt}$. If no ATP (Process 1 in Figure 6-4) or not enough ATP bound by the asymmetric complex was hydrolyzed by the time of challenge (Process 2 in Figure 6-4), stable symmetric complex would be formed with both the labeled ($GroES^{F5M}$) and unlabeled $GroES^{wt}$ on board and no FRET signal change would be observed. On the other hand, as time elapsed and enough ATP was hydrolyzed, the symmetric complex would still be formed but be very unstable and tend to revert to the asymmetric complex by releasing the GroES from the ring with less ATP (and thus more ADP) bound, in this case the bound $GroES^{F5M}$, and thus a FRET signal change occurred (Process 3 in Figure 6-4). Since ATP hydrolysis by $GroEL^{D398A}$ is found to be much slower than GroES release ($0.0006\ s^{-1}$ *VS* $60\ s^{-1}$) as presented in Section 6.3.1 of this chapter, it is justifiable to assume that during the measurement of GroES release was taken, no further ATP hydrolysis had occurred.

6.2.3 Preparation of subunit-mixed GroEL tetradecamer the subunit mixed $GroEL_{14}$ comprises both $GroEL^{wt}$ and $GroEL^{D398A}$ subunits. Experiments done with it provide critical insight into the nature of ATP hydrolysis by the symmetric complex leading to BoS. Since the GroEL oligomeric construct is extremely stable [89-90], it is difficult to find the right conditions to dissociate the GroEL oligomer into the folded monomer. Therefore, we sought to completely denature GroEL, and after mixing the two different kinds of unfolded GroEL monomer together, we refolded and reconstituted GroEL subunits into fully active tetradecameric state.

A

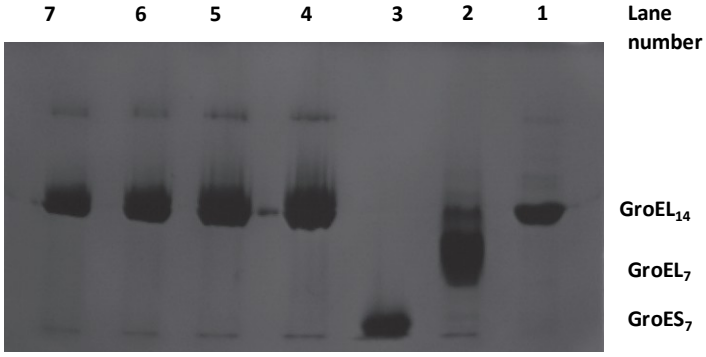
7
6
5
4
3
2
1
Lane number
GroEL14
GroEL7
GroES7

B

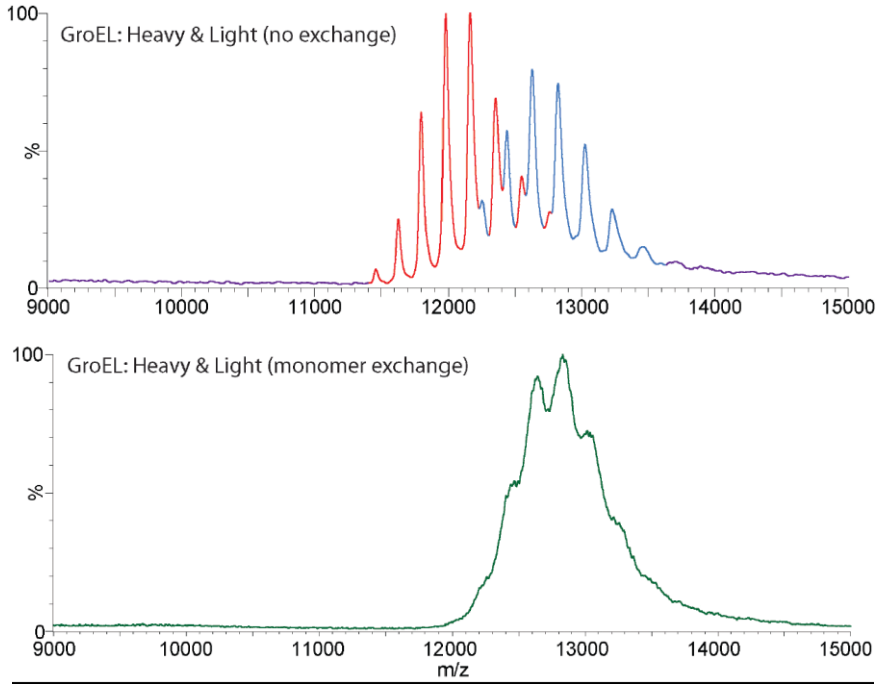
GroEL: Heavy & Light (no exchange)
100
%
0
9000
10000
11000
12000
13000
14000
15000
GroEL: Heavy & Light (monomer exchange)
100
%
0
9000
10000
11000
12000
13000
14000
15000
m/z

C

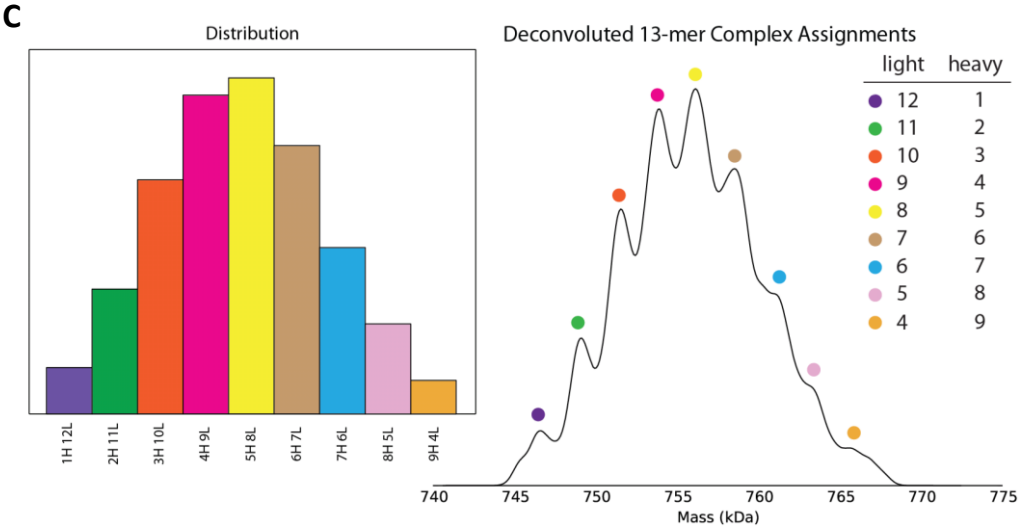
Distribution
1H 12L
2H 11L
3H 10L
4H 9L
5H 8L
6H 7L
7H 6L
8H 5L
9H 4L
Deconvoluted 13-mer Complex Assignments
light
heavy
12 1
11 2
10 3
9 4
8 5
7 6
6 7
5 8
4 9
740
745
750
755
760
765
770
775
Mass (kDa)

Figure 6-2: Characterization and validation of stochastically reconstituted mixed-subunit $GroEL_{14}$. **(A)** Characterization of reconstituted $GroEL_{14}$ from urea denatured state by 4.5% native PAGE. The lanes are identified as follows: Lane 1, $GroEL_{14}$; Lane 2, SR1 ($GroEL_7$); Lane 3, $GroES_7$; Lane 4 and 6, two independent repeats of renatured and reconstituted $GroEL_{14}$ from 6M-urea-denatured state in the presence of ATP; Lane 5 and 7, two independent repeats of renatured and reconstituted $GroEL_{14}$ from 6M-urea-denatured state in the presence of ADP. **(B)** and **(C)** Native state Mass spectrometry validation of stochastic mixing between $GroEL^{light}$ and $GroEL^{heavy}$ (purified by my colleague Nicolas Corsepius by using $N^{15}H_4Cl$ and C^{13}-Glucose containing M9 minimum media) subunit in reconstituted $GroEL_{14}$. The MS analysis and the figure is performed and generated by our collaborator Dr. Weston Struwe in Dr. Justin Benesch's lab. The upper and the lower panels in B show the m/z spectrum of 1:1 mixed light/heavy GroEL subunit with no subunit exchanged (upper panel) and urea-treated and reconstituted $GroEL_{14}$. C shows the deconvoluted $GroEL_{13}$ (one subunit knocked out in MS most likely occurs during the cleaning of the protein by removal of the adduction of salt and solvent during the ESI process [125]) mass distribution. Inset is the distribution of subunit-mixed $GroEL_{13}$ of different compositions.

The GroEL re-naturation and reconstitution protocol was adopted from a published procedure [91]. 30μM GroEL subunit of different ratios of $GroEL^{wt}$ to $GroEL^{D398A}$ were denatured in 6M urea (buffered with 50mM TrisHCl at pH 7.5) for 90min and then the solution was diluted 20 times by combining with refolding buffer consisted of 50mM TrisHCl, 5mM $MgCl_2$, 500mM NH_4Cl, 2mM DTT, and 5mM ATP or ADP. After 30min incubation at room temperature or overnight at 4^oC, the sample was concentrated by using the centricon concentrator and then washed thoroughly by using buffer of 50mM TrisHCl and 10mM $MgCl_2$ to remove ATP and residual urea. The reconstitution efficacy was checked by native PAGE (Figure 6-2A) which shows that other than a small fraction of GroEL molecules (<5%) may exist in an aggregated high molecular weight form, the majority were successfully reconstituted back to tetradecameric state. The stochasticity of subunit mixing and reconstituting into $GroEL_{14}$, though well expected based on the infinitesimal affect on GroEL conformation brought

about by the amino acid substitution D398A, was checked by high resolution native state MS performed by Dr. Weston Struwe in Dr. Justin Benesch's lab (Figure 6-2B and C).

The E315C mutant was introduced into both $GroEL^{wt}$ and $GroEL^{D398A}$ background to facilitate labeling of the reconstituted $GroEL_{14}$ with IAEDANS. Protein labeling follows the same protocol as described in Chapter 5. FRET experiments were performed to determine partition of the mixed-subunit $GroEL_{14}$ of different mixing ratio into the asymmetric and the symmetric complex upon being mixed with ATP and $GroES^{F5M}$ as described in Chapter 5.

6.2.4 Application of binomial distribution theory in solving BoS problem For the simple case of *7ATP/nATP*, the application of binomial distribution function was initially developed by my colleague Nicholas Corsepius and the readers are encouraged to read the corresponding chapter of his thesis for a stricter mathematic treatment for derivation of the following equations. Here, only a more intuition-based approach was taken instead: the probability $P(n)$ of having n ATP remained un-hydrolyzed in one asymmetric complex after on average $7-N$ Pi has been released per asymmetric complex is given in Equation 6.1:

$$P(n) = \frac{7!}{n! \cdot (7-n)!}(P(H))^n \cdot (1-P(H))^{(7-n)} \quad \text{Equation 6.1}$$

In Equation 6.1, $P(H)$ is the probability for ATP hydrolysis and equals the ensemble average fraction of ATP remaining un-hydrolyzed, i.e. $P(H) = N/7$, which intuitively makes good sense since the more ATP that remains un-hydrolyzed the more likely ATP hydrolysis is going to occur. In the time domain (N is the dependent variable of time t, $N=f(t)$), ATP hydrolysis by GroEL proceeds with a well defined exponential burst phase with a rate constant k, that is, $\frac{7-N(t)}{7} = 1 - e^{-k \cdot t}$. Plugging the expression

into Equation 6.1 results in Equation 6.2 which relates ensemble hydrolysis of ATP on time domain to the distribution of microscopic nucleotide binding state of the asymmetric complex at the corresponding time point:

$$P(n,k) = \frac{7!}{n! \cdot (7-n)!}(e^{-k \cdot t})^n \cdot (1 - e^{-k \cdot t})^{(7-n)} \quad \text{Equation 6.2}$$

If BoS occurs at hydrolysis of the lth ATP, we can express its probability $P(BoS)$, by summing up $P(n,k)$ for n taking from 0 to $7-l$ (Equation 6.3).

$$P(BoS) = \sum_{n=0}^{7-l} \frac{7!}{n! \cdot (7-n)!}(e^{-k \cdot t})^n \cdot (1 - e^{-k \cdot t})^{(7-n)} \text{ Equation 6.3}$$

By the same line of logic, binomial distribution theory can be applied to the more complex case where ATP hydrolysis occurs stochastically from both GroEL rings (*mATP/nATP*). All possible microscopic states resulted (not considering different geometric arrangements within one ring) are given in Figure 6-8. For each state, its probability $P(m,n)$ can be calculated with Equation 6.4:

$$P(m,n) = \frac{7!}{m! \cdot (7-m)!} \cdot \frac{7!}{n! \cdot (7-n)!} P(H)^{14-m-n} \cdot (1 - P(H))^{m+n} \quad \text{Equation 6.4}$$

which is just a double application of binomial distribution function to both GroEL rings since ATP hydrolysis of the two rings are independent of each other. $P(H)$ is similarly defined as in Equation 6.1. From Equation 6.4, a separate parameter, De, can be defined as the degeneracy of each microscopic state mATP/nATP (illustrated in inset of Figure 6-8):

$$De = \frac{7!}{m! \cdot (7-m)!} \cdot \frac{7!}{n! \cdot (7-n)!} \quad Equation\ 6.5$$

The combined probability of the $S \times S$ square (upper left as marked by the dashed blue line in Figure 6-8) $P(S \times S)$ is given in Equation 6.5:

$$P(S \times S) = \sum_{m=7-S}^{7} \sum_{n=7-S}^{7} P(m,n) \qquad \text{Equation 6.6}$$

And according to the 'hydrolysis number rule' (Section 6.4), $P(BoS) = 1 - P(S \times S)$.

6.3 Results

6.3.1 BoS shows a similar dependence on ATP hydrolysis for both GroELwt and GroEL^{D398A} Combining the FRET *VS* time and the Pi release *VS* time traces in Figure 5-5 results in a single trajectory of FRET *VS* Pi release (Figure 6-3A red) which reveals sigmoidal dependence of BoS on ATP hydrolysis: BoS starts after ~3 ATP have been hydrolyzed and is completed at ~12 ATP. It argues against the assumption that ATP hydrolysis within a ring is concerted [77], because if that were true, BoS would occur from the very beginning of such plot and progress linearly as all 14 ATP being hydrolyzed. As a matter of fact, such sigmoidal dependence implies that not all ATP hydrolysis leads to BoS but rather only some critical ATP hydrolysis events can lead to BoS.

In order to rule out the possibility that the sigmoidal dependence merely reflects the co-occurrence of the two events that are not a cause-and-effect relationship, we altered the time domain of our study on both BoS and ATP hydrolysis by using the ATPase deficient mutant GroEL^{D398A} which hydrolyzes ATP 1000 slower than GroEL^{wt} (Figure 6-3B). The same FRET pair (IAEDANS/F5M) was used to monitor BoS of GroEL^{D398A} symmetric complex, and hydrolysis of ATP by the mutant was followed by coupling Pi release to phosphorolysis of 2-amino-6-mercapto-7-methylpurine ribonuleosde (Figure 6-1) and measured by absorption change at 360nm (Section 6.2.1).

In both cases, the measurements were conducted under single turnover conditions by including an ATP depletion system (Hexokinase plus glucose) after the GroEL^{D398A} symmetric complex being rapidly formed. The results are shown in Figure 6-3B from which a similar FRET *VS* Pi release trajectory was generated (blue in Figure 6-3A) and overlaid with that of GroEL^{wt}. The similarity between the two is immediately apparent indicating the same fundamental process of BoS occurs despite a 1000 fold difference in time scales. It therefore provides a strong evidence for relating BoS to ATP hydrolysis of the GroEL/ES symmetric complex.

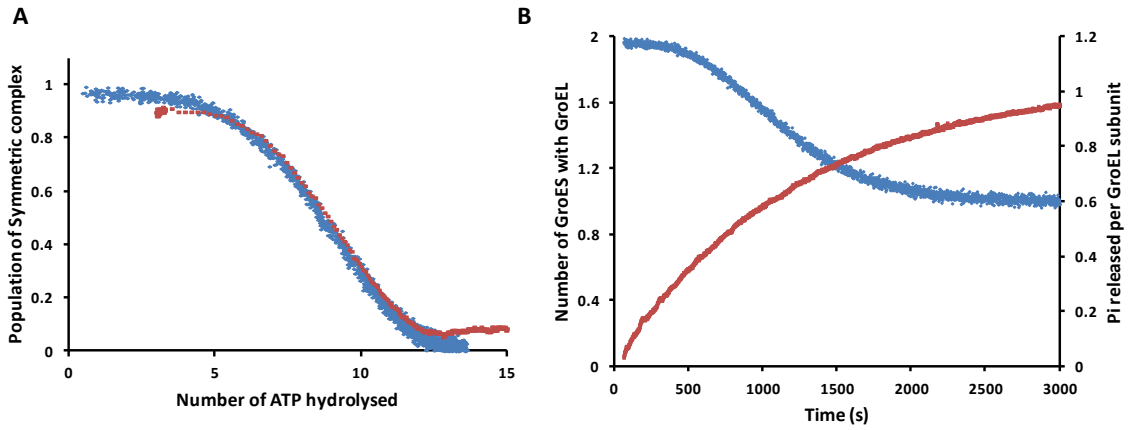

Figure 6-3: Both the GroEL^{wt} and GroEL^{D398A} symmetric complex break into the asymmetric complex (BoS) and they shows similar sigmoidal dependence on ATP hydrolysis despite 1000 times difference in their ATP hydrolysis rates. (A) The decay of the population of the symmetric GroEL:ES_2 complex was plotted against the average number of ATP that was hydrolyzed during the initial turnover for both GroEL^{wt} (red) and GroEL^{D398A} (blue). The two BoS traces were generated by plotting corresponding FRET trajectories *VS* Pi release traces. The GroEL^{wt} BoS trace was generated from kinetic traces shown in Figure 5-5 in Chapter 5, while the GroEL^{D398A} BoS trace was generated from data shown in B. **(B)** FRET measurement (blue, plotted on the left y-axis) and Pi release measurement (red, plotted on the right y-axis) conducted with pre-formed GroEL^{D398A} symmetric complex. In both cases 10 units of hexokinase plus 10mM glucose were included to deplete free ATP, and thus prevent symmetric complex from reforming. If the quenching system was omitted, very little breakage of symmetric complex was observed on this time scale [13]. All FRET measurements were conducted in a Perkin Elmer fluorometer and the reaction was initiated by manually adding 0.5mM ATP. The first data point was collected 60sec after the reaction was initiated. The Pi release measurement was conducted as described in Section 6.2.1. The Pi release trace

was fitted with a single exponential equation and the rate was found to be 0.0045min^{-1} for this measurement.

6.3.2 A minimum of 4 to 5 ATP are required to be hydrolyzed in one ring for the symmetric complex to be broken As discussed in more details in the discussion section of this chapter (and also in Figure 6-8), BoS is a complex function of the nucleotide binding state of both GroEL rings (*mATP/nATP*). We approach this complicated problem by starting with a special case to simplify the analysis with the aim that the insight we've obtained from this simpler special case may provide constraints in helping solving the problem in a more general sense.

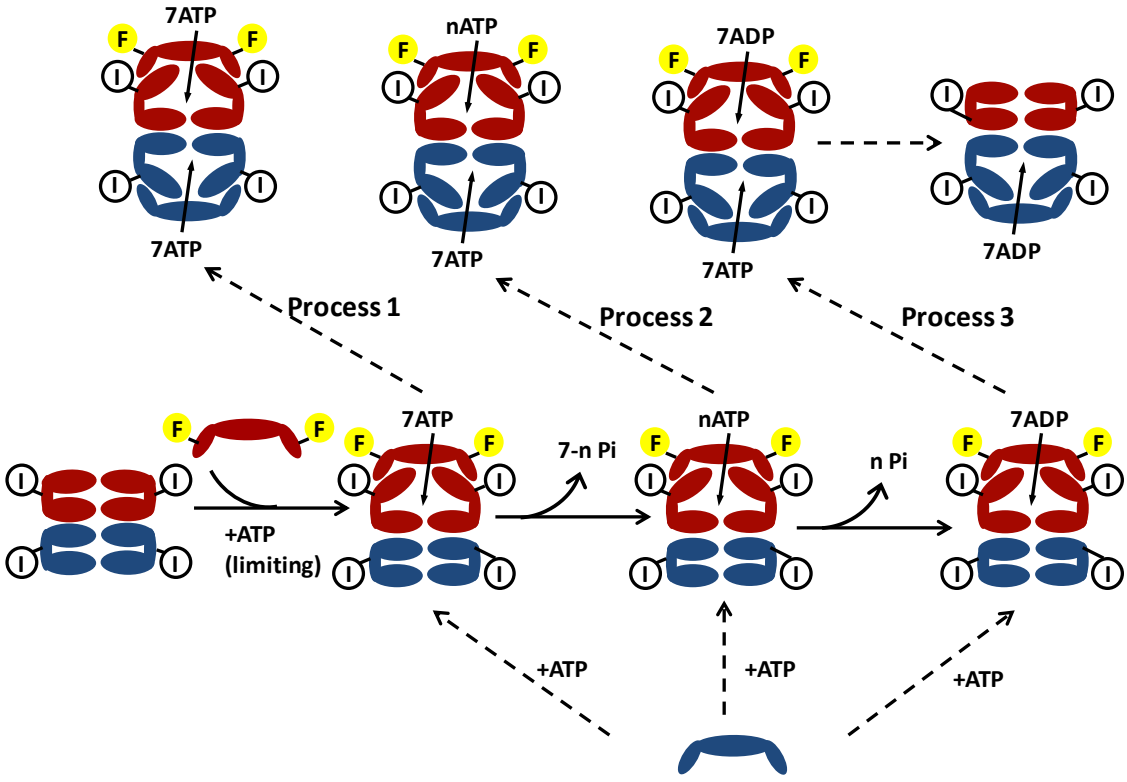

Figure 6-4: Schematic representation of how the BoS experiment was set up and performed under *7ATP/nATP* conditions. In detailed description of the experiment can be found in Section 6.2.2. 'I' and 'F' stand for IAEDANS and fluorescence-5-malieamide labeled respectively.

The special case is set up in the following way. Instead of forming symmetric complex and allowing ATP hydrolysis to occur in both rings to induce BoS, the asymmetric complex was formed by limiting the [ATP] and [GroES] applied, and as ATP hydrolysis occurs in a single ring (the red colored ring, Figure 6-4), at different time points, excess GroES and ATP were introduced to induce formation of the symmetric complex either as a relatively long living species if insufficient number of ATP has been hydrolyzed (Process 1&2, Figure 6-4), or a mere transient intermediate if enough ATP has been hydrolyzed (Process 3, Figure 6-4). The 'ATP bullet' is formed by using IAEDANS-GroEL^{D398A} and GroES^{F5M} and challenged by GroES^{wt} and ATP to allow *i)* BoS to be followed by FRET signal decrease caused by release of GroES^{F5M}, and *ii)* enough time for challenging 'ATP bullet' with excess ligands before changed of nucleotide binding state as ATP gets hydrolyzed. Therefore, for any symmetric complex that is formed, transient or not, we always deal with the situation of *7ATP/nATP*, i.e. a 'full house' of ATP in one ring (the blue colored ring in Figure 6-4) and another ring (the red colored ring in Figure 6-4) with partially hydrolyzed ATP with the number '*n*' depends on the time elapsed before challenging the 'ATP' bullet. The microscopic number *n* can be related to macroscopic averaged parameter such as Pi released/GroEL$_{14}$ at corresponding time point by applying binomial distribution theory since hydrolysis of ATP by GroEL is found to be stochastic (Section 6.3.1 & 6.3.3).

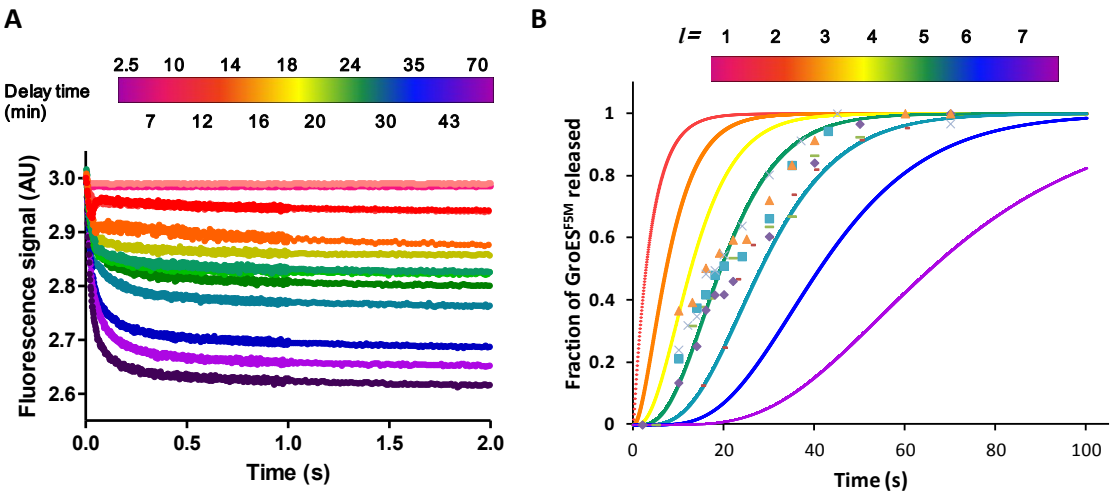

Figure 6-5: BoS under *7ATP/nATP* condition as reflected by release of GroES^{F5M} from GroEL^{D398A} ATP 'bullet' when challenged with GroES^{wt} and excess ATP. (A) FRET trajectories of release of GroES^{F5M} from GroEL^{D398A} ATP 'bullet' at different delay times indicated by the color code shown above the plot. **(B)** Results of six independent sets of measurements of the sort shown in A are plotted against corresponding delay time. The simulation was done by using Equation 6.3 with l, the number of ATP needs to be hydrolyzed for BoS to occur, taking integer values from 1 to 7. The simulated curves are shown as solid lines colored coded as indicated above the plot.

An example set of FRET kinetic trajectories is shown in Figure 6-5A. Figure 6-5B is generated from Figure 6-5A by plotting the percentage of GroES^{F5M} released efficiently at a rate close to 60s^{-1} against the time point at which the challenge was performed. As would be expected, as time goes by, more and more bound ATP get hydrolyzed, and increasing fraction of GroES^{F5M} is released rapidly indicating there are less and less stably formed symmetric complexes.

To determine the minimal number of ATP to be hydrolyzed for BoS to occur (or the largest n as in *7ATP/nATP*), time dependent BoS was simulated according to Equation 6.3 with l (the lth ATP to be hydrolyzed when BoS occurs) taking integer values from 1 to 7. The rate of ATP hydrolysis by the GroEL^{D398A} asymmetric complex k was determined to be 0.036±0.008min^{-1} (three independent measurements) in a similar

way as in Figure 6-3B. The set of simulated BoS curves are shown as solid lines in Figure 5B. It appears the majority of experimental data points distribute between l =4 and 5, or $n \leq 3$ or 2 of *7ATP/nATP* in order for BoS to occur.

6.3.3 BoS studied with subunit-mixed GroEL$_{14}$ To study BoS that occurs under conditions other than *7ATP/nATP*, I prepared a series of subunit mixed GroEL$_{14}$ with different wild-type to D398A ratios (Section 6.2.3). Stochastic mixing between the two different kinds of subunits is checked by both TMR dimer experiments (Figure 2B) and high resolution native state MS (Figure 6-2B). Due to the 1000 fold difference in ATP hydrolysis rate between the wild-type and the mutant subunit, there is a very long time window during which only ATP bound to the wild-type subunit is hydrolyzed to ADP, while ATP to D398A subunit remains unhydrolyzed. Consequently, stochastic mixing of the two kinds of subunits in subunit-mixed GroEL$_{14}$ results in stochastic distribution of unhydrolyzed ATP (bound to mutant subunit) during this long time window. Varying the macroscopic ratio of wild-type/D398A subunit in preparing the mixed GroEL$_{14}$ allows sampling different distributions of nucleotide binding state (*mATP/nATP*). Since subunit mixing is stochastic, the distribution of microscopic *mATP/nATP* can again be related to the macroscopic wild-type/D398A subunit ratio. On the other hand, BoS of mixed subunit GroEL$_{14}$ of different compositions is reflected by the population of the asymmetric complex formed at the beginning of the long window period which is in turn measured by FRET based experiments described in Section 6.2.3.

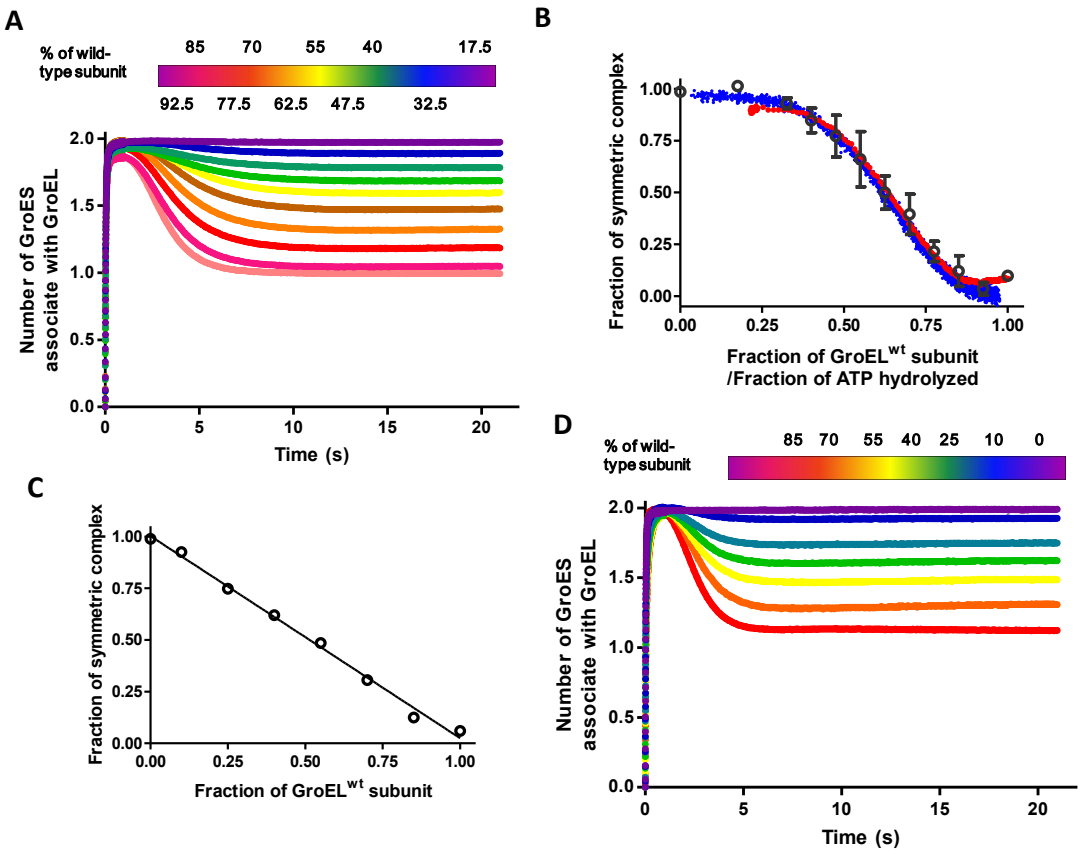

Figure 6-6: BoS of subunit-mixed GroEL$_{14}$ (A and B) or GroEL^{wt} and GroEL^{D398A} mixed on tetradecamer level (C and D) followed by FRET. **(A)** FRET trajectories of subunit-mixed GroEL$_{14}$ with varying fractions of GroEL^{wt} subunit. The traces were generated by mixing IADEANS-labeled subunit-mixed GroEL$_{14}$ with GroES^{F5M} and 0.5mM ATP in stopped-flow device in a similar fashion as those shown in Figure 5-5 and 5-6 of Chapter 5. The fractions of GroEL^{wt} of these traces are identified by the color code shown above the data plot. **(B)** The result of BoS of subunit-mixed GroEL$_{14}$ (black open circles) were overlaid with BoS trajectories of both GroEL^{wt} (red) and GroEL^{D398A} (blue) on the time domain, the latter two were taken from Figure 6-3A. Error bars represent standard deviations generated from three independent repetitions. **(C)** The results of BoS of tetradecamer mixed GroEL^{wt} and GroEL^{D398A}. The plot shows a linear dependence (R^2=0.9945) on the fraction of GroEL^{wt} present, a trend quite different from that of the subunit-mixed shown in B. The raw FRET data are shown in D. **(D)** The FRET experiments were performed in a very similar way as in A except that the mixed GroEL^{wt} and GroEL^{D398A} were not subjected to urea treatment so they are mixed as intact separated tetradecamers rather than subunits. The traces of different fractions of GroEL$^{wt}_{14}$ are identified as the color code shown above the plot.

An example plot of one such FRET measurement is shown in Figure 6-6A. The steady-state level of each trace was converted to the population of the symmetric

complex and plotted against the composition of mixed $GroEL_{14}$ (Figure 6-6B). Much to our delight and expectation, it overlaps with the FRET *VS* Pi release trajectory almost perfectly. The observation indicates that hydrolysis of ATP by a homogeneous $GroEL_{14}$ ($GroEL^{wt}$ or $GroEL^{D398A}$) as time elapses (the FRET VS Pi release trace) can be well represented by hydrolysis of ATP by spatially stochastically mixed subunits. And thus we take it as the most important evidence to support the stochastic ATP hydrolysis model by GroEL (Figure 6-8).

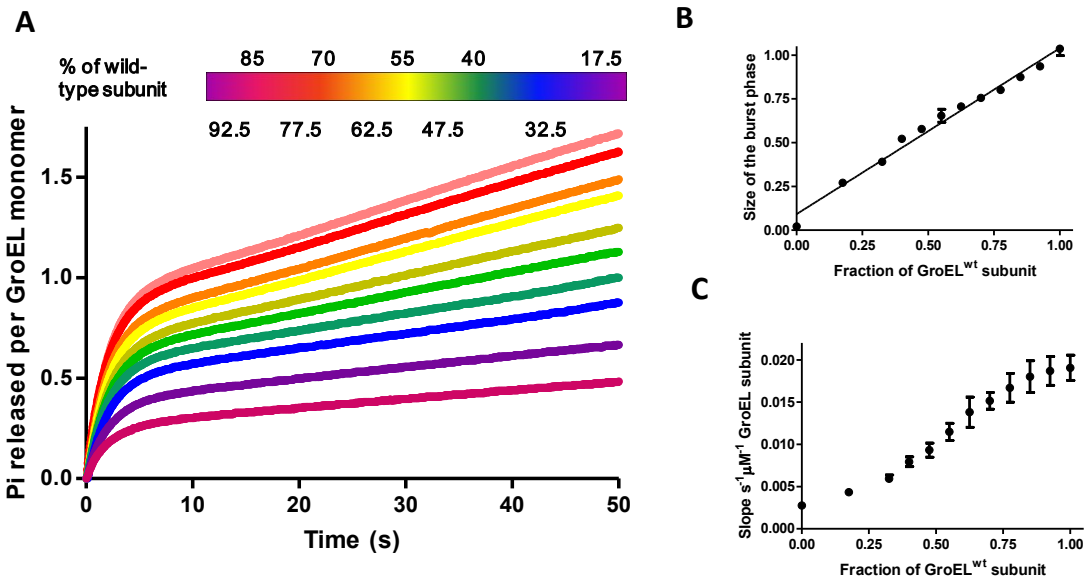

Figure 6-7: Pi release measurements performed with subunit-mixed $GroEL_{14}$. (A) The measurements were conducted with unlabeled protein sample in the same way as described in Chapter 3 with PBP-MDCC. The fraction of $GroEL^{wt}$ subunit of each trace is identified as the color code shown above the plot. **(B)** Plot the size of the burst phase against fraction of $GroEL^{wt}$ subunit. The former shows a linear dependence on the latter (slope=0.95±0.04, R^2=0.9856). **(C)** Plot the linear steady-state rate against fraction of $GroEL^{wt}$ subunit. The plot now shows a sigmoidal dependence. In both B and C, the error bars are standard deviations calculated from results of three independent repetitions of Pi release measurements of the sort shown in A.

Measurements of pre-steady state ATP hydrolysis by the mixed $GroEL_{14}$ was also performed (Figure 6-7). From this set of measurements we've learned that on one hand, the normal intrinsic ATPase activity of $GroEL^{wt}$ subunit is not affected by the ATPase

deficient mutant present side-by-side in the same ring because the kinetics of the burst phase of all mixed $GroEL^{14}$ tested appear unaltered (Figure 6-7A). On the other hand, the size of the Pi release burst is linearly proportional to the fraction of $GroEL^{wt}$ subunit (Figure 6-7B) for obvious reason (hydrolysis of ATP bound by $GroEL^{D398A}$ subunit would occur much later. However, we do notice even for our '100%' $GroEL^{D398A}$ sample the burst size of ATP hydrolysis and the linear steady-state are not zero. We've also seen similar phenomenon when ADP release from $GroEL^{D398A}$ asymmetric complex was followed (Figure 4-3 of Chapter 4). We therefore attribute such low level of wild-type like ATPase activity to a small fraction of endogenous $GroEL^{wt}$ subunit expressed from the chromosome copy of the *GroE* gene. Different from the linear dependence of Pi burst size, the slope of the linear phase of Pi release trajectories are sigmoidally correlated with the fraction of $GroEL^{wt}$ subunit (Figure 6-7C), indicating a complex dependence on both the fraction of $GroEL^{wt}$ subunit and the population of asymmetric complex that is capable of turning over (it intersects with y-axis above zero which may be also due to the trace amount of $GroEL^{wt}$ present in $GroEL^{D398A}$ sample). Last but not least, a set of control experiments was also performed (Figure 6-6D) which demonstrates that if $GroEL^{wt}$ and $GroEL^{D398A}$ are mixed only at the tetradecamer level, the dependence of the symmetric complex is linearly correlated with the fraction of $GroEL^{wt}$ (Figure 6-6C) rather than sigmoidal as in the case of mixing at subunit level.

6.4 Discussion

From the experimental evidence presented here, we've learned that ATP hydrolysis by GroEL is stochastic from individual subunit of both rings and the stochastic hydrolysis gives rise to BoS. In a special case, when one ring is fully occupied by ATP,

only 4 or 5 ATP needs to be hydrolyzed from the other ring for GroES to depart and BoS to occur. But in real life, ATP hydrolysis occurs in both rings at the same time. The set of experiments done with subunit mixed $GroEL_{14}$ containing both wild-type and D398A subunits allows us to convert hydrolysis of ATP from the time domain (Figure 6-3) to the space domain (Figure 6-6). And the good agreement between the two not only unambiguously demonstrates the stochasticity of ATP hydrolysis but also provide a wealth of information regarding how stochastic hydrolysis of ATP between the two GroEL rings leads to BoS. The question is: how can we extract the useful information in helping solve the BoS problem.

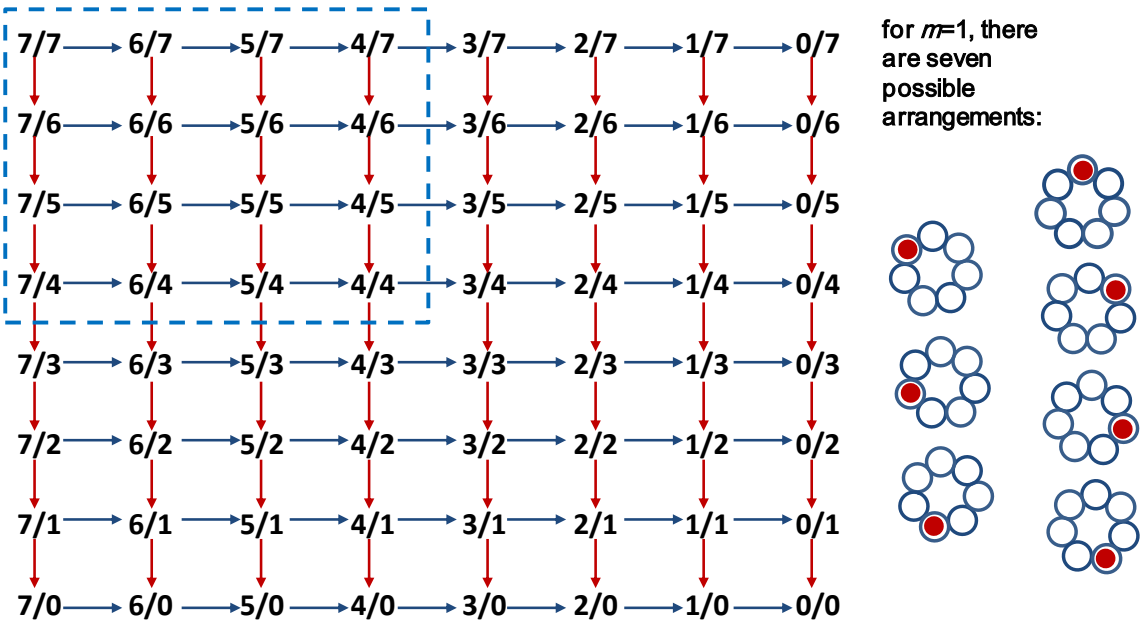

Figure 6-8: the nucleotide binding states (*mATP/nATP*) as a result of stochastic hydrolysis of ATP of the two rings. The two numbers of the like, *m/n*, are the number of ATP remains unhydrolyzed on each GroEL ring. Blue horizontal arrows represent a single hydrolysis event on one ring, and red vertical arrows represent hydrolysis on the other ring. It therefore forms an 8×8 matrix of stochastic ATP hydrolysis. Each element of the matrix represents a microscopic nucleotide binding state with degeneracy calculated by Equation 6.5 as a result of different space arrangement of unhydrolyzed ATP (inset). Different ways of grouping these states into the BoS competent and

incompetent make different rules describing how BoS occurs. The square marked by the blue dashed lines shows one simple way based on the hydrolysis number rule.

The complexity of dealing with stochastic ATP hydrolysis from all fourteen subunit from both GroEL rings, as illustrated in Figure 6-8, makes it less straightforward in application of binomial distribution theory as in the special case of *7ATP/nATP*. Especially the difficulty lies in finding out a set of rules for classification of the microscopic nucleotide binding state of $GroEL_{14}$ *mATP/nATP* into groups corresponding to BoS competent (BoS occurs much faster than additional ATP hydrolysis), BoS incompetent (additional ATP hydrolysis occurs much faster than BoS), and BoS partially competent (BoS and ATP hydrolysis occurs at a comparable rate). To simplify the problem, the third group can be omitted given the fact that despite a 1000 times difference in ATP hydrolysis rate, BoS trajectories of both $GroEL^{wt}$ and $GroEL^{D398A}$ almost entirely overlap with one another (Figure 6-3A). It means that either the third case doesn't exist at all or doesn't account to a measurable extent. The rationales for the latter are provided by the following simple calculations. Assuming all the free energy gain (~27.3kJ/mol Pi [92]) due to loss of favorable interaction formed between γ-phosphate and GroEL nucleotide binding pocket is committed to BoS, according to Eyring's equation [93], the rate acceleration of BoS by one ATP hydrolysis event can be calculated as $k_1/k_2=exp(\Delta G/RT)=4700$ fold at 37°C. Therefore, hydrolysis of ATP makes such a huge difference that we can take BoS as an all-or-none event switched on by a single critical ATP hydrolysis event.

To approach this slightly simplified complex problem, we can start with making simple rules regarding how to group each individual *mATP/nATP* into the BoS competent and incompetent, and test if such a rule can well describe the experimental results. One

such simple rule is that as long as one ring hydrolyzes sufficient a number of ATP (S), its bound GroES departs and BoS occurs ('hydrolysis number rule'). According to such a rule, the matrix shown in Figure 6-8 can be divided into two parts: all states within the left upper square with dimension of $S \times S$ (one example square with S=4 is marked by the dashed blue line in Figure 6-8) are BoS incompetent and the rest to the right and below are competent. By plugging value of $P(H)$ (the ensemble fraction of ATP remains unhydrolyzed) into Equation 6.6, BoS can be simulated with S taking integer values between 1 to 6 (solid lines in Figure 6-9A).

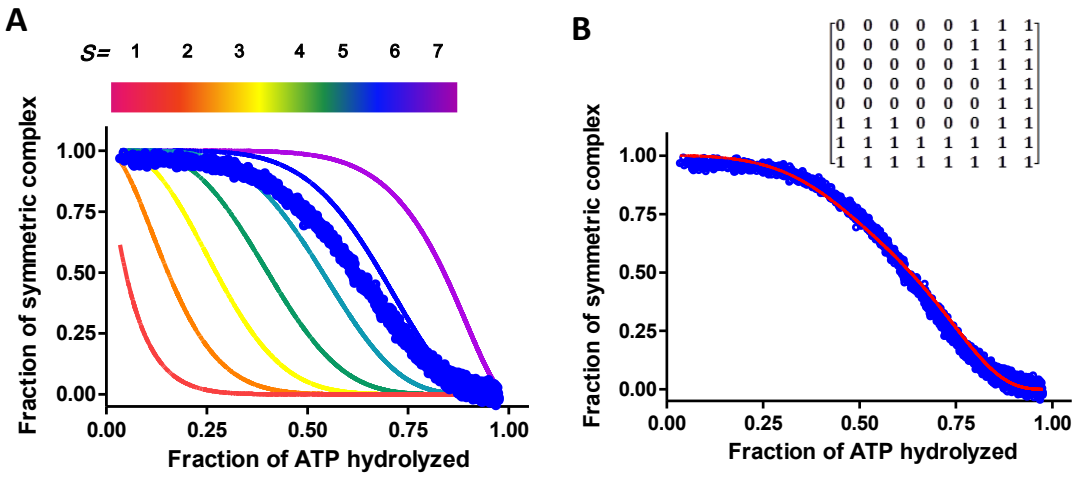

Figure 6-9: Simulation results based on the 'hydrolysis number rule' (A) and the 'difference adjusted rule' (B). In both cases, the experimentally obtained BoS of GroEL^{D398A} on the time domain is also shown (blue). **(A)** The simulated curves were generated by applying Equation 6.6 with S taking integer values between 1 and 7. The color code is shown above the plot. **(B)** Simulation (red) done with Equation 6.8 with optimized $\boldsymbol{P_{BOS}}$ shown in the inset.

Not surprisingly the majority of the experimental data points falls between the curve S=4 and S=5, indicating at least four or five ATP are needed to be hydrolyzed per ring for BoS to occur, a similar conclusion was reached in the special case of *7ATP/nATP*. However, none of the simulated curves track the experimental data very

well, and this is probably due to the oversimplified assumption made by the simple 'hydrolysis number rule'. Instead of taking the shape of an $S\times S$ square, the collective of BoS incompetent states may appear in a different way.

A more sophisticated way for grouping individual *mATP/nATP* state into the BoS competent or the BoS incompetent can be designed on top of the 'hydrolysis number rule': for BoS to occur, the number of ATP bound to the opposite ring should also be considered. The larger the difference between *m* and *n*, the more likely GroES is to be discharged from the ring with smaller number of ATP which we termed the 'difference adjusted number rule'. A matrix idea of solving the problem was developed by my colleague Nicolas Corsepius [68] and is briefly rephrased here as follows: the 8×8 matrix $\boldsymbol{BoSM}$ was introduced as the BoS matrix. Each individual element of the matrix, $BoSM(i,j)$, is the product of the probability of the corresponding *mATP/nATP* state $P(m,n)$ (Equation 6.4) and the probability for BoS to occur at this particular nucleotide binding state $P_{BOS}(i,j)$. Because BoS either occur or doesn't occur, the value of $P_{BOS}(i,j)$ can only takes 1 (occur) or 0 (not occur). *m* and *n* of *mATP/nATP* are related to matrix index *i* and *j* by $i,j = 8-m,n$, so that $BoSM(i,j)$ can be expressed as follows:

$$BoSM(i,j) = P'(8-i,8-j)\cdot P_{BOS}(i,j) \quad \text{Equation 6.8}$$

in which $P'(8-i,8-j) = P_{adjust}(i,j)\cdot P(8-i,8-j)$ represents the hydrolysis path adjusted probability of the *(8-i)ATP/(8-j)ATP* state (Figure 6-10). The parameter for adjustment $P_{adjust}(i,j)$, otherwise equals 1, can be calculated according to Equation 6.9 for the microscopic states marked in Figure 6-10 in the black dashed lined rectangle.

$$P_{adjust}(i,j) = \frac{\left(1-P_{BOS}(i-1,j)\right)\cdot P'^{(9-i,8-j)} + \left(1-P_{BOS}(i,j-1)\right)\cdot P'(8-i,9-j)}{P(9-i,8-j)+P'(8-i,9-j)}$$

Equation 6.9

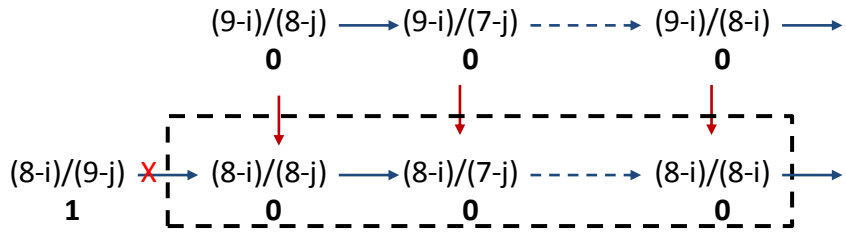

Figure 6-10: A portion of the nucleotide binding state matrix taken from Figure 6-8. For a given microscopic state *(8-i)ATP/(8-j)ATP* shown in the figure (i and j are the corresponding index of BoSM matrix), its probability for been populated can no longer be simply described by the binomial distribution probability (P(8-i,8-j), Equation 6.4) if one of the two up-stream microscopic state is BoS competent [(8-i) /(9-j), its $P_{BOS}=1$] while itself is BoS incompetent ($P_{BOS}=0$). This is simply because the path leading from the BoS competent state to BoS incompetent state is closed: after the symmetric complex breaks it cannot be reformed by additional hydrolysis of ATP. Therefore, the probability for populating all the downstream microscopic states incompetent of BoS (in black dashed line rectangle) needs to be adjusted by the parameter P_{adjust} calculate with Equation 6.9 to eliminate the contribution to the downstream BoS incompetent states from the upstream BoS competent state.

The sum of all the elements of the matrix $\boldsymbol{BoSM}$, $\sum\sum BoSM(i,j)$ at a given $P(H)$ value (related to the ensemble fraction of ATP not hydrolyzed) is the probability of BoS across all microscopic nucleotide binding states and it therefore can be fitted to the experimental data to obtain the optimized arrangement of BoS competent and incompetent *mATP/nATP* states in the form of matrix $\boldsymbol{P_{BOS}}$ in which $P_{BOS}(i,j)$ only takes integer values of 0 or 1, and $P_{BOS}(i,j) = P_{BOS}(j,i)$ since the two GroEL rings are indistinguishable, and $i,j \in [1,8]$ (Figure 9B inset).

The resulted optimized $\boldsymbol{P_{BOS}}$ fits the experimental data much better than the simple 'Hydrolysis number rule' (Figure 6-9B red solid line), and we believe the optimized $\boldsymbol{P_{BOS}}$ shown in Figure 9B inset is the best description of BoS in light of available experimental evidence. Then, the next question to ask is what we can learn from

the optimized $\boldsymbol{P_{BOS}}$ about BoS, in particular, why such way of ATP hydrolysis, i.e. sufficient number of ATP hydrolysis and difference between the rings, can lead to BoS.

From the last three lines/rows of $\boldsymbol{P_{BOS}}$ where the number '1' dominants, it appears that the total number of ATP hydrolyzed per ring is the major factor and the difference in number of ATP remain unhydrolyzed between the two rings ($|m\text{-}n|$ in *mATP/nATP*) is minor in inducing BoS: BoS mainly occurs after five ATP in one ring have been hydrolyzed but exceptions do exist including 4ATP/2ATP, 3ATP/2ATP, 2ATP/2ATP, 2ATP/3ATP, and 2ATP/4ATP where $|m\text{-}n|\leq 2$. On the other hand, BoS will occur under any conditions if more than six ATP have been hydrolyzed in one ring (the last two rows/columns of $\boldsymbol{P_{BOS}}$).

The differential roles played by these two factors in inducing BoS may reflect the fact that ATP hydrolysis affects the stability of the symmetric complex from at least two aspects: on one hand, hydrolysis of ATP destabilize the symmetric complex by weakening the interaction between GroEL and GroES that is rather independent of the opposite ring; on the other hand, ATP hydrolysis can also induce changes in the inter-ring interface that destabilize the whole symmetric complex via certain inter-ring allostery effect which may be dependent on changes occurring in the opposite ring. In the next chapter, I present experimental work with a GroEL mutant K105A that is almost entirely devoid of BoS. Study on this mutant greatly improves our understanding of the structural basis of the occurrence of BoS as well as other inter-ring communication related phenomenon which can be largely explained by the destabilization of the symmetric complex caused by stochastic ATP hydrolysis (Figure 7-7).

Chapter 7: Inter-ring allostery is the structural basis for BoS to occur

7.1 Introduction

Inter-ring allosteric signal transduction is arguably indispensible for the normal function of the *GroE* system. The two-ringed arrangement of this molecular machine is absolutely essential for its normal function as reflected by studies conducted with a single-ring mutant of GroEL, SR1, which cannot hydrolyze ATP in steady state in the presence of its cochaperonin GroES [39] and cannot support growth of *E. coli* cells under heat-shocked conditions [94].

At least three aspects of the chaperonin function reflect such allostery: *i)* the negative cooperativity in terms of steady-state ATP hydrolysis [22, 95], *ii)* discharge of GroES from the *cis* ring of the acceptor state complex ([$GroEL_7$-$(ADP)_7$-$GroES_7$]-[$GroEL_7$]) upon being challenged by ATP [55-56], and *iii)* breakage of symmetry (BoS) described in the last chapter. The negative cooperativity, as described in detail in Section 1.3 of Chapter 1, has long been speculated to be caused by inter-ring allosteric communication since either disrupting the two ring structure in the case of SR1 [39] or completely rearranging the inter-ring interface [34] result in lost of this unique property. Both the discharge of GroES and BoS actually refer to the same phenomenon with the former being a special case of the latter as pointed out in Section 6.3.2 of Chapter 6. As pointed out in the last chapter, stochastic hydrolysis of ATP leads to discharge of GroES from the GroEL ring with less ATP bound, and both the number of ATP being hydrolyzed and the difference in terms of number of ATP between the two rings matter

for BoS to occur. It therefore appears that the two GroEL rings can communicate and are aware of the nucleotide binding state (ATP/ADP) of each other.

Allosteric signal transduction is frequently found to be associated with change of contact between structural elements [96-101]. There are two sets of contacts between the two GroEL rings as each subunit interfaces with two other subunits in the opposing ring. The 'right side' contact comprises an important salt-bridge between E461 and R452 [14], and all the four mutations that create SR1 (R452E, E461A, S463A and V464A) are found on this side of contact between rings [102]. It is therefore, believed that the 'right side' contact is mainly responsible for holding the two GroEL rings together. The 'left side' contact, on the other hand, involves a structural element that directly connects the ATP binding sites of opposing GroEL subunits across the ring. Helix D has long been speculated as playing the critical role in inter-ring communication [34, 100] with its N-terminal residues such as G88 (involving the main chain amide proton) forming electrostatic interaction with the γ-phosphate of ATP and its C-terminus comes head-to-head with its counterpart across the ring. The nature of the contacting point is however, of much debate. Some suggests it being the ionic interaction between E434 and K105 of the opposite ring [103] while another study claims it should be the *Van der waals* interaction between the two A109s across the ring [34, 123]. The distance between E434 and K105A of the opposite ring is too far away (>9Å) to be considered as a salt-bridge [104-105], while a single *Van der waals* interaction such as the one formed between A109s is too weak to account for the dramatic effects of inter-ring allostery.

The structural basis for the inter-ring communication of GroEL has only became clear in light of recent progress of structural characterization of the GroEL:ES_2 football

complex [16]. A new type of inter-ring contact was proposed: the positively charged K105 form electrostatic interaction across the ring with the C-terminus of Helix D which is negatively charged due to the helix dipole. In the football complex, both sets of such interaction were found to be broken, while in the bullet complex, one set was reformed between K105 of the *cis* ring and C-terminus of Helix D of the *trans* ring. Based on these changes, a model was proposed to account for the inter-ring communication in response to ATP binding and hydrolysis: as the football complex formed in the presence of ATP and GroES, the N terminus of helix D (G88) of both GroEL rings form favorable electrostatic interactions with the ATP γ-phosphate, and such interaction draws the two Helices D apart from one another. ATP hydrolysis and release of Pi breaks the interaction involving ATP γ-phosphate. As a result, a potential is built for driving the Helix D back to its original position to reform the salt bridge between its C-terminus and K105 across the ring. As more ATP is hydrolyzed and enough potential is accumulated in one ring, Helix D of all the subunits of this ring move closer to the their counterpart on the opposite ring, which in turn triggers the departure of GroES bound to the same ring.

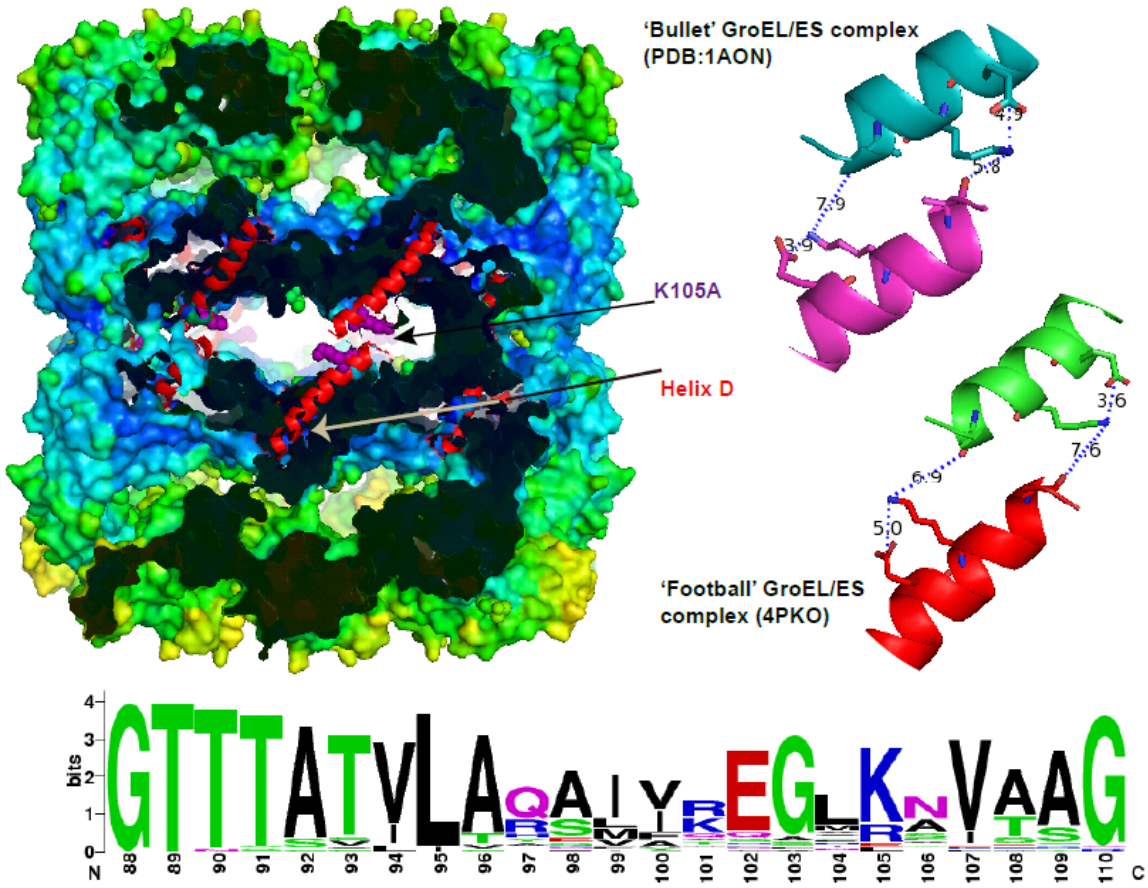

Figure 7-1: Position of Helix D and K105 in the inter-ring interface. Left, the apo-GroEL structure is sliced to show the position of Helix D (red) and K105 (magenta). Right, the relative position between K105 in one ring and the carbonyl of A109 of the opposite ring in both the asymmetric complex (upper right) and the symmetric complex (lower right). Bottom, amino acid sequence alignment result of Helix D across 40 different organisms selected by [106]. The sequence alignment is created by the online program weblog (http://weblogo.berkeley.edu/logo.cgi).

To put such model in direct test, I substitute lysine at 105 with alanine to disrupt the electrostatic interactions between K105 and the C-terminus of Helix D. I examined the mutant K105A. Not only its negative cooperativity of ATP hydrolysis was almost entirely eliminated but also its BoS happens at a rate at least 1000 fold slower than that of GroEL^{wt} football complex. In addition, I measured the formation of K105A football under equilibrium conditions in the presence of ADP, and by comparing the obtained free energy change with that of GroEL^{wt} football formation I calculated the change of free

energy ($\Delta\Delta G$) brought about by this amino acid substitution to be ~75kJ/mol corresponding to ~10.6 kJ/mol per such electrostatic interaction, a number in good agreement with those from literature characteristic of electrostatic interactions [104].

7.2 Method specific to Chapter 7

GroELK105A mutant was created by site directed mutagenesis as described in [39]. The same mutation was also introduced to the GroELE315C background to allow protein labeling for FRET measurements. The steady-state ATPase activity assay and pre-steady state FRET measurements were conducted in the same way as described in previous chapters.

7.3 Results

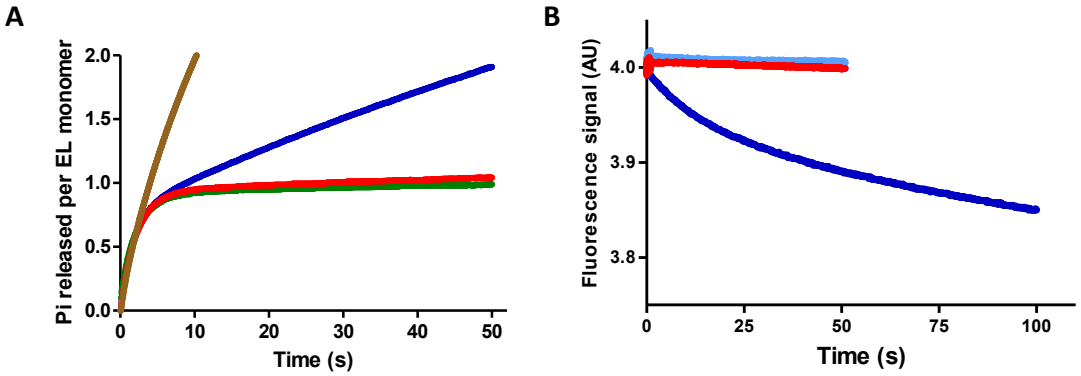

Figure 7-2: Pre-steady state study of ATP hydrolysis (A) and release of GroES (B) by GroEL^{K105A}. (A) The K105A mutation doesn't interfere with the GroEL intrinsic ATPase activity shown by the Pi release measurements. All the pre-steady state measurements were initiated by mixing 1μM GroEL subunit with 0.5mM ATP and other ingredient if specified. The Pi release trajectories are identified as: brown, GroEL^{K105A} only; blue, GroEL^{K105A} plus GroES; green, GroEL^{K105A} plus GroES and BeF_3; red, GroEL^{wt} plus GroES and BeF_3. **(B)** GroES^{F5M} can be displaced from preformed GroEL^{K105A}/ES^{F5M} complex in the presence of 1mM ADP by mixing in large molar excess of GroES^{wt} (blue) but cannot be displace from GroEL^{wt}/ES^{F5M} complex (red), nor from GroEL^{K105A}/ES complex if BeF_3 was also included (light blue).

7.3.1 BoS of GroELK105A football does not readily occur despite ATP hydrolysis As suggested by the crystal structure [14, 16], K105 is involved in a critical

contacting point connecting ATP binding sites across the ring. Consistent with the above notion, we've found that despite unaltered intrinsic ATPase activity (Figure 7-2A) and positive cooperativity of steady-state ATP hydrolysis (Figure 7-3B blue), substituting the lysine with alanine results in lost of negative cooperativity from GroEL steady-state ATP hydrolysis profile (Figure 7-3A blue) and the dramatically increased steady-state symmetric complex population in the absence of SP (Figure 7-4A blue). Under the same conditions, the wild-type football, formed by mixing apo-GroEL with GroES and ATP, readily convert to bullet complex as bound ATP hydrolyzed to ADP (Figure 7-4A purple).

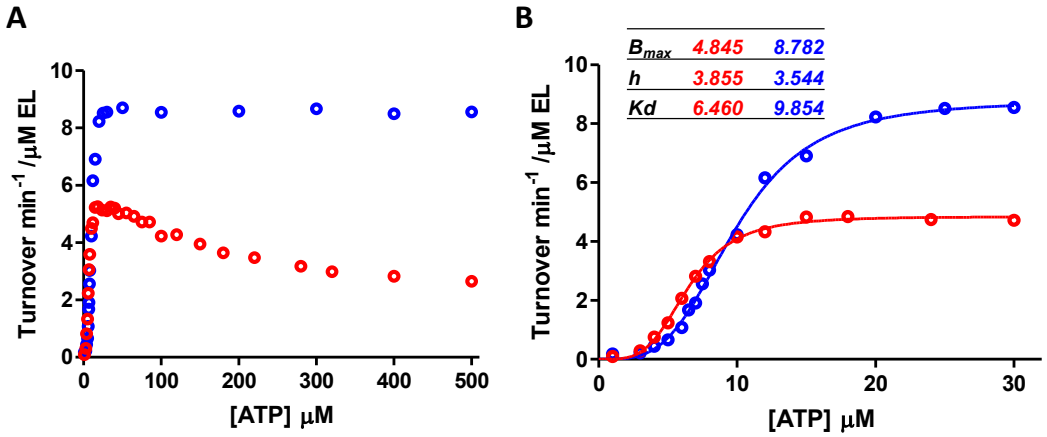

Figure 7-3: Comparison between GroEL^{wt} (red) and GroEL^{K105A} (blue) steady-state ATP hydrolysis. Release of Pi was measured by using PBP-MDCC as described in Chapter 3 at 10mM [K^+]. **(A)** The turnover of ATP by GroEL^{K105A} is much faster than that of GroEL^{wt} at saturating [ATP] and lacks the characteristic negative cooperativity. **(B)** Zooming into the range of lower [ATP], both GroEL^{wt} and GroEL^{K105A} show a similar level of positive cooperativity. The continuous lines are generated by fitting the steady-state data up to 30μM ATP with Hill equation: $y=B_{max}*[ATP]^h/([ATP]^h+K_d^h)$, in which h is Hill coefficient, K_d is dissociation constant of ADP, and B_{max} represents ATPase turnover number at the plateau . The fitting results are shown in the inset.

The much higher steady-state football population of K105A is not caused by accelerated ADP release due to the mutation but by impaired inter-ring communication as demonstrated in Figure 7-4B. In the case of GroEL^{wt}, in the absence of SP, the rate of

GroES^{F5M} dissociation from GroEL^{IAEDANS} by large molar excess of GroES^{wt} is limited by the slow spontaneous release of ADP (the same conclusion can also be drawn from Figure 5-7 of Chapter 5), the rate determining step (RDS) of the bullet cycle (Figure 7-4B pink); while in the presence of SP, chasing off GroES^{F5M} is limited by ATP hydrolysis due to the tremendously accelerated ADP release caused by SP binding to GroEL (Figure 7-4B red) which results in a shift of RDS to ATP hydrolysis. Since ATP hydrolysis is ~5 times faster than spontaneous ADP release, turning over of the *GroE* system, reflected by the rate of GroES^{F5M} 'wash-off', is much accelerated by the presence of SP. On the other hand, GroEL^{K105A} displays a much slower GroES wash-off rate irrespective of the presence of SP (Figure 7-4B blue and light blue, both ~0.02s^{-1}). As we learn from Figure 7-4A, the symmetric football is the predominant species under such condition. Therefore, it leads us to believe that the K105A mutation affects not the rate of ADP release but the actual breakage of football complex which results in the tremendously enhanced football population observed at steady state.

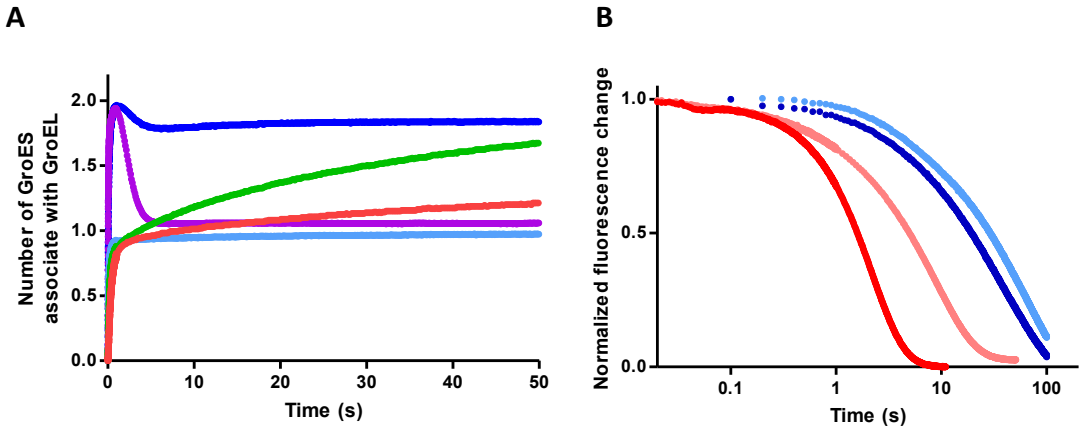

Figure 7-4: GroEL^{K105A} shows a high level of steady-state football population due to impaired inter-ring communication. (A) The FRET measurements showing GroEL/ES complex formation under conditions identified as follows: purple, IAEDANS labeled GroEL^{wt} mixed with GroES^{F5M} and ATP; light blue, IAEDANS labeled GroEL^{wt} mixed with GroES^{F5M} and ADP plus BeF_3; blue, the same with purple but using IAEDANS-GroEL^{K105A} instead of GroEL^{wt}; green, the same with blue but using IAEDANS-

$GroEL^{K105A}$ instead of $GroEL^{wt}$; red, IAEDANS-$GroEL^{K105A}$ mixed with $GroES^{F5M}$ and ADP. **(B)** $GroES^{F5M}$ 'washout' measurements shows that the release of GroES from $GroEL^{K105A}$ football is much slower than $GroEL^{wt}$ and is not due to slow release of ADP since SP cannot accelerate the rate of GroES release from $GroEL^{K105A}$ football. The 'washout' experiments were performed in the same manner as in Chapter 5 by mixing in $GroES^{wt}$ to the turning over system of $GroEL^{IAEDANS}$, $GroES^{F5M}$, ATP and SP (if specified). The traces are identified as: red, $GroEL^{wt}$; blue, $GroEL^{K105A}$; dark color, plus SP; light color, without SP.

7.3.2 $GroEL^{K105A}$ football can be formed more readily than that of the wild-type

The $GroEL^{K105A}$ football does not only exist longer than that of the wild-type but also appears to be formed more readily as reflected by the following two sets of experiments. In one set, we've found that $GroEL^{K105A}$ football can even be formed in the presence of ADP (Figure 7-4A red), and including BeF_3 drives the formation of football to almost completion (Figure 7-4A green). The latter may be achieved by 'locking' GroES to the $GroEL^{K105A}$ football complex since ADP•BeF_3 mimics ATP in the GroEL nucleotide binding pocket [92] (Figure 7-2B light blue). Such observation is in direct contrast with $GroEL^{wt}$ which cannot form the symmetric complex to any observable amount even in the presence of ADP·BeF_3 (Figure 7-4A light blue).

The second set of experimental data that indicates $GroEL^{K105A}$ football can be formed more readily is shown in Figure 7-5. In the figure, the formation of the symmetric complex was compared between $GroEL^{wt}$ (Figure 7-5A) and $GroEL^{K105A}$ (Figure 7-5B) in the presence of varying [ATP]. To avoid complication from BoS as ATP being hydrolyzed, we used $GroEL^{D398A}$, a mutant that hydrolyzes ATP 1000 times slower than $GroEL^{wt}$, as wild-type surrogate at the 105 position. It is quite clear from the data that as [ATP] decreases, the formation of the symmetric complex turns from a single-step transition at saturating [ATP] to biphasic at lower [ATP]. As [ATP] drops to below 50μM, the addition of the two GroES molecules proceeds at two clearly distinguishable

steps, and at even lower [ATP] (≤5μM), only bullets can be formed. It therefore appears that though recruitment of GroES by the two GroEL rings pre-occupied by ATP happens simultaneously, occupying the two GroEL rings by ATP is stepwise, that is, transition from $[EL^{T}]:[EL^{T}]$ to $[EL^{T}]:[EL^{R}\cdot ATP]$ happens much faster than transition from $[EL^{T}]:[EL^{R}\cdot ATP]$ to $[EL^{R}\cdot ATP]:[EL^{R}\cdot ATP]$. On the other hand, binding of ATP by the two $GroEL^{K105A}$ rings and the formation of the K105A football proceeds with a single step within the range of [ATP] applied (500-10μM). All the kinetic trajectories thus obtained can be well fitted with the sum of two exponential phases: a lag phase which corresponds to ATP populating both GroEL rings at the same time (Step 1 in the kinetic scheme of Figure 7-5C) and an exponential enhancement phase where football was formed (Step 2 in the kinetic scheme of Figure 7-5C). As expected, the rate constant of the former linearly correlates with [ATP] applied with a 2rd order rate constant of $9.6\times10^{5}M^{-1}S^{-1}$, similar values for ATP binding can be found in [35, 107] ; and the rate constant of the latter shows a hyperbolic dependence of [ATP] which can be well described by the two-step kinetics (Figure 7-5C).

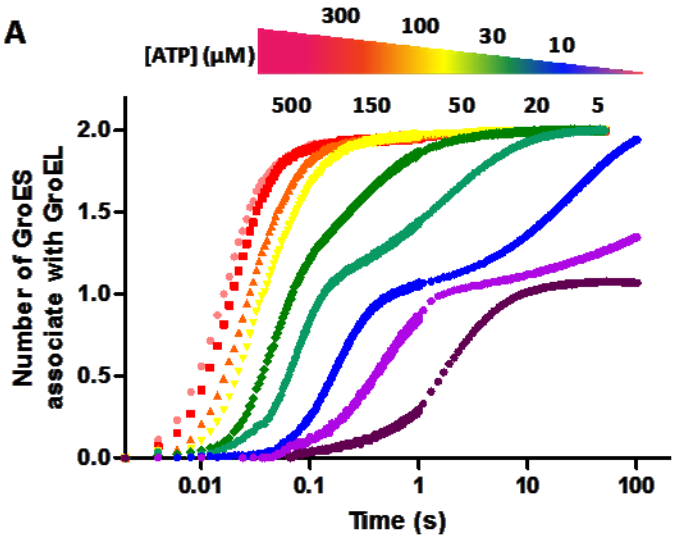
A
[ATP] (μM)
300
100
30
10
500
150
50
20
5
Number of GroES associate with GroEL
2.0
1.5
1.0
0.5
0.0
0.01
0.1
1
10
100
Time (s)

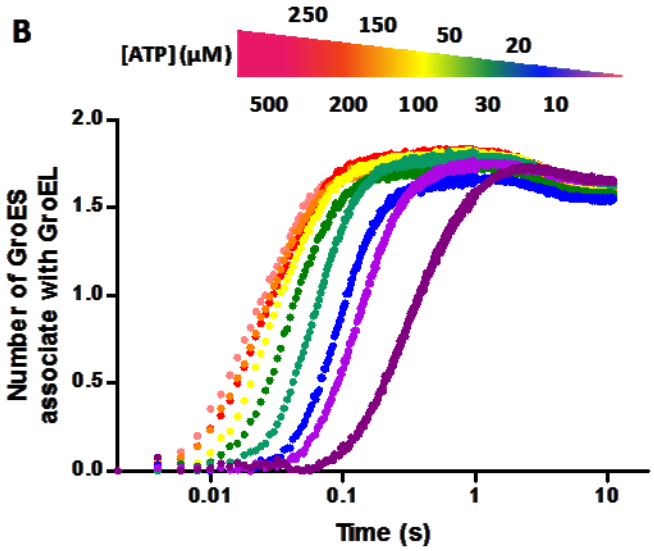
B
[ATP] (μM)
250
150
50
20
500
200
100
30
10
Number of GroES associate with GroEL
2.0
1.5
1.0
0.5
0.0
0.01
0.1
1
10
Time (s)

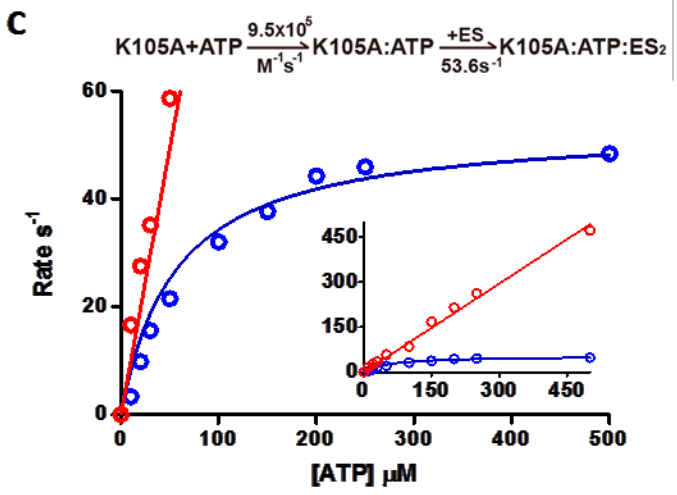
C
K105A+ATP
9.5x10^5
M^-1s^-1
K105A:ATP
+ES
53.6s^-1
K105A:ATP:ES2
Rate s^-1
60
40
20
0
0
100
200
300
400
500
[ATP] μM
450
300
150
0
0
150
300
450

Figure 7-5: IAEDANS labeled GroEL^{D398A} (A) or GroEL^{K105A} (B) in complex with GroES^{F5M} at varying [ATP]. The measurements were initiated by introducing varying [ATP] to a mixture of apo-GroEL^{IAEDANS} and GroES^{F5M}. The traces are identified as the colored code shown on top of each plot which also specified [ATP] applied. **(C)** The kinetic trajectories shown in B were fitted with the sum of two exponential terms: $y=Amp_1*exp(-k_1*t)-Amp_2*exp(-k_2*t)+B$. The rates constants of the two phases ($k_1>k_2$) were plotted against [ATP] applied (red, k_1, and blue, k_2). The two sets of data can be best described by the two-step kinetic scheme shown above the plot. The continuous lines are generated by simultaneously fitting the two sets of data points with the following two equations respectively to generate the same set of kinetic parameters: $k_1=slope*[ATP]$, and $k_2=1/\{1/(slope*[ATP])+1/k_{ES}\}$, in which, *slope* is the 2rd order rate constant of ATP binding to GroEL^{K105A}, and k_{ES} is the rate of GroES association with GroEL^{K105A} occupied by ATP. The fitting results are shown in the kinetic scheme as well. Given a GroES^{F5M} subunit concentration of 7μM as applied in this set of experiments, a pseudo first order rate of 53.6s^{-1} corresponds to a 2rd order rate constant of $5.36\times10^{7}M^{-1}s^{-1}$, a value very close to the one reported in Chapter 5 as well as those from literature [40, 55]. So does the directly fitted 2rd order rate constant of ATP binding ($9.5\times10^{5}M^{-1}s^{-1}$) [35, 107].

7.3.3 The thermodynamics of formation of GroEL^{K105A} football in the presence of ADP

Since the K105A symmetric complex is in equilibrium with the asymmetric complex in the presence of ADP (Figure 7-4A red and Figure 7-2B), it allows us to evaluate the energetics associated with this critical inter-ring communication hub by comparing the thermodynamics of formation of GroEL^{K105} 'football' with that of the wild-type.

The free energy of formation of the K105A symmetric complex was determined by measuring the dissociation constant of the second GroES (i.e. the equilibrium constant of the reaction shown in Figure 7-7) in two different ways. In one way, the FRET signal between GroEL^{IAEDANS} and GroES^{F5M} was employed to monitor the formation of the K105A symmetric complex (Figure 7-6A) in the presence of saturating [ADP] (1mM). The clear biphasic shape of the kinetic trajectories indicates that addition of the two GroESs to form GroEL^{K105A} football is sequential with the bullet complex formed first at a rate much faster than the subsequent step. Under the condition applied, varying

[GroES] only resulted in change of the amplitude of the slower phase (corresponding to the formation of the symmetric complex) while the amplitude of the faster phase (formation of the asymmetric complex complex) was unaffected. This allows us to focus just on the equilibrium established between the asymmetric complex and the symmetric complex for this set of experiments. By converting the average number of GroES associated with GroEL to the population of 'football' and plotting it against [GroES] applied, we can obtain the dissociation constant of the second GroES from the $GroEL^{K105A}$ symmetric complex as 1.9±0.2μM by fitting the data plot with the quadratic binding equation (Figure 7-6A legend). The moderate quality of fitting as well as the uncertainty of the K_d value obtained can be largely attributed to the unusually high concentration of $GroES^{F5M}$ required which results in higher background, poorer signal to noise, and prevents us from titrating sufficient amount of GroES to drive complete formation of 'football'.

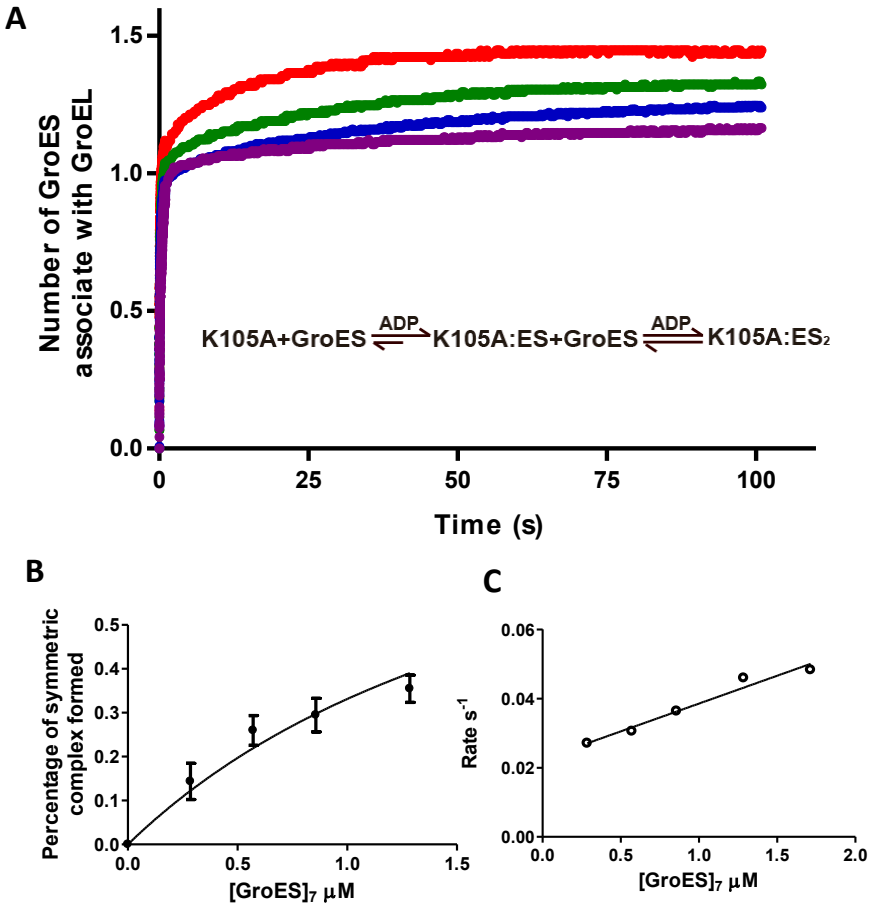

Figure 7-6: Determining the energetics of formation of the football complex by FRET (A) 2µM of IAEDANS labeled GroEL^{K105A} subunit pre-equilibrated with 1mM ADP was mixed with GroES^{F5M} of varying concentrations. **(B)** The population of football complex formed was plotted against [GroES^{F5M}] and the data set was fitted with the quadratic binding equation to extract K_d for binding of the second GroES ($y = \left[([EL_{14}{:}ES_7]^{total} + [ES_7] + K_d) - \sqrt{([EL_{14}{:}ES_7]^{total} + [ES_7] + K_d)^2 - 4[EL_{14}{:}ES_7]^{total}[ES_7]}\right]/(2[EL_{14}{:}ES_7]^{total})$, in which, $[EL_{14}{:}ES_7]^{total}$=0.147µM. The best fit value for Kd is 1.9±0.2µM. Error bars are standard deviations of the plateau value of the symmetric complex population from the six individual traces that are averaged into the kinetic trajectories shown in A. **(C)** The rate constants of the slow phase of kinetic traces shown in A are plotted against $[GroES]_7$ applied. The best fit linear equation is Rate=0.016$[GroES]_7$+0.022, which yields an apparent dissociation constant of 0.022/0.016=1.38µM.

A K_d of 2µM corresponds to a free energy change (ΔG_{k105A}) of -34kJ/mol at 37°C. To evaluate the free energy contribution of this salt bridge ($\Delta\Delta G$), one also needs to know the free energy change for the formation of the wild-type 'football' (ΔG_{wt}) under identical

conditions. This value is not readily measurable because the football complex with both rings occupied by ADP ([$GroES_7$-$(ADP)_7$-$GroEL_7$]-[$GroEL_7$-$(ADP)_7$-$GroES_7$]) exists only transiently. However, we can estimate it roughly from published related kinetic parameters concerning formation (k_{on}) and breakage (k_{off}) of the wild-type ADP football. As a rough estimate of k_{off}, we used the rate of discharge of the GroES from the cis-ring of the acceptor bullet complex upon being challenged by ATP and excess GroES (~$60s^{-1}$ at 37°C [40]) because this step was found to proceed via a similar transient football complex ([$GroES_7$-$(ADP)_7$-$GroEL_7$]-[$GroEL_7$-$(ATP)_7$-$GroES_7$]) [108]. In the same study[108] that established the associative mechanism by which the asymmetric complex exchanges GroES, k_{on} is estimated to be ~$6.5\times10^{-6}M^{-1}s^{-1}$. Based on these two numbers, we can calculate ΔG_{wt} to be ~41kJ/mol, a huge free energy penalty which explains why formation of the wild-type 'football' with ADP is often not observable. $\Delta\Delta G$ is therefore ~-75kJ/mol or ~-10.6kJ/mol for each broken charge-helix dipole interaction (Figure 7-7A) (since there are only seven sets of such interaction being broken as 'football' formed from 'bullet'), a value falls well in the range reported in literature [104].

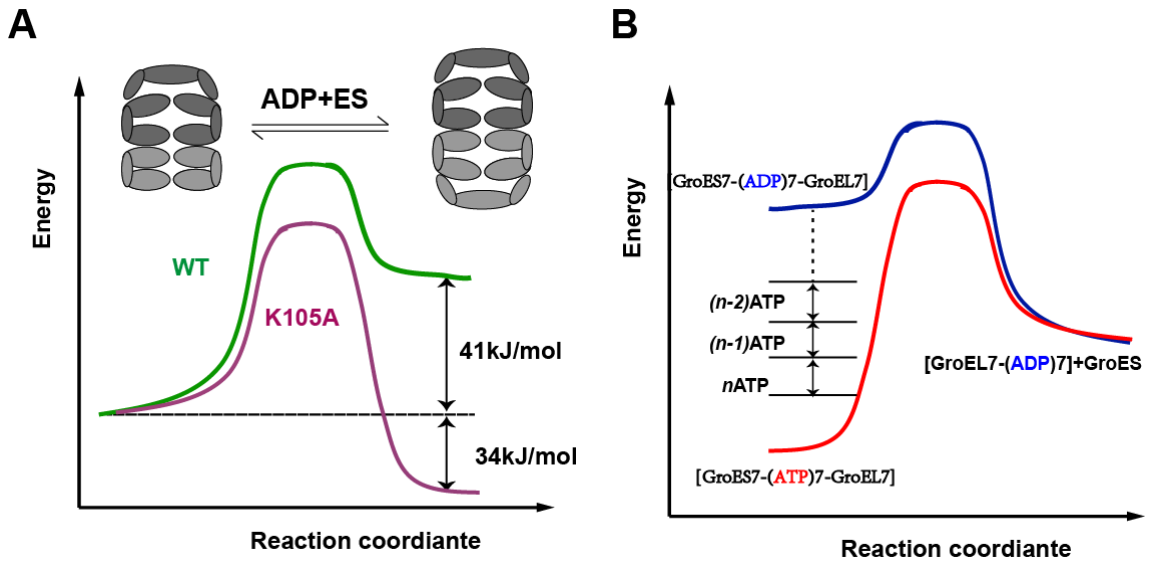

Figure 7-7: (A) The reaction diagram shows that by introducing the mutation K105A, an energetically unfavorable reaction, i.e. formation of the symmetric complex in the presence of ADP from the asymmetric complex, was turned into a favorable one. The free energy changes were calculated as described in the main text. **(B)** The reaction diagram illustrates how hydrolysis of ATP may destabilize the GroEL/ES complex and bring about discharge of GroES. Only one ring was examined in this simple illustration.

7.4 Discussion

Helix D, as the most important structural element connecting the nucleotide binding sites across the ring, has long been suspected to play a role in inter-ring communication. However, the nature of the inter-ring allostery has only been elucidated by a recent structural survey on the folding active symmetric football complex. The point of action is identified as the electrostatic interaction between the positively charged lysine 105 and the negatively charge C-terminus of Helix D (carbonyl oxygen of A109) across the ring [16]. Formation of the symmetric complex is accompanied by disruption of this inter-ring interaction while BoS results in its reestablishment.

The experimental characterization of the mutant K105A presented in this chapter serves to test the model describing the structural basis for BoS as proposed in [16]. The experimental evidence presented here clearly indicates that substituting the positively charged lysine 105 with alanine at the GroEL inter-ring interface results in a dramatic change of the way the two rings interact with one another. On the one hand, BoS of the $GroEL^{K105A}$ 'football' is less readily to occur (at least 1000 times slower than the wild-type football as shown in Figure 7-4B) despite unaltered intrinsic ATPase activity. This is most likely due to the impaired inter-ring communication which cannot carry the allosteric signal from one ring to the other as efficiently as the $GroEL^{wt}$. On the other hand, we've found that there is less energetic cost for the formation of $GroEL^{K105A}$ 'football' as reflected by the two sets of experimental data underlining the dramatic

contrast between this mutant and the wild-type: *i)* GroEL^{K105A} 'football' can be formed with ADP while the wild-type cannot (Figure 7-4A), and *ii)* the formation of GroEL^{K105A} 'football' proceeds with a single step even at low [ATP], but as for GroEL^{wt}, ATP binding to one ring tremendously slows down ATP binding to the other ring which results in a distinctive two-step formation of the wild-type football at low [ATP] (Figure 6-5). It therefore appears that rather than being closely coordinated, the allosteric transitions undergone by the two rings of GroEL^{K105A} become more independent of one another. The fact that this mutant also lost the characteristic negative cooperativity from its steady-state ATPase profile further highlights the importance of the lysine 105 as a critical allosteric communication contact.

By taking advantage of the fact that in the presence of ADP, the GroEL^{K105A} 'football' is in equilibrium with the 'bullet', we determined the free energy change associated with formation of its symmetric complex. By comparing with that of the wild-type, we've found that there is approximately 10.6kJ/mol/interaction free energy change associated with removing the positive charge from position 105. The magnitude of such free energy is in good keeping with identifying K105 as involved in forming electrostatic interaction with the negatively charged C-terminus of Helix D, and therefore, we take it as the energetic contribution of the salt bridge involved [104-105].

The experimental evidence thus presented is in perfect agreement with the view offered in [16]. For GroEL^{wt}, ATP occupancy of one ring slows down ATP binding to the other ring and it is reflected from the sequential recruitment of the two GroES at dramatically different rates at lower [ATP]; while for GroEL^{K105A}, such inter-ring negative cooperativity in terms of ATP binding is absent. Such observation is consistent

with the structural change at the inter-ring interface surrounding Helix D accompanying the transition from the asymmetric bullet complex to the symmetric football complex. By comparing the crystal structures of chaperonins at these two different states, one can find that as ATP and GroES bind to the trans-ring of the asymmetric complex, it requires breaking the salt bridge formed between the *cis* K105 and the *trans* C-terminus of Helix D which is found, as presented here, to entail a free energy penalty of 10.6kJ/mol/interaction. Such free energy penalty is removed by disrupting the electrostatic interaction involving K105 by substituting it with alanine, and thus we found the much slower binding of ATP and GroES to the second ring of $GroEL^{wt}$ is absent in $GroEL^{K105A}$. Though the energetics of each individual interaction is modest, when combined together for all fourteen subunits, it becomes so huge that removing it by the lysine to alanine mutation turns a thermodynamically unfavorable process, i.e. formation of the symmetric complex in the presence of ADP, into a favorable one (Figure 7-7A).

As pointed out in [16], the disruption of the salt bridge formed between K105 and Helix D C-terminus as the symmetric complex forms appears to be caused by the conformational change induced by ATP binding particularly by the new interactions formed between the negatively charged γ-phosphate of ATP and several positively charged residues in the N-terminus of Helix D. When ATP binds to the *trans* ring of the asymmetric complex, the resulted twisting and sliding of Helix D brings apart K105 of the original *cis* ring from the C-terminus of Helix D of the old *trans* ring. As ATP is hydrolyzed, the favorable interactions that hold Helix D in its new position are diminished. And thus, Helix D tends to return back to its original position under the drive to reform the salt bridge between K105 and C-terminus of Helix D of the opposite ring.

This may be one of the most important sources of potential energy that drives BoS to occur, given the free energy change of -10.6kJ/mol/interaction *VS* -27.6kJ/mol/γ-phosphate binding [92]. And indeed, in the last chapter, I summarize how stochastic hydrolysis of ATP results in BoS with two simple rules: sufficient number of ATP (≥6) need to be hydrolyzed within the ring from which GroES is discharged (the 'hydrolysis number rule'), and if only five ATP are hydrolyzed, BoS can still occur provided the opposite ring has less than 2 ATP that have been hydrolyzed (the 'difference adjusted rule'). The study presented here provides a sound structural foundation for these two rules. Since hydrolysis of ATP destabilizes the symmetric complex, its free energy level rises progressively as more and more ATPs are hydrolyzed until enough ATP (≥6) being hydrolyzed to allow BoS to occur spontaneously and rapidly as shown in the last chapter (Figure 7-7B). The step size of free energy rise can be as large as 27.6kJ/mol/ATP hydrolysis [92] if all the free energy related to interactions involving γ-phosphate of ATP is utilized to destabilize the complex as ATP being hydrolyzed and Pi released; and it can be as small as 10.6kJ/mol/interaction if only the energetics associated with K105 is considered. Therefore, for the former, each ATP hydrolysis event results in between 1700 and 4700 fold of rate acceleration ($k_1/k_2=exp(\Delta G/RT)$), which explains why BoS appears as an all-or-none event as reflected by the 'hydrolysis number rule'.

As for the difference adjusted rule, it would be hard to rationalize if K105 were solely responsible for inter-ring communication. As a matter of fact, it is not as reflected by a multitude of experimental observations shown in this chapter: *i)* in the presence of ATP, the GroEL^{K105A} symmetric complex population at steady-state is ~90% but not 100% (Figure 7-4A); *ii)* BoS of the GroEL^{K105A} symmetric complex does occur though at

a much slower rate (Figure 7-4B); *iii)* though the kinetics of formation of GroEL^{K105A} 'football' in the presence of ATP is indistinguishable from that of the GroEL^{K105A} 'bullet' (Figure 7-5B), we can see clearly that formation of GroEL^{K105A} 'football' is biphasic in the presence of ADP (Figure 7-6A) and binding of the second GroES is much less tight than the first GroES (Figure 7-6, binding of the first GroES is too tight to be measured with such experimental setup). All these lines of evidence indicate that there must be additional contacting site for transmitting allosteric signal across the ring, which may be responsible for BoS events underlying the 'difference adjusted rule'. However, we do notice that they only account for a small portion of all the BoS competent states (Figure 6-8).

Chapter 8: SP refolding optimization by the symmetric complex under turning over conditions

8.1 Introduction

From work presented in the last 4 chapters, we've learnt that *i)* the GroEL/ES symmetric complex becomes the predominant species in the presence of saturating [SP] (denatured α-Lactalbumin, α-LA for short), and *ii)* stochastic ATP hydrolysis induces breakage of the symmetric complex into the asymmetric complex to allow rapid turnover of the system. The latter may result in accelerated refolding of SP. However, up till this point, a major issue has been left untouched, i.e. how the optimized SP refolding is achieved by GroEL cycling in the symmetric cycle. The work presented in this chapter helps to answer this critical question on at least two accounts: *i)* how many SP can be processed by the symmetric complex in the GroEL functional cycle, *ii)* what is the advantage for chaperonins to populate as a highly dynamic system i.e. the symmetric complex of the symmetric cycle over a relatively static one, e.g. SR1.

As for the first aspect, a new FRET system was developed to meet the special requirements for measurement of SP encapsulation by GroEL/ES complex. Two widely used model SPs were chosen to perform such measurement: malate dehydrogenase from pig heart mitochondria (MDH) and ribulose-1,5-bisphosphate carboxylase/oxygenase from *Rhodospirillum rubrum* (Rubisco). In both cases, close to two SPs were found to be encapsulated by the symmetric complex under 'actively turning over' conditions. In addition, measurements on SP encapsulation efficiency also indicate that this process can only occur efficiently if the natural order of ligand arrival to the GroEL trans-ring is

sustained, i.e. SP binding first, followed by ADP release, and then ATP binding and GroES binding to complete SP encapsulation.

For the second one, one obvious benefit bestowed by a system of chaperonin that is actively turning over is that GroEL can accelerate some of its SPs refolding by repetitively unfolding them, induced by ATP binding according to the iterative annealing theory [64] (Section 1.5 of Chapter 1). On the other hand, with respect to SPs that shows no sign of being forcefully unfolded by GroEL, the benefits may not be so obvious. Among those SPs, we chose MDH for our study [109]. Contrary to what is generally perceived that GroEL can only assist refolding of SP when present in stoichiometric quantity (i.e. moles of SP/moles of GroEL ring ≈ 1) [9-10, 27, 38], the work presented here shows that even with a large molar excess of denatured MDH (dMDH) over GroEL ring (10:1), up to 70% of MDH activity can be recovered at rate much faster than the spontaneous MDH refolding ($0.080\pm0.009 min^{-1}$ *VS* $0.029\pm0.007 min^{-1}$). When the same refolding assays were repeated under non-turnover conditions (using SR1 or using ATP depletion system consisted of HK and Glucose), GroEL can only recover MDH stoichiometrically. It therefore appears that, being able to turnover not only makes GroEL an iterative annealing machine, but also allows it to mediate refolding of multiple SP molecules at a given amount of time as long as these denatured molecules remain 'rescuable' (have not formed high order irreversible aggregates).

8.2 Methods specific to Chapter 8

8.2.1 Preparation of denatured Rubisco and MDH Rubisco was over expressed from a plasmid containing His-tagged Rubisco from *Rhodospirillum rubrum*, a gift from Dr. Grant Pearce, and purified in essentially the same way as $GroES^{his}$ (Section 2.5 of

Chapter 2). MDH from pig heart mitochondria was purchased from Roche Applied Science. The concentrations of Rubisco and MDH were measured at 280 nm using the extinction coefficients of 67,000 $cm^{-1}M^{-1}$ and 6,800 $cm^{-1}M^{-1}$ respectively. Rubisco was denatured by incubating a 20-30μM Rubisco solution with 8M freshly made acid urea (20mM Glycine-HCl, pH=2.5) for 10min on ice. MDH was denatured in 6M freshly prepared urea.

8.2.2 Labeling MDH and Rubisco with QSY-7 maleimide MDH^{QSY7} was prepared as follows: 100μM denatured MDH in freshly made urea was mixed with 110μM QSY-7 maleimide (Sigma Aldrich) and incubated with agitation in dark for 1 hour at room temperature. Unreacted dye was removed by extensive wash using an YM-10 microcon (Millipore Corporation). The extent of labeling (~1 mol QSY7 /mol MDH subunit) was measured at 560nm to determine the dye concentration and Bradford assay for MDH concentration. The extinction coefficient used for the QSY-7 is 90,000 $cm^{-1}M^{-1}$. Rubisco was labeled in essentially the same way as described in [86] by incubating native Rubisco sample (~200 μM) with 2-3 times of QSY-7 for 1 hour before quenching the reaction with 1mM DTT. The unreacted fluorescence dye was removed by PD-10 gel filtration.

8.2.3 MDH refolding assay The recovery of enzymatic activity by 6M urea-denatured MDH refolded in the presence of chaperonins was monitored spectroscopically. dMDH was added to a solution containing 50 mM Tris-OAc pH 7.5, 100 mM KOAc, 10 mM $Mg(OAc)_2$, 0.2 mM PEP, 1 mM DTT, 5 units PK, 12.5 μM GroES, plus GroEL of concentration as indicated in Figure 8-6 legends. The final MDH concentration was 0.5 μM and MDH refolding was carried out at 30°C. The MDH

refolding was initiated by addition of 1 mM ATP, and at various time points, 10 µl of this refolding reaction was removed and diluted to a 890 µl solution containing 100 mM TrisOAc pH 7.5, 50mM EDTA, 0.15 mM NADH, 1µM GroEL subunit (to capture free dMDH) and incubated on ice for at least 10min before subject to MDH activity assay. The assay was carried out at 30°C and initiated by addition of 0.5 mM oxaloacetate. The decrease in absorbance at 340 nm was monitored over 4min. The slopes of the steady-state trace of MDH at different time points were normalized to that of native MDH of the same concentration (5.6nM) and expressed as % of MDH activity recovered.

MDH refolding assay in the presence of SR1 was performed in a similar way but requires an additional step to break the SR1-GroES complex to release encapsulated MDH monomer for reconstitution of enzymatically active MDH dimer. SR1-GroES complex was broken by mixing an aliquot of MDH refolding solution (10µl) with equal volume of solution containing 200mM EDTA (pH=7.5) and 14µM GroEL and rapidly frozen by submersed in liquid methanol pre-chilled at -80°C. The frozen solution containing broken SR1-GroES complex and free MDH monomers was incubated at 30°C for 15min for the MDH dimer to form from refolded MDH monomer before adding 880µl solution containing 100 mM Tris pH 7.5, 50mM EDTA, 0.15 mM NADH to perform MDH activity assay.

8.3 Results

8.3.1 The Stoichiometry of SP encapsulation by the symmetric complex It has been shown in Chapter 5 that the steady state population of the symmetric complex and the asymmetric complex can be quantitatively measured by employing a calibrated FRET system, and that an equilibrium exists between the two complexes that is dependent upon

the concentration of an SP that cannot fold (α-LA). However, the K_d of GroEL for α-LA is much higher than the concentration of $GroEL_{14}$ suitable for FRET measurement (Figure 5-6 of Chapter 5 and also [110]), and thus under these conditions, there is only a very small fraction of α-LA being encapsulated by chaperonins making encapsulation measurement very difficult. Therefore, in this study, two authentic tightly bound SPs (Rubisco and MDH) were employed.

Their ability to promote formation of the symmetric complex was first investigated. As shown in Figure 8-1, the two rings of the apo-$GroEL^{IAEDANS}$ are first equilibrated with varying quantities of either dRubisco (Figure 8-1A) or dMDH (Figure 8-1B), and subsequent addition of ATP and $GroES^{F5M}$ leads to formation of the symmetric complex to different extents (experimental setup illustrated in Figure 8-1E). When the final steady-state level of the symmetric complex was plotted against corresponding [SP], we can see that the two sets of data points take the shape of squared binding curves (Figure 8-1F blue and red circles), indicating stoichiometric binding of both SPs to GroEL. Under such tight binding conditions, no dissociation constant of the binding of either MDH or Rubisco to GroEL can be determined. Similar phenomena have been observed by others [27, 55]. Both of the two tight binding curves break at $[SP]/[GroEL]_7=1$ (dashed line in Figure 8-1F), and at saturating [SP], the symmetric complex was formed up to ~90%. Since SP and GroES share the same set of binding sites on GroEL, the two SP molecules that associate with GroEL must be encapsulated within the two enclosed chambers as a result of formation of the symmetric complex.

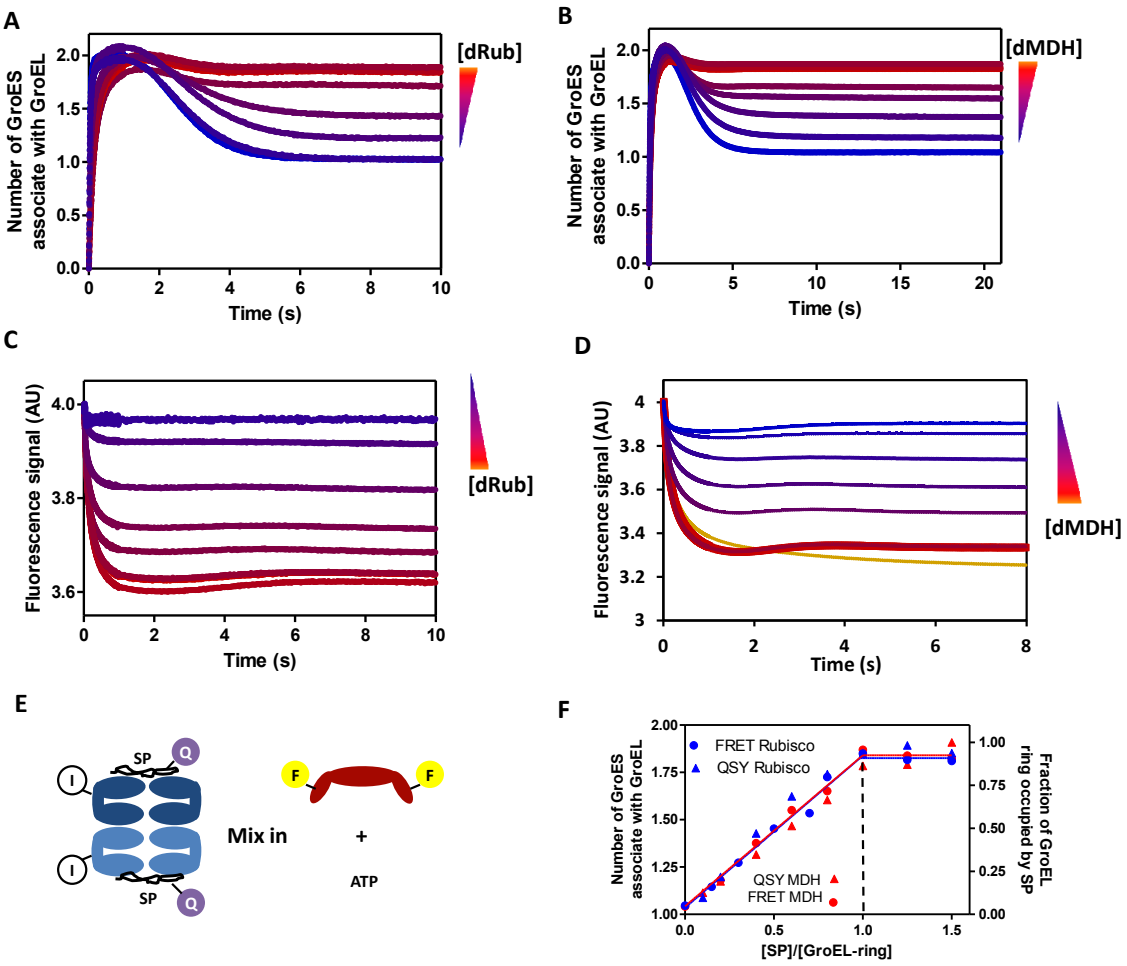

Figure 8-1: The "football" complex encapsulates two misfolded proteins simultaneously. (A) Pre-steady state formation of GroEL:GroES$_2$ monitored by FRET. Concentrations of dRubisco applied in the measurements are as follows (from top to bottom): 0.43μM, 0.357μM, 0.286μM, 0.229μM, 0.171μM, 0.114μM, 0.057μM and 0μM. 2μM GroEL^{IAEDANS} subunit (0.3μM rings), 4μM GroES^{F5M} subunit, and 0.5mM ATP were used for all the measurements. The reactions were initiated by introducing ATP+GroES^{F5M} into solution containing GroEL^{IAEDANS} pre-incubated with dRubisco (illustrated in E). The summary plot of this set of experiment is shown in F as blue circle. **(B)** Pre-steady state formation of GroEL:GroES$_2$ monitored by FRET in the presence of denatured MDH. The experiments were performed in essentially the same way as those shown in A, and the steady-state level of football were plotted against corresponding [dMDH] shown in F. **(C)** Encapsulation of dRubisco by GroEL:GroES$_2$ shown by titrating GroEL ring with dRubisco^{QSY7} reported by the quenching of F5M labeled GroES. The experiments were performed under the same condition as those in A. The bottom yellow trace was generated by also including 1mM $BeCl_2$ and 10mM NaF to restrict the measurement to single turnover condition and was used as 100% SP occupation level. The summary plot of this set of experiment is shown in F as blue triangles. **(D)** Encapsulation of dMDH by GroEL:GroES$_2$ shown by titrating GroEL ring with dMDH^{QSY7} reported by the quenching of F5M labeled GroES. The experiments

were performed in essentially the same way as those summarized in C, and the summary plot was shown in F. **(E)** Cartoon illustration of the experimental setup for both the GroEL/ES complex measurements [FRET pair: $GroEL^{IAEDANS}$ (I) and $GroES^{F5M}$ (F)] and SP encapsulation measurements [FRET pair: $GroES^{F5M}$ (F) and SP^{QSY7} (Q)]. **(F)** Determination of SP (dMDH in red and dRubisco in blue) encapsulation stoichiometry by the GroEL:$GroES_2$ complex. Two different ways are employed: (i) the FRET signal between $GroEL^{IAEDANS}$ and $GroES^{F5M}$ using unlabeled SPs (circles), and (ii) quenching of $GroES^{F5M}$ by SP^{QSY7} upon SP encapsulation and formation of the GroEL:SP_2:$GroES_2$ complex (triangle).

The fact that the symmetric complex contains two SPs can also be demonstrated by directly monitoring the SP encapsulation event. This set of experiments was performed with QSY-7 labeled MDH and Rubisco in which the QSY-7 quenches fluorescence emitted from F5M labeled on GroES (Figure 8-2A) upon SP being encapsulated. The advantages of labeling SP with 'black hole' quenchers like QSY-7 and monitoring proximity between SP and GroES rather than GroEL are at least two fold: *i)* the fluorescence signal is devoid of complications from the conformational and environmental change associated with SP encapsulation since the dye labeled on SP (QSY-7) doesn't fluoresce (Figure 8-2B red); *ii)* SPs bound to the trans-ring can be distinguished from those encapsulated on the basis that quenching of $GroES^{F5M}$ fluorescence only occurs if SP labeled with QSY-7 is encapsulated in the same ring to which the $GroES^{F5M}$ molecule caps (Figure 8-2B brown). This can also be expected based on the much smaller Foster distance of this FRET pair (61Å [111]) than the distance from GroES bound to one ring to the center of the enclosed chamber of the opposite ring (>120Å, [14, 16]) given the sixth power dependence of FRET efficiency on distance change.

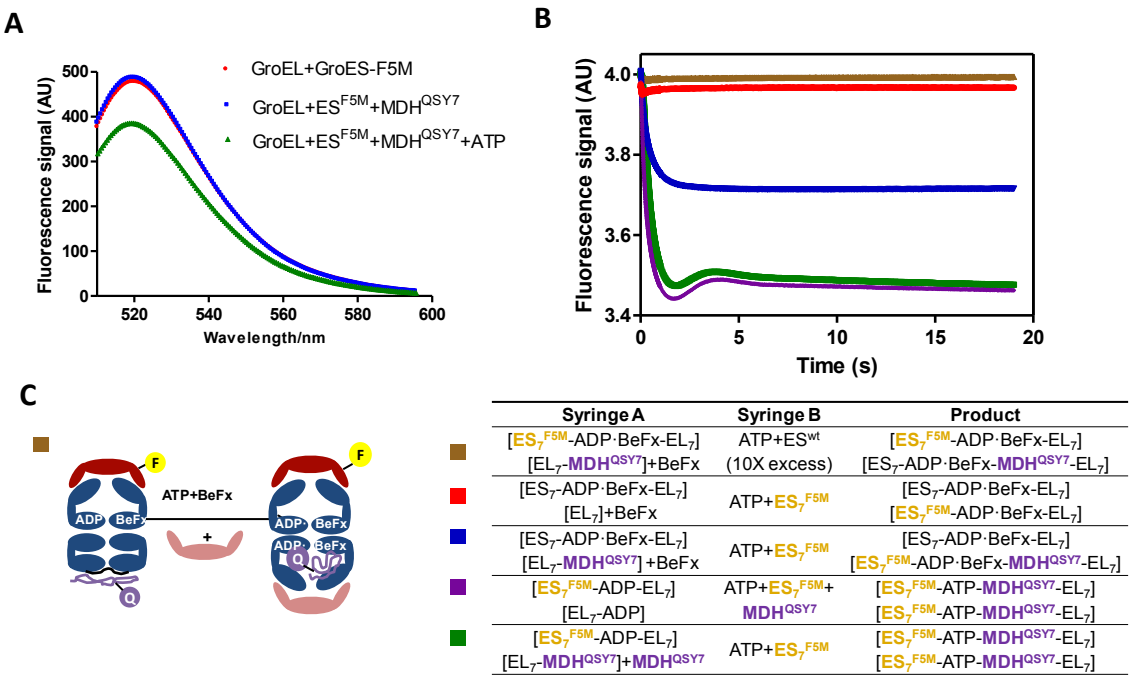

Syringe A	Syringe B	Product
[ES_7^{F5M}-ADP·BeFx-EL_7] [EL_7-MDH^{QSY7}]+BeFx	ATP+ES^{wt} (10X excess)	[ES_7^{F5M}-ADP·BeFx-EL_7] [ES_7-ADP·BeFx-MDH^{QSY7}-EL_7]
[ES_7-ADP·BeFx-EL_7] [EL_7]+BeFx	ATP+ES_7^{F5M}	[ES_7-ADP·BeFx-EL_7] [ES_7^{F5M}-ADP·BeFx-EL_7]
[ES_7-ADP·BeFx-EL_7] [EL_7-MDH^{QSY7}] +BeFx	ATP+ES_7^{F5M}	[ES_7-ADP·BeFx-EL_7] [ES_7^{F5M}-ADP·BeFx-MDH^{QSY7}-EL_7]
[ES_7^{F5M}-ADP-EL_7] [EL_7-ADP]	ATP+ES_7^{F5M}+ MDH^{QSY7}	[ES_7^{F5M}-ATP-MDH^{QSY7}-EL_7] [ES_7^{F5M}-ATP-MDH^{QSY7}-EL_7]
[ES_7^{F5M}-ADP-EL_7] [EL_7-MDH^{QSY7}]+MDH^{QSY7}	ATP+ES_7^{F5M}	[ES_7^{F5M}-ATP-MDH^{QSY7}-EL_7] [ES_7^{F5M}-ATP-MDH^{QSY7}-EL_7]

Figure 8-2: Direct measurement of SP encapsulation by SP^{QSY7}/$GroES^{F5M}$ quench pair. (A) Steady state fluorescence quenching of $GroES^{F5M}$ by $dMDH^{QSY7}$. Quenching of $GroES^{F5M}$ only occurs in the presence of $dMDH^{QSY7}$, ATP and GroEL. 2µM $GroEL^{wt}$, 3µM $GroES^{F5M}$, 0.429µM $dMDH^{QSY7}$, and 0.5mM ATP were used. **(B)** Calibration of SP encapsulation with the MDH^{QSY7}/$GroES^{F5M}$ quench pair. The experimental set-up is listed in the table beneath the graph and the color code is to the left of the table. The square brackets define the ligand content of each GroEL ring. Both the red and the purple traces were offset by a slight fluorescence signal value (0.025) to reveal the brown and green traces respectively. One measurement (the brown trace) was further illustrated by cartoons in C. **(C)** Cartoon illustration of the brown trace shown in B.

A proof-of-concept experiment is shown in Figure8-2B where the asymmetric acceptor-state complex was equilibrated with a molar equivalent (to GroEL rings) of MDH^{QSY7}. This was then mixed in the stopped-flow device with ATP and $GroES^{F5M}$. Including BeF_3 in the assay before mixing in ATP and $GroES^{F5M}$ leads to a two fold reduction of the amplitude of quench of $GroES^{F5M}$ fluorescence (Figure 8-2B blue *VS* green). This is because BeF_3 prevents discharge of GroES from the *cis* ring and thus only trans-ring is available for SP encapsulation, while in its absence, both rings can be

populated with MDH^{QSY7} and $GroES^{F5M}$ and consequently the amplitude of the quench becomes twice as much (Figure 8-2B green).

Next, the efficiency of SP encapsulation was directly quantitatively measured under conditions comparable to the $GroEL^{IADEANS}$-$GroES^{F5M}$ FRET measurements (Figure 8-1 A and B). Apo-GroEL was pre-incubated with varying amounts of SP^{QSY7} (MDH or Rubisco) before mixing in ATP and $GroES^{F5M}$ in the stopped-flow device. These experiments were performed either in the absence of BeF_3 so as to permit multiple turnovers or in its presence. The latter serves as the bench mark for 100% encapsulation since it permits only one round of ATP hydrolysis per GroEL ring (Figure 8-1 C and D). Plotting the SP encapsulation efficiency against corresponding [SP] yields a similar tight binding curve as in the case of GroEL/ES complex formation measurements (Figure 8-1F). Moreover, these curves also have the break point at $[SP]/[GroEL]_7=1$ and a plateau level of up to ~90% GroEL rings being occupied by SP, indicating again, that both rings of the symmetric "football" complex are occupied by SP^{QSY7}.

8.3.2 SP catalyzed ADP/ATP exchange guarantees efficient SP encapsulation It is conventionally accepted that SP binds first to the T-state GroEL molecule followed by ATP binding which converts the conformation of GroEL to the R state, and eventually GroES binds to the R state GroEL ring to complete SP encapsulation and formation of the *cis* chamber [9-10, 57]. As reviewed in more detail in Section 1.5 of Chapter 1, an active folding model was proposed based on the stretching force exerted on SP bound to GroEL as a result of ATP induced conformational change (forceful unfolding) [61-62, 64, 112]. Recently, a contrary view has been proposed [35] which claims ATP binding precedes the binding of SP and therefore the ATP induced forceful unfolding, if there

were any, would simply not occur. This argument is based upon the measured 2nd order rate constants for the binding of ATP ($2x10^5$ $M^{-1}s^{-1}$) and SP ($6x10^6$ $M^{-1}s^{-1}$) to apo-GroEL ring. The [ATP] in *E coli.* (~10mM according to [113]) exceeds the concentration of SP by some 5000-fold [taken here to be maximally equivalent to the concentration of $GroEL_{14}$ (2.6μM [114])]. If such conditions prevail within *E coli* cells, then the binding of ATP to GroEL will occur 200 times faster than the binding of SP.

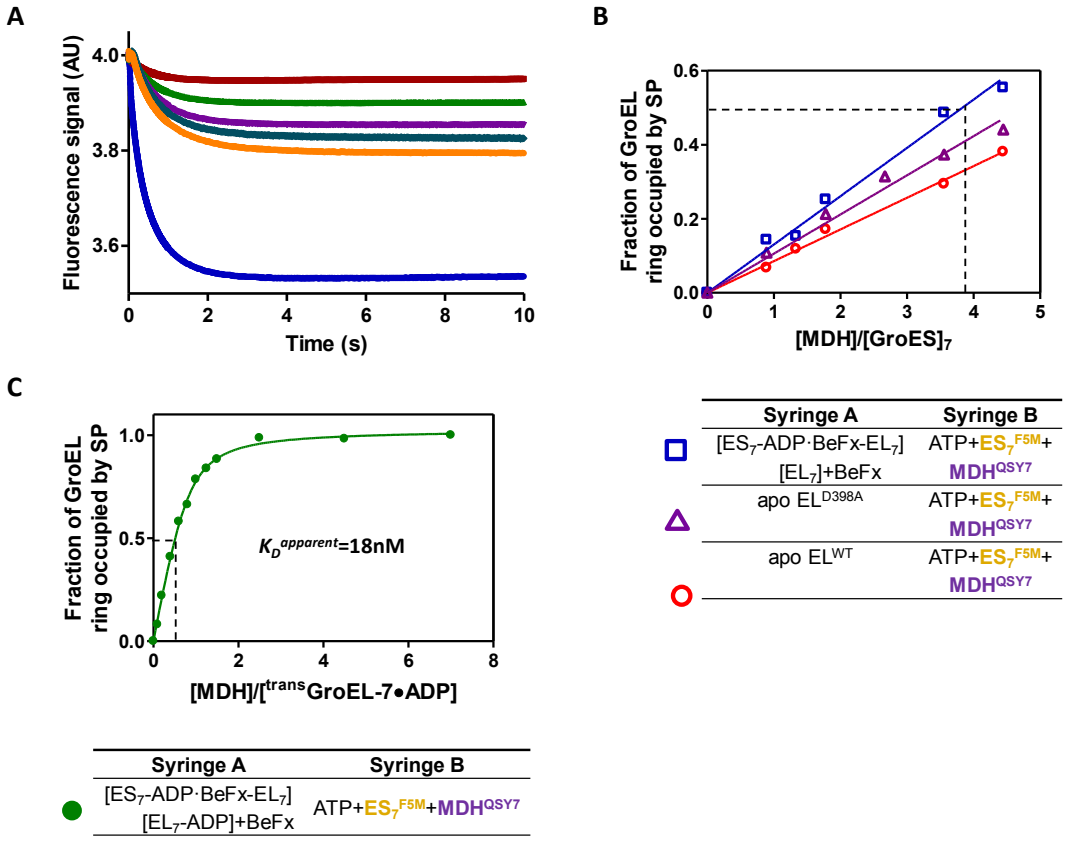

Figure 8-3: The experimental demonstration of the consequences of permitting ATP to bind to GroEL before SP (MDH^{QSY7}) and $GroES^{F5M}$. (A) The kinetic traces resulted from mixing 2μM $GroEL^{D398A}$ subunits with 0.5mM ATP, 2.25μM $GroES^{F5M}$ and MDH^{QSY7} of varying concentrations. The traces of different [MDH^{QSY7}] applied are identified as, red, 0.13μM; green, 0.25μM; purple, 0.38μM; navy blue, 0.51μM; orange, 0.64μM. The royal blue trace was obtained by pre-incubating SP accepting species with 0.286μM $MDH^{QSY7}$and 1mM BeF_3 before introducing $GroES^{F5M}$ and ATP. This trace was set as the 100% encapsulation level to which the steady-state level of all the other traces in the same panel were normalized and converted to the fraction of GroEL ring occupied by SP as plotted in B. Three additional sets of similar experiments done with

different initiation species (specified below) were also performed (raw data not shown) and processed in the same way. The results are shown in B and C. **(B)** Summary plot of experiments of the kind shown in A initiated with the acceptor state complex (blue square), apo-GroEL^{D398A} (purple triangle), and apo-GroEL^{wt} (red circle). The slope of the regression line is used to calculate the [MDH]/[GroES$_7$] ratio required to achieve half occupancy of GroEL rings by SP, which is roughly marked by the dashed line in the plot. The commonplace of all the three sets of experiments is that ATP is permitted to bind to GroEL ring prior to SP and GroES, and consequently results in very inefficient SP encapsulation. **(C)** The plot was generated by introducing varying amounts of MDH^{QSY7} to the asymmetric resting state complex in the presence of BeF_3. Both MDH^{QSY7} and ATP (0.5mM) were introduced simultaneously. The presence of ADP on the trans ring ensures that SP binds before ATP and GroES^{F5M}. This SP-catalyzed ADP/ATP exchange permits efficient SP encapsulation which is evident from the much lower [MDH]/[GroES$_7$] (~1.2) required to occupy 50% of GroEL ring. Assuming that equilibrium between the unfolded protein and GroEL is established prior to encapsulation, an apparent dissociation constant of 18nM was obtained by fitting the data set with the quadratic binding equation:

$$y = \left[\left([EL]_7{}^{total} + [MDH] + K_d\right) - \sqrt{\left([EL]_7{}^{total} + [MDH] + K_d\right)^2 - 4[EL]_7{}^{total}[MDH]}\right] / \left(2[EL]_7{}^{total}\right).$$

This analysis is however flawed for it fails to consider that the physiological GroEL state to accept SP is the resting state ([^{cis}GroEL$_7$-ADP$_7$-GroES$_7$]-[^{trans}GroEL$_7$-ADP$_7$]) [12, 40, 112] in which ADP occupies the trans-ring and blocks ATP binding until SP binding induced rapid release of ADP. Consequently, the SP accelerated ADP/ATP exchange enforces the order of ligand arrival as: SP first, followed by ATP and GroES. What will happen if ADP was removed from the trans-ring and the acceptor state ([^{cis}GroEL$_7$-ADP$_7$-GroES$_7$]-[^{trans}GroEL$_7$]) was used to accept SP, ATP, and GroES? The consequence of such treatment is demonstrated both experimentally (Figure 8-3) and conceptually (Figure 8-4).

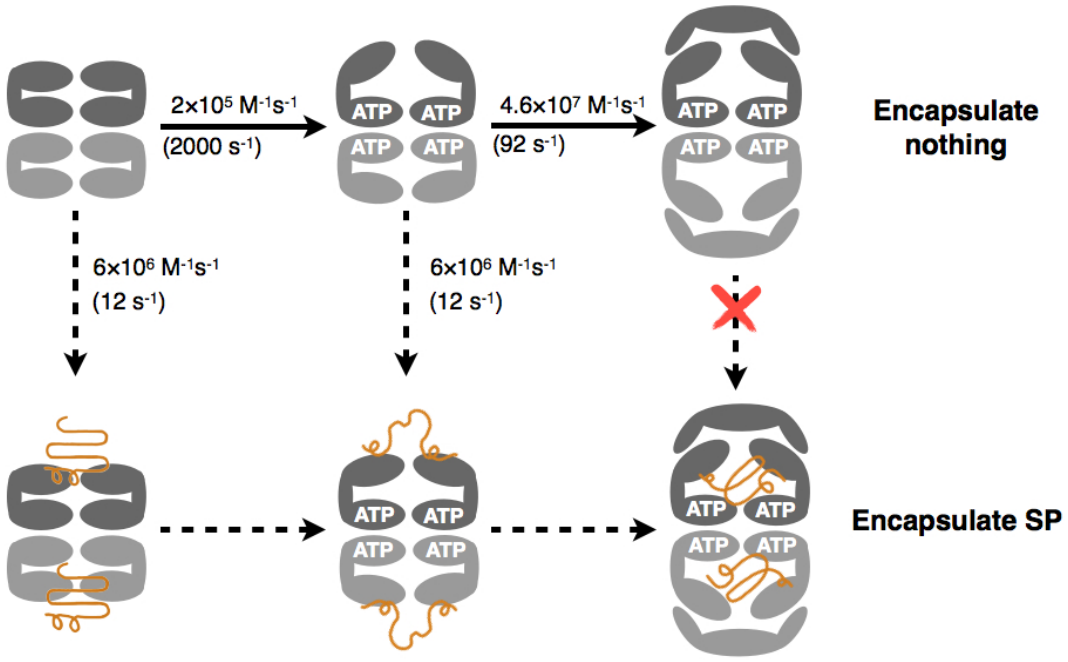

Figure 8-4: An alternative mechanism of chaperonin-nucleotide exchange (reproduced from [16]). This proposal [35] is based on the results of experiments performed in the absence of GroES and purports to describe the situation in vivo. The 2nd order rate constants are experimentally determined values; the pseudo-1st order constants in parenthesis were obtained using values for the [ATP] and [SP] in vivo in *E. coli* of 10mM and 2.6μM (set as equivalent to the in vivo $[GroEL]_7$) respectively [113-114]. However, this analysis is conceptually flawed for it fails to consider the subsequent binding of GroES and SP to the binary GroEL-ATP complex. Since the 2nd order rate constant for the binding of GroES to GroEL-ATP (4.6 x10^7 $M^{-1}s^{-1}$) is almost 10-fold greater than that for the binding of SP, this mechanism leads the formation of the biologically unproductive ternary complex, GroEL-ATP-GroES, which precludes the binding of SP.

In the set of experiments using the $dMDH^{QSY7}$/$GroES^{F5M}$ quench pair introduced above, ATP, $GroES^{F5M}$, $dMDH^{QSY7}$ were simultaneously presented to the acceptor state complex pre-incubated with BeF_3. After mixing, $GroES^{F5M}$ was present at a slight molar excess over GroEL ring while $[MDH^{QSY7}]$ varies. A control in which GroEL was **pre-incubated** with a molar equivalent of MDH^{QSY7} (to GroEL rings) before mixing with ATP, BeF_3 and $GroES^{F5M}$ established the maximum encapsulation, and all other measurements were normalized to it for calculating the % occupancy of GroEL ring by SP. The same experiments were repeated with three additional initiation states: the apo-

GroEL^{wt}, the apo-GroEL^{D398A}, and the resting state complex. In the first three cases where SP and ATP were introduced simultaneously to an empty GroEL ring, to occupy 50% of GroEL rings by SP, at least 4 fold of [MDH] over [$GroES_7$] is required (Figure 8-3B, the dashed line). This result, indicating a very poor encapsulation efficiency, is in good keeping with the fact that GroES can associate with GroEL much faster than SP does (2rd order rate constant of binding to GroEL by GroES ~$4\times10^7 M^{-1}s^{-1}$ [12, 40, 55], and by SP ~$6x10^6$ $M^{-1}s^{-1}$ [35, 110]; illustrated in Figure 8-4).

On the other hand, when ATP and MDH^{QSY7} were simultaneously presented to the resting state complex with ADP occupying the *trans* ring, efficient encapsulation of the MDH^{QSY7} is restored as evident from the much lower [MDH]/[$GroES_7$] ratio required to achieve half occupancy of GroEL rings by SP (Figure 8-3C dashed line, ~1.2) despite a slight drop of MDH affinity compared with that of the acceptor state complex (Figure 8-3C, the binding is no longer stoichiometric since the curve take a shape of an isotherm). The contrast of SP encapsulation efficiency between these two groups of very similar experiments highlights the fact that premature ATP binding and inefficient SP encapsulation can be effectively prevented by the slow dissociation of ADP remaining from the previous cycle. A similar conclusion can also be drawn by noticing that the green trace in Figure 8-2B (SP and ATP/GroES simultaneously presented to the resting state complex *trans* ring) almost overlaps with the purple trace (SP pre-incubated with the *trans* ring of the acceptor complex). Moreover, in response to the assertion made in [35, 110], with SP binding preceding ATP binding, it is still possible for GroEL to do its work in disrupting any residual non-native structural elements left on SP as predicted by the active refolding theory.

8.3.3 Probing the benefits of chaperonin turnover Rapid turnover is another important feature when GroEL functions in the symmetric cycle. It is ultimately driven by ATP hydrolysis induced BoS (breakage of symmetry) with a rate of ~$0.5s^{-1}$. It is intriguing to ask why nature design this molecular machine in such a way: since refolding of SP usually takes up to minutes to be completed [27, 64, 115], it is hardly justifiable for this huge energy cost (in the form of ATP) if what GroEL does is just to encapsulate SP to create an aggregation-free environment for spontaneous refolding to occur.

Based on what is known about the chaperonins, one potential benefit bestowed by rapid turnover may come from the iterative annealing effect, i.e., as GroEL turnover, SPs are subject to rounds of unfolding (powered by ATP binding) and refolding (when they are encapsulated or released into the solution) to optimize the search for the folding global minimum. Indeed, Rye et.al. have found that Rubisco refolds approximately two times faster in the presence of 'actively turning over' chaperonins than being simply encapsulated [112]. This modest refolding rate enhancement can at least partially account for the cost of extra energy associated with a turning over system.

Another source of potential benefit for operating a dynamic system rather than a static one is that by turning over, GroEL can visit and mediate refolding of multiple SP molecules and the faster the turnover rate the more SPs it can process in a given amount of time. If the above assumption is correct, one should expect that even sub-stoichiometric amount of GroEL can do just as well as using molar excess of GroEL over SP for recovery of lost SP activity. This is exactly what we see from the replot of a previously published result on GroEL-assisted Rubisco refolding [64] (Figure 8-5). If each GroEL ring can only exert its influence on refolding of a single Rubisco, we would

expect the yield of refolded SP to rise linearly as the $[GroEL]_7$/[SP] increases and then plateau as $[GroEL]_7$/[SP] rise over 1 (as the dashed line in Figure 8-5A shows). In reality, we see the yield of Rubisco refolding rises hyperbolically and the area between the dashed line and the actual data points can be interpreted as the benefits brought about by turnover. This strongly indicates that GroEL can productively mediate multiple SP refolding by operating in the highly dynamic, turning over symmetric cycle.

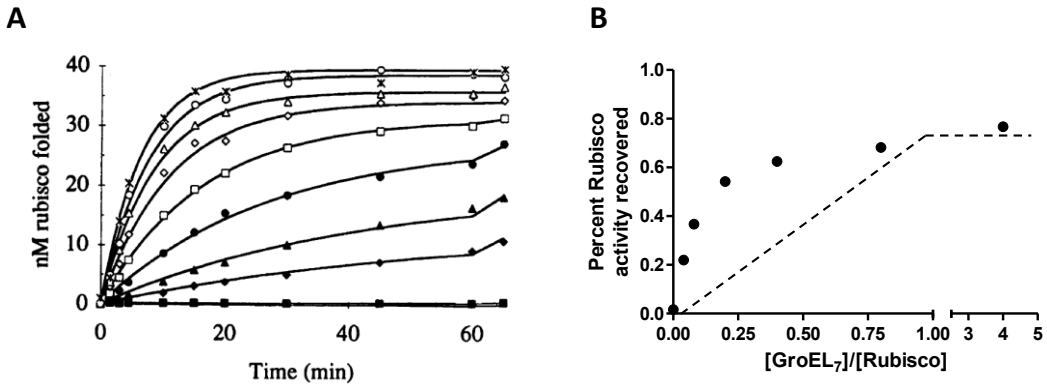

Figure 8-5: GroEL can handle refolding of multiple Rubisco molecules under turning over conditions. (A) Rubisco refolding assay results taken from Mathew Todd et.al [64]. **(B)** The final yield of Rubisco recovered (beyond 60min) was plotted against the corresponding $[GroEL]_7$/[Rubisco] applied. The dashed line shows what the yield of Rubisco is supposed to look like if the assay were repeated with a static chaperonin system (e.g. SR1).

To test if what is observed with Rubisco can also be applied to other chaperonin SPs, I performed a set of similar analysis with MDH which is known to form relatively stable mis-folded state after diluting from denaturant (also confirmed in Figure 8-6D). The results are shown in Figure 8-6. It is immediately apparent that the same principle applies to MDH as well: though MDH refolding occurs faster as higher $[GroEL_7]$/[SP] is applied (Figure 8-6A), the final yield of active MDH remains largely unaltered even as little as one $GroEL_7$ per ten dMDH was employed under turning over conditions (red, Figure 8-6C). On the other hand, when SR1 (not capable of turnover) was used, only

stoichiometric amount of native MDH can be recovered (blue, Figure 8-6C). In addition, if the refolding assay performed at [GroEL$_7$]/[SP]=1/10 was repeated in the presence of an ATP-depletion system (10unit HK plus 10mM Glucose), we've found a dramatic drop of the final yield of MDH activity from ~70% to ~20%, the latter only slightly higher than that of the spontaneous MDH refolding (Figure 8-6C, inset). Such observation further underlines the benefits brought about by a turning-over system. Being able to mediate refolding of multiple SPs in a short time period may be critical in the normal functionality of the *GroE* for cell survival from heat stress, which is discussed in greater detail in the following section.

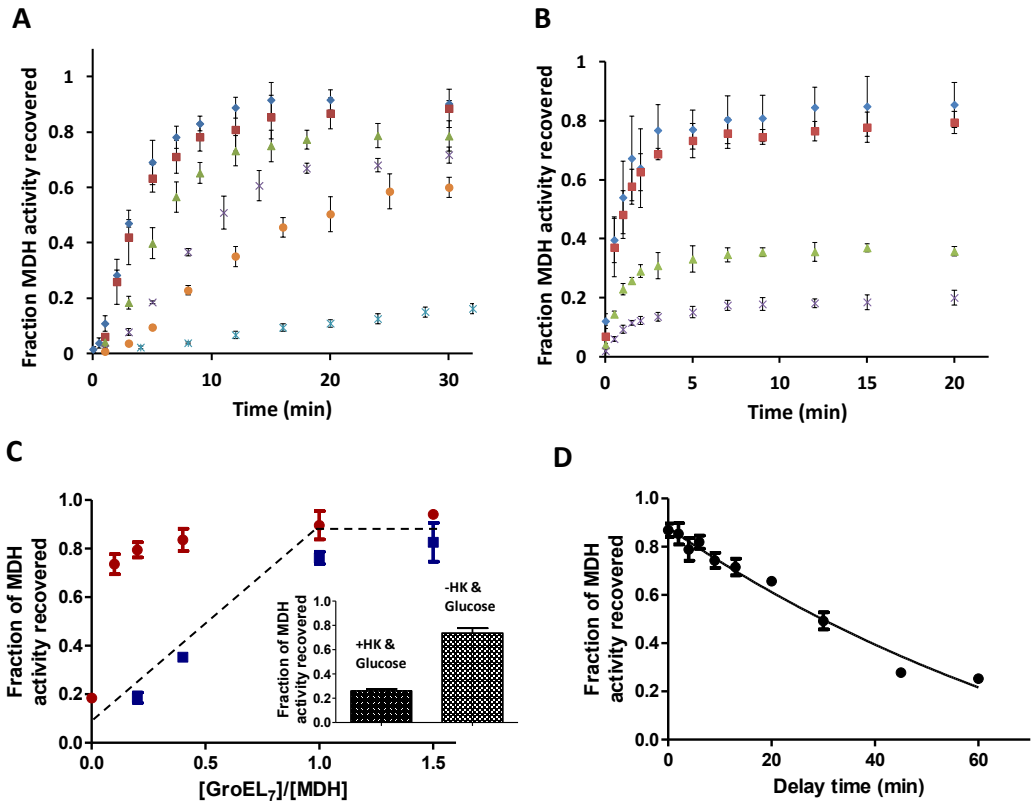

Figure 8-6: Time course of GroEL (A) or SR1 (B) mediated MDH refolding. The experiments were performed as described in Section 6.2.3. The concentrations of GroEL$_7$ or SR1$_7$ applied are: blue, 0.75μM; red, 0.5μM; green, 0.2μM; purple, 0.1μM; orange, 0.05μM. light blue is MDH spontaneous refolding. **(C)** Fraction of MDH recovered is plotted against corresponding [GroEL]$_7$/[MDH] applied. Red, GroEL-mediated MDH

refolding, and blue, the SR1-mediated. The dashes line shows what the yield of MDH is supposed to look like if the assay were repeated with a static chaperonin system. It traces very well with the experimental points of MDH refolding in the presence of SR1. *Inset* shows the consequence of turning a dynamic system into a static one by removing ATP with HK and glucose. Both were performed with $[GroEL]_7$/[MDH]=0.1. **(D)** The spontaneous MDH refolding was initiated by diluting urea 100 fold with refolding buffer (Section 6.2.3) plus 12.5μM GroES subunit and 1mM ATP, and after a delay time, 7μM GroEL subunit was introduced. The same [MDH] was applied as in A and B. This is to probe the kinetics of formation of irreversible aggregates that render MDH irredeemable. The data points were fitted with a single exponential decay with a rate constant of $0.010\pm0.007 min^{-1}$. All the error bars shown in the figure are standard deviations of three independent repeats.

8.4 Discussion

When GroEL shifts gear from the asymmetric cycle to the symmetric cycle by the presence of SP, this molecular machine makes two important adjustments: the symmetric complex becomes the predominant species and the overall turnover rate increases approximately 5 fold from $\sim0.1s^{-1}$ limited by spontaneous ADP release in the asymmetric cycle to $\sim0.5s^{-1}$ for BoS to occur in the symmetric cycle. Work presented in this chapter demonstrates that accompanying the first adjustment made by the chaperonin system, GroEL turns into a parallel processing machine with both rings available for SP encapsulation (Section 6.3.1) and are capable of processing SP refolding, possibly via an active refolding mechanism (Section 6.3.2). It is beyond the scope of this thesis to investigate if GroEL does refold SP via the active refolding mechanism, but the work presented here reveals a delicately designed timing mechanism which, at least, permits GroEL to actively mediate refolding of its SP: slow spontaneous release of ADP from GroEL *trans* ring prevents premature ATP binding, and it is only after SP binds to the *trans* ring that ADP quickly dissociates followed by ATP binding and GroES binding. Therefore, as long as these conditions prevail, the spontaneous release of ADP is slow, the order of ligand arrival will always be SP first, and then ATP, followed by GroES. In

this order, it will not only allow SP to be subject to the stretching force generated by ATP-binding-induced GroEL conformational change, prerequisite for active refolding to occur (the fact that such conformational change can do work is demonstrated by my colleague Nicolas Corsepius [63], and the benefits it brings about in SP refolding is reported in [112]), but also it guarantees efficient SP encapsulation as shown in Figure 8-3 and 8-4.

As the other important feature of the GroEL symmetric cycle, turning over at a faster pace is just as important as populating in the symmetric state in adjusting the *GroE* system fit for its duty, i.e. assisting refolding of denatured SPs. The active refolding of SP by GroEL is achieved by first forcefully unfolding SPs to rescue them from kinetically trapped states. And then, unfolded SPs are released from its binding site and encapsulated briefly in the enclosed chamber formed between both GroEL rings and GroESs. SPs committed to reaching their native states tend to have lower affinity for GroEL and are less likely to be re-captured, while SPs fall again into the kinetic trap will have to be recaptured and go through the same iteration for another trial to reach their native conformations. It is therefore formulated as the iterative annealing mechanism [64]. From it, one obvious benefit for turning over at a higher rate is to give SPs as many chances as possible to be refolded before formation of irreversible aggregates.

Another source of benefit lies upon the ability of a turning over system to mediate multiple SPs refolding at very short time intervals determined by the turnover rate. This is by no means to say that these two benefits can be separated, but rather they are very closely related. If the only thing GroEL did was to create a segregated environment free of aggregation, then we would not be able to observe the much greater final yield

associated with the turning over system when sub-stoichiometric amount of $GroEL_7$ to SP was applied. This is simply because the duration of encapsulation is much shorter than that of SP refolding. Consequently, after each round of GroEL functional cycle, most of the SP emerged from the GroEL cavity would be no different from before encapsulation. Therefore, the fact that we do observe much higher final yield under turning over conditions with substoichiometric amount of $GroEL_7$ to SP strongly indicates that GroEL must be able to do something more than just passively segregating SPs so that when SP emerges from each round of turnover, it is quite different from what it was before. The forceful unfolding could be one such mechanism that allows SP to progress dramatically forward to reach the native state after being rescued from kinetic traps. Another possible candidate could be the active breaking down of lower order reversible aggregates into denatured monomer by GroEL in the case of MDH as suggested by Clarke et.al [115].

We do notice that both Rubisco and MDH can form relatively stable mis-folded state without collapsing into high order aggregates after removal of denaturant for a fair amount of time (for Rubisco, [64]; for MDH, Figure 8-6D). For SPs that can rapidly form irreversible aggregates such as rhodanese [116], sub-stoichiometric amount of GroEL may not work as well as the stoichiometric one. This is because when aggregate formation occurs at a rate comparable to the turnover rate, it poses a very high demand for GroEL at any time in preventing aggregate formation which is mainly achieved via passive segregation of SP. However, this is not to say that the benefits carried by rapid turnover of the chaperonin system are only limited to a certain category of SPs under some selected *in-vitro* conditions. *In vivo*, GroEL/ES are known to work hand in hand with other classes of chaperones such as DnaJ/K system, ClpB, and small Hsps (IbpA,

IbpB etc.) [117]. In particular, the expression level of small Hsps is known to be sensitive to temperature increase [118-119]. Under heat stress, these small chaperones are considered to play a major role in capturing denatured proteins to prevent formation of large aggregates [117]. Given the relatively low abundance of GroEL molecule within cells (~2.6μM in rings [114]) in comparison with the total *in-vivo* protein concentration (350mg/ml [120]), the maximum amount of SP GroEL/ES can handle can be estimated as follows: 2.6μM × 60kDa (the biggest SP GroEL can encapsulate)=0.16mg/ml. Approximately 30% of the total protein population can be recognized by GroEL in denatured states [124]. Even if assuming there are 100 fold increases of the [GroEL/ES] as a result of heat shock induced expression, it only makes up 1/7 of all potential SPs that require chaperonins' assistance. To be able to cope with the rest 6/7, the chaperonins have to turnover rapidly in order to accomplish the refolding of multiple SPs. However, under these *in-vivo* conditions, the success of the task does not rely on SPs forming a relatively stable mis-folded state as in the case of Rubisco and MDH, but is dependent on the action of the small Hsp proteins that capture and prevent formation of irreversible aggregates for maintaining a dynamic pool of denatured but folding-competent SPs. The collaboration between GroEL/ES and small Hsps, therefore, extends what can be achieved beyond the limit of both as individuals, and as we can see is critical for cell survival of heat stress.

Chapter 9: Summary and future perspectives

At the height of classical physics, Lord Kelvin once remarked 'there is nothing new to be discovered in physics now. All that remains is more and more precise measurement' (on the annual meeting of the British Association for the Advancement of Science, 1900). However, this was followed by the era of quantum physics and theory of relativity. Though on a much humbler ground, we believe we are in a very similar situation: after years of research work, it is quite remarkable to have so many surprises born out of research on the *GroE*. The work presented in this dissertation not only helps to resolve some of the long standing disputes in this field but also reveals a few interesting leads that may inspire future research to reveal the hidden secrets of the chaperonins.

The fundamentally important GroEL functional cycle is the primary research subject dealt with by this dissertation with especially emphasis on the three aspects in dispute of the cycle, e.g. the identity of the rate determining step, the physiological order of arrival of ligands (ATP, SP and GroES) to GroEL trans-ring, and the role of the symmetric GroEL-$GroES_2$ "football" complex in the overall chaperonin cycle. To achieve such goal, multiple spectroscopic probes were employed to determine the pre-steady state kinetics of the chaperonin cycle, i.e. ATP hydrolysis, release of hydrolysis product ADP, and formation of GroEL/ES complexes. From the multi-facet pre-steady state kinetic survey (Chapter 3 to 5, and 8) and inspired by our colleagues [46], we propose a two cycle model to account how the GroE-optimized SP refolding is achieved via its functional cycle: *i)* in the absence of SP, ADP release is the rate-determining step (RDS) of the whole cycle and consequently, the asymmetric GroEL-$GroES_1$,"bullet" which

precedes this step, is the pre-dominant species; *ii)* in the presence of SP, the release of ADP is greatly accelerated while the intrinsic ATPase activity of GroEL remained unaffected, and consequently ATP hydrolysis becomes the RDS and the symmetric GroEL-$GroES_2$,"football" becomes the predominant species.

The release of ADP from the *trans* ring of GroEL is found to be the key regulatory step of the whole GroEL functional cycle. In the absence of SP, slow ADP release from the asymmetric resting-state complex [^{cis}GroEL-ADP-GroES : ^{trans}GroEL-ADP] prevents further ATP binding and hydrolysis. Binding of SP to this complex accelerates ADP release dramatically, permitting two important adjustments; *i)* rapid release of ADP allows GroEL nano-machine to turn over at its maximal rate, set by its intrinsic ATPase activity and *ii)* the change of the RDS alters the nature of predominant species; from an inert asymmetric resting state complex to a highly dynamic symmetric complex that can accommodate refolding of two SPs simultaneously. The GroEL-trans ring recruits SP first causing rapid ADP-ATP exchange, followed by association with GroES and encapsulation of SP into the 'folding chamber'.

The delicate design of this molecular machine underlying the two cycle model inspires us to further pursues how it turns over in the dynamic folding active symmetric cycle. The work can be ultimately phrased as solving a problem of breakage of symmetry (BoS). The work presented in chapter 6 demonstrates that BoS is caused by stochastic ATP hydrolysis among all 14 subunits between the two GroEL rings. Application of the binomial distribution theory allows deconvolution of the averaged ensemble into stochastically coexisting microscopic states which in turn makes it possible for us to pinpoint the critical ATP hydrolysis events that lead to BoS. The work that characterizes

the inter-ring communication mutant GroEL^{K105A} identifies it as one of the most critical site responsible for BoS (Chapter 7): its BoS can only occur 1000 times slower than that of the wild-type, and of all the free energy gain (27.6kJ/mol) by the GroEL/ES complex associated with hydrolysis of ATP and release of Pi, almost a half can be attributed to the drive for reforming the electrostatic interaction between the ε-amino group of K105 and the carbonyl group of A109 across the inter-ring plate (10.6kJ/mol).

One unsolved mystery born directly out of what we've learned about BoS is that there are likely more communication hubs involved other than K105. As discussed in more detail by the end of Chapter 7, the mode of action by K105 cannot account for all BoS events caused by ATP hydrolysis. By comparing the crystal structure of the symmetric complex with the asymmetric complex, my colleague Xue Fei has also identified change of a salt bridge of the 'right side' contact (R452-E461) [16]. This salt bridge breaks as BoS occurs. Given the fact that signal of ATP hydrolysis can be transmitted all the way from the equatorial domain to the apical domain to cause discharge of GroES, it is highly likely that such allostery can also be transmitted horizontally and vertically across the inter-ring interface which weaves a complex transmission network spreading all across the GroEL molecule and centered by the nucleotide binding pocket. Since we know very little about these allosteric transduction pathways, carefully designed mutagenesis survey instructed by structural characterization and molecular dynamic simulation study may help to ultimately reveal the secret of how this molecular machine utilizes the energy release by ATP binding and hydrolysis to do its work.

Another problem that has puzzled the field from the very beginning is that what GroEL does to assist refolding of its denature SPs. Though this dissertation cannot provide a straightforward answer to the question, I believe we are very close to it. As demonstrated in Chapter 5, the adjustment made by the *GroE* system in response to the presence of SP by turning over faster appears to favor the active refolding mechanism over the pure passive segregation one. In addition, the work presented in Chapter 8 shows that under turning over conditions, even sub-stoichiometric amount of chaperonins can rescue denatured SPs to a similar extend as the stoichiometric one can do. It indicates that GroEL must be able to do something more than just passive encapsulation to promote SP refolding. To find out what GroEL does, it is necessary to conduct a full-flank survey on how SP refolds both in the presence and absence of GroEL. A recent progress made on H/D exchange coupled to MS detection allows following H/D protection factor at the amino acid resolution as SP refolds [121-122], and its application in the GroEL-mediated SP refolding may eventually provide an answer to this question and put an end to the long standing dispute over it.

Appendix I: Residual plots for kinetic traces in Chapter 3

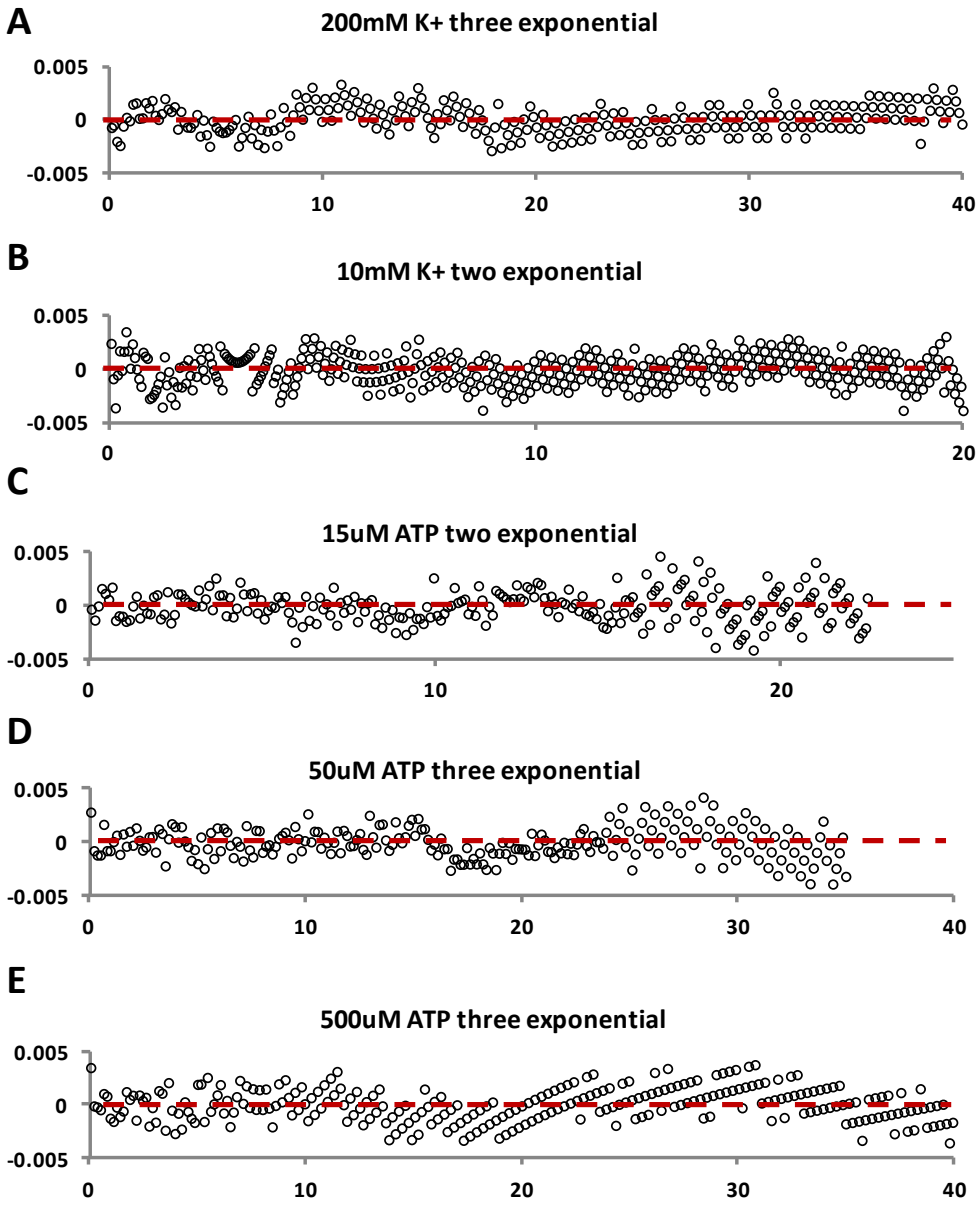

Figure A-1: Least squares error analysis of the experimental data shown in Figure 3-5. Plots A, D and E (at high [K^+] or high [ATP]) were fitted to an expression containing exponential terms for all three phases (lag, burst, delay) plus a linear steady state term. For plots B and C (at low [K^+] or low [ATP]) an expression containing two exponential terms (for the lag and burst phases) plus a linear steady state term, suffices. Under these conditions, the rates of the burst and of the delay approach one another (Figure 3-5 inset) and consequently cannot be kinetically resolved.

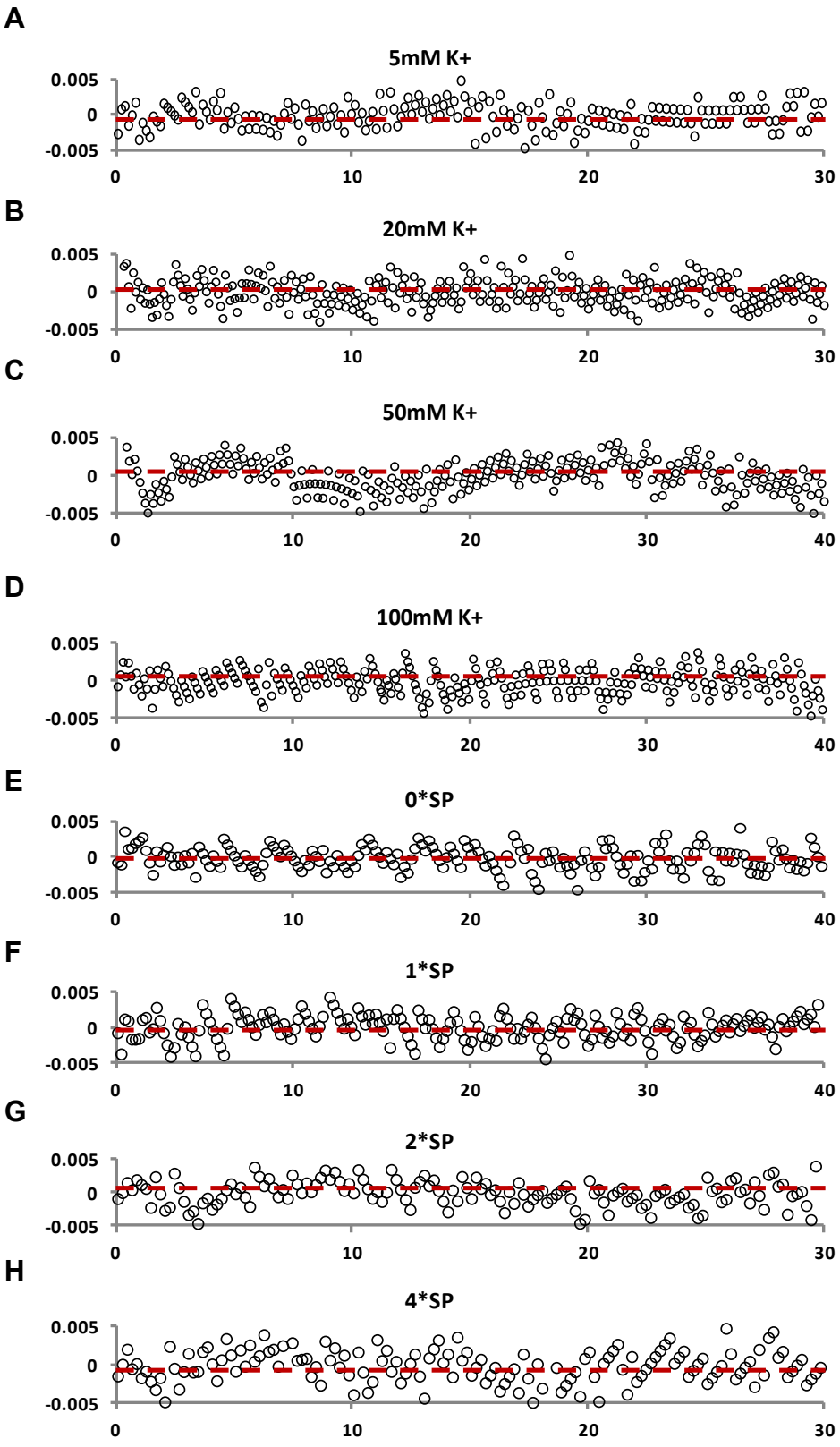

Figure A-2: Least squares error analysis of the experimental data shown in Figure 3-9.

Appendix II: ODE analysis of Pi release trajectory reveals an additional step responsible for ADP release in the GroEL functional cycle

A minimal kinetic scheme of GroEL catalyzed ATP hydrolysis was developed based on the appearance of the four phases as shown in Scheme 3-1.

Validation experiments were performed to confirm the assignment of the phases as discussed in more detail in the result section of this chapter. Confirmation was also done by fitting the experimental data with the following ODEs developed based on Scheme 3-1 to obtain the individual microscopic rate constant.

$$\frac{dA}{dt} = -A \cdot k_1 + D \cdot k_4$$
$$\frac{dB}{dt} = A \cdot k_1 - B \cdot k_2$$
$$\frac{dC}{dt} = B \cdot k_2 - C \cdot k_3$$
$$\frac{dD}{dt} = C \cdot k_3 - D \cdot k_4$$

, in which capital letter *A* to *D* stand for concentrations of the kinetic species as designated by the blue letter in Scheme 3-1. The ordinary differential equations are solved numerically by using Matlab 7.0 ODE solver *ode15s* and fit to the experimental data by using Matlab 7.0 function *lsqcurvefit*. The details of fitting and program scripts are provided in as follows:

```
function y=mech(t,x)% function file transcribing the ODEs into Matlab readable format %
global k;                                          % rate constant vector %
y(1)=-k(3)*x(1);                    % y is dconcentration/dt, and x is concentration %
y(2)=k(3)*x(1)-k(1)*x(2);
y(3)=k(1)*x(2)-k(2)*x(3);
y(4)=k(2)*x(3)-k(3)*x(4);
y(5)=k(3)*x(4)-k(1)*x(5);
y(6)=k(1)*x(5)-k(2)*x(6);
```

```
y(7)=-k(2)*x(2);
y=[y(1);y(2);y(3);y(4);y(5);y(6);y(7)];

function ysum=fitdata(a,x)                % function file globally fit the two set of data %
global k;                                                          % rate constant vector %
k(1)=a(1);
k(2)=a(2);
k(3)=a(3);
 time=[];
[t1,y1]=ode15s(@mech,time,[a(4),0,0,0,0,0,0]);
[t2,y2]=ode15s(@mech,time,[0,a(5),0,0,0,0,0]);
lamda=a(6);
rest=y1(:,3) +y1(:,4)+y1(:,5)*(lamda+1);          % simulate resting state FRET trace %
acceptor=y2(:,3)+y2(:,4)+y2(:,5)*(lamda+1);    % simulate acceptor state FRET trace %
ysum=[rest;acceptor];
```

Load the two variable vectors *time* and *expdata* (experimental data) in the form:

```
time/expdata=[rest;acceptor];
```

into Matlab workspace. Then execute the following scripts sequentially:

```
options=optimset('MaxFunEvals',4500,'MaxIter',5000,'Jacobian','on');
 % adjust function Isqcurvefit performance %

 [x,resnorm,residual,exitflag,output,lambda,jacobian]=lsqcurvefit(@fitdata,[initial   value
for fit],time,expdata,[lower limit of parameter search],[ upper limit of parameter search]);
% call function Isqcurvefit to optimize the user-defined function fitdata %

[sigma2, stder, Corr] = NLRStat(resnorm, jacobian)          % use to calculate sum of
square of residuals (sigma2), standard deviations (stder) and correlation matrix (Corr) %
```

Due to the fact that the four phases of Pi release trajectory are well separated from each other, the rates obtained by fitting the data with Equation 1 can be used as microscopic rate constant for individual step especially for the burst phase and the delay phase. The following ODE analysis were conducted to extract individual microscopic rate constant and the results are compared with the rates of the four phases to test if the usage of the latter as subjugate of the former is justifiable.

	k_1/lag phase rate	k_2/burst phase rate	k_3/delay phase rate	k_4/steady-state rate	*[Pi]:[EL]*/burst amplitude
ODE analysis	11.1±0.7	0.484±0.004	0.224±0.006	0.0294±0.001	0.46±0.02
Exp analysis	11.3±0.9	0.514±0.005	0.145±0.009	0.01209±0.00003	0.495±0.005

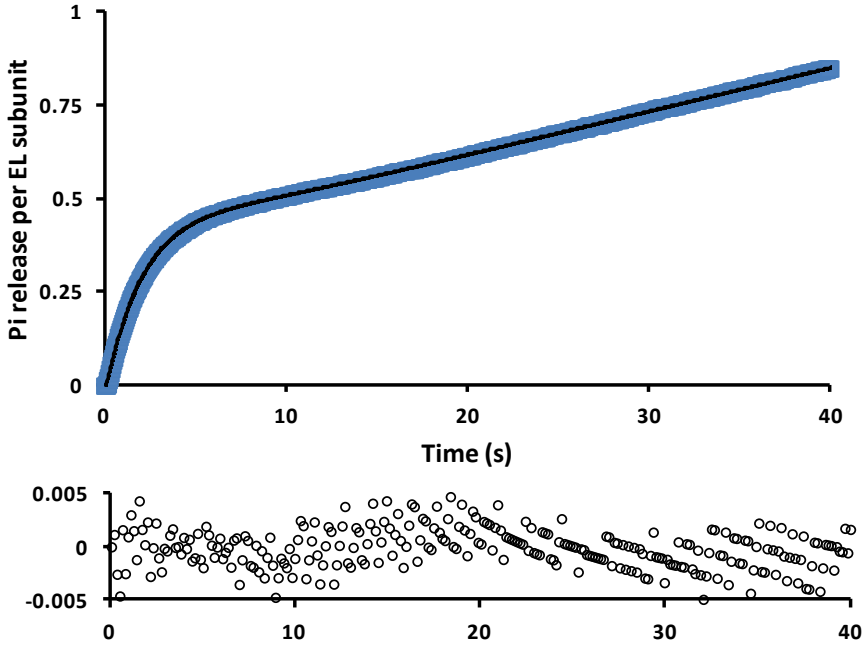

Figure A-3: ODE analysis of the Pi release trajectory. The data shown in Figure 3-3 was fitted with the ODEs developed based on Scheme 3-1 as described in Section 3.2.4. The blue trace is the experimental data and the black curve is the ODE fitting line. The results obtained by both methods were presented and compared in the table above the data plot. The residuals of the ODE fitting were plotted in lower panel.

It appears from the table in Figure A-3 that the two sets of rate constants obtained in different ways agree with each other very well, and thus it is legitimate to use the two sets of rate constant interchangeable. However, I do notice that there is an additional conformation change step included in the ODE analysis between the hydrolysis of ATP and release of ADP (the minimal kinetic model in Scheme 3-1). This additional step is indispensible in modeling the delay phase of the Pi release trajectory. Although in our exponential analysis we assign the delay phase as the ADP release step, in actuality, it could be either ADP release or the slow conformation change that eventually leads to ADP release. Based on the similarity of the value of rate constant, here I re-assign the

delay phase to this conformational change step which is indistinguishable from the actual ADP release step by merely following Pi release. However, experimental evidence is presented in Chapter 4 for the existence of this elusive conformational change by directly measuring ADP release from GroEL molecule.

References

1. Rasmussen, B.F., et al., *Crystalline ribonuclease A loses function below the dynamical transition at 220 K.* Nature, 1992. **357**(6377): p. 423-4.

2. Zavodszky, P., et al., *Adjustment of conformational flexibility is a key event in the thermal adaptation of proteins.* Proc Natl Acad Sci U S A, 1998. **95**(13): p. 7406-11.

3. Tsou, C.L., *Active site flexibility in enzyme catalysis.* Ann N Y Acad Sci, 1998. **864**: p. 1-8.

4. Fersht, A., *Structure and Mechanism in Protein Science*. fourth ed. 2002, New York: W.H.Freeman and Company. P 536.

5. Taverna, D.M. and R.A. Goldstein, *Why are proteins marginally stable?* Proteins, 2002. **46**(1): p. 105-9.

6. Onuchic, J.N., Z. Luthey-Schulten, and P.G. Wolynes, *Theory of protein folding: the energy landscape perspective.* Annu Rev Phys Chem, 1997. **48**: p. 545-600.

7. Hartl, F.U., A. Bracher, and M. Hayer-Hartl, *Molecular chaperones in protein folding and proteostasis.* Nature, 2011. **475**(7356): p. 324-32.

8. Lorimer, G.H., *A personal account of chaperonin history.* Plant Physiol, 2001. **125**(1): p. 38-41.

9. Fenton, W.A. and A.L. Horwich, *Chaperonin-mediated protein folding: fate of substrate polypeptide.* Q Rev Biophys, 2003. **36**(2): p. 229-56.

10. Lin, Z. and H.S. Rye, *GroEL-mediated protein folding: making the impossible, possible.* Crit Rev Biochem Mol Biol, 2006. **41**(4): p. 211-39.

11. Horovitz, A. and K.R. Willison, *Allosteric regulation of chaperonins.* Curr Opin Struct Biol, 2005. **15**(6): p. 646-51.

12. Ye, X. and G.H. Lorimer, *Substrate protein switches GroE chaperonins from asymmetric to symmetric cycling by catalyzing nucleotide exchange.* Proc Natl Acad Sci U S A, 2013. **110**(46): p. E4289-97.

13. Yang, D., X. Ye, and G.H. Lorimer, *Symmetric GroEL:GroES2 complexes are the protein-folding functional form of the chaperonin nanomachine.* Proc Natl Acad Sci U S A, 2013. **110**(46): p. E4298-305.

14. Xu, Z., A.L. Horwich, and P.B. Sigler, *The crystal structure of the asymmetric GroEL-GroES-(ADP)7 chaperonin complex.* Nature, 1997. **388**(6644): p. 741-50.

15. Chen, L. and P.B. Sigler, *The crystal structure of a GroEL/peptide complex: plasticity as a basis for substrate diversity.* Cell, 1999. **99**(7): p. 757-68.

16. Fei, X., et al., *Formation and structures of GroEL:GroES2 chaperonin footballs, the protein-folding functional form.* Proc Natl Acad Sci U S A, 2014. **111**(35): p. 12775-80.

17. Bartolucci, C., et al., *Crystal structure of wild-type chaperonin GroEL.* J Mol Biol, 2005. **354**(4): p. 940-51.

18. Boisvert, D.C., et al., *The 2.4 A crystal structure of the bacterial chaperonin GroEL complexed with ATP gamma S.* Nat Struct Biol, 1996. **3**(2): p. 170-7.

19. Hunt, J.F., et al., *The crystal structure of the GroES co-chaperonin at 2.8 A resolution.* Nature, 1996. **379**(6560): p. 37-45.

20. Ranson, N.A., et al., *ATP-bound states of GroEL captured by cryo-electron microscopy.* Cell, 2001. **107**(7): p. 869-79.

21. Fei, X., et al., *Crystal structure of a GroEL-ADP complex in the relaxed allosteric state at 2.7 A resolution.* Proc Natl Acad Sci U S A, 2013. **110**(32): p. E2958-66.

22. Horovitz, A., et al., *Review: allostery in chaperonins.* J Struct Biol, 2001. **135**(2): p. 104-14.

23. Lin, Z., F.P. Schwartz, and E. Eisenstein, *The hydrophobic nature of GroEL-substrate binding.* J Biol Chem, 1995. 270(3): p. 1011-4.

24. Viitanen, P.V., et al., *Chaperonin-facilitated refolding of ribulosebisphosphate carboxylase and ATP hydrolysis by chaperonin 60 (groEL) are K+ dependent.* Biochemistry, 1990. **29**(24): p. 5665-71.

25. Clark, A.C., B.S. Karon, and C. Frieden, *Cooperative effects of potassium, magnesium, and magnesium-ADP on the release of Escherichia coli dihydrofolate reductase from the chaperonin GroEL.* Protein Sci, 1999. **8**(10): p. 2166-76.

26. Todd, M.J., P.V. Viitanen, and G.H. Lorimer, *Hydrolysis of adenosine 5'-triphosphate by Escherichia coli GroEL: effects of GroES and potassium ion.* Biochemistry, 1993. **32**(33): p. 8560-7.

27. Goloubinoff, P., et al., *Reconstitution of active dimeric ribulose bisphosphate carboxylase from an unfoleded state depends on two chaperonin proteins and Mg-ATP.* Nature, 1989. **342**(6252): p. 884-9.

28. Yifrach, O. and A. Horovitz, *Nested cooperativity in the ATPase activity of the oligomeric chaperonin GroEL.* Biochemistry, 1995. **34**(16): p. 5303-8.

29. Monod, J., J. Wyman, and J.P. Changeux, *On the Nature of Allosteric Transitions: A Plausible Model.* J Mol Biol, 1965. **12**: p. 88-118.

30. Koshland, D.E., Jr., G. Nemethy, and D. Filmer, *Comparison of experimental binding data and theoretical models in proteins containing subunits.* Biochemistry, 1966. **5**(1): p. 365-85.

31. Gresham, J.S., *Allostery and GroEL: Exploring the tenets of nested cooperativity*, in *Chemistry and Biochemistry*. 2004, University of Maryland: College Park.

32. Grason, J.P., *Allostery in GroEL: Its role in the refolding of protein substrates*, in *Chemistry and Biochemistry*. 2003, University of Maryland: College Park.

33. Poso, D., A.R. Clarke, and S.G. Burston, *A kinetic analysis of the nucleotide-induced allosteric transitions in a single-ring mutant of GroEL.* J Mol Biol, 2004. **338**(5): p. 969-77.

34. Sewell, B.T., et al., *A mutant chaperonin with rearranged inter-ring electrostatic contacts and temperature-sensitive dissociation.* Nat Struct Mol Biol, 2004. **11**(11): p. 1128-33.

35. Tyagi, N.K., W.A. Fenton, and A.L. Horwich, *GroEL/GroES cycling: ATP binds to an open ring before substrate protein favoring protein binding and production of the native state.* Proc Natl Acad Sci U S A, 2009. **106**(48): p. 20264-9.

36. Tyagi, N.K., W.A. Fenton, and A.L. Horwich, *ATP-triggered ADP release from the asymmetric chaperonin GroEL/GroES/ADP7 is not the rate-limiting step of the GroEL/GroES reaction cycle.* FEBS Lett, 2010. **584**(5): p. 951-3.

37. Yifrach, O. and A. Horovitz, *Allosteric control by ATP of non-folded protein binding to GroEL.* J Mol Biol, 1996. **255**(3): p. 356-61.

38. Horwich, A.L., *Protein folding in the cell: an inside story.* Nat Med, 2011. **17**(10): p. 1211-6.

39. Grason, J.P., et al., *Setting the chaperonin timer: the effects of K+ and substrate protein on ATP hydrolysis.* Proc Natl Acad Sci U S A, 2008. **105**(45): p. 17334-8.

40. Grason, J.P., J.S. Gresham, and G.H. Lorimer, *Setting the chaperonin timer: a two-stroke, two-speed, protein machine.* Proc Natl Acad Sci U S A, 2008. **105**(45): p. 17339-44.

41. Madan, D., Z. Lin, and H.S. Rye, *Triggering protein folding within the GroEL-GroES complex.* J Biol Chem, 2008. **283**(46): p. 32003-13.

42. Lorimer, G., *Protein folding. Folding with a two-stroke motor.* Nature, 1997. **388**(6644): p. 720-1, 723.

43. Schmidt, M., et al., *Symmetric complexes of GroE chaperonins as part of the functional cycle.* Science, 1994. **265**(5172): p. 656-9.

44. Todd, M.J., P.V. Viitanen, and G.H. Lorimer, *Dynamics of the chaperonin ATPase cycle: implications for facilitated protein folding.* Science, 1994. **265**(5172): p. 659-66.

45. Sameshima, T., et al., *Football- and bullet-shaped GroEL-GroES complexes coexist during the reaction cycle.* J Biol Chem, 2008. **283**(35): p. 23765-73.

46. Sameshima, T., et al., *Denatured proteins facilitate the formation of the football-shaped GroEL-(GroES)2 complex.* Biochem J, 2010. **427**(2): p. 247-54.

47. Llorca, O., et al., *The formation of symmetrical GroEL-GroES complexes in the presence of ATP.* FEBS Lett, 1994. **345**(2-3): p. 181-6.

48. Azem, A., et al., *The protein-folding activity of chaperonins correlates with the symmetric GroEL14(GroES7)2 heterooligomer.* Proc Natl Acad Sci U S A, 1995. **92**(26): p. 12021-5.

49. Corrales, F.J. and A.R. Fersht, *Kinetic significance of GroEL14.(GroES7)2 complexes in molecular chaperone activity.* Fold Des, 1996. **1**(4): p. 265-73.

50. Sparrer, H., K. Rutkat, and J. Buchner, *Catalysis of protein folding by symmetric chaperone complexes.* Proc Natl Acad Sci U S A, 1997. **94**(4): p. 1096-100.

51. Llorca, O., et al., *Symmetric GroEL-GroES complexes can contain substrate simultaneously in both GroEL rings.* FEBS Lett, 1997. **405**(2): p. 195-9.

52. Hayer-Hartl, M.K., J. Martin, and F.U. Hartl, *Asymmetrical interaction of GroEL and GroES in the ATPase cycle of assisted protein folding.* Science, 1995. **269**(5225): p. 836-41.

53. Hayer-Hartl, M.K., K.L. Ewalt, and F.U. Hartl, *On the role of symmetrical and asymmetrical chaperonin complexes in assisted protein folding.* Biol Chem, 1999. **380**(5): p. 531-40.

54. Behlke, J., O. Ristau, and H.J. Schonfeld, *Nucleotide-dependent complex formation between the Escherichia coli chaperonins GroEL and GroES studied under equilibrium conditions.* Biochemistry, 1997. **36**(17): p. 5149-56.

55. Rye, H.S., et al., *GroEL-GroES cycling: ATP and nonnative polypeptide direct alternation of folding-active rings.* Cell, 1999. **97**(3): p. 325-38.

56. Rye, H.S., et al., *Distinct actions of cis and trans ATP within the double ring of the chaperonin GroEL.* Nature, 1997. **388**(6644): p. 792-8.

57. Horwich, A.L., G.W. Farr, and W.A. Fenton, *GroEL-GroES-mediated protein folding.* Chem Rev, 2006. **106**(5): p. 1917-30.

58. Koike-Takeshita, A., M. Yoshida, and H. Taguchi, *Revisiting the GroEL-GroES reaction cycle via the symmetric intermediate implied by novel aspects of the GroEL(D398A) mutant.* J Biol Chem, 2008. **283**(35): p. 23774-81.

59. Georgescauld, F., et al., *GroEL/ES chaperonin modulates the mechanism and accelerates the rate of TIM-barrel domain folding.* Cell, 2014. **157**(4): p. 922-34.

60. Horwich, A.L., A.C. Apetri, and W.A. Fenton, *The GroEL/GroES cis cavity as a passive anti-aggregation device.* FEBS Lett, 2009. **583**(16): p. 2654-62.

61. Shtilerman, M., G.H. Lorimer, and S.W. Englander, *Chaperonin function: folding by forced unfolding.* Science, 1999. **284**(5415): p. 822-5.

62. Lin, Z., D. Madan, and H.S. Rye, *GroEL stimulates protein folding through forced unfolding.* Nat Struct Mol Biol, 2008. **15**(3): p. 303-11.

63. Corsepius, N.C. and G.H. Lorimer, *Measuring how much work the chaperone GroEL can do.* Proc Natl Acad Sci U S A, 2013. **110**(27): p. E2451-9.

64. Todd, M.J., G.H. Lorimer, and D. Thirumalai, *Chaperonin-facilitated protein folding: optimization of rate and yield by an iterative annealing mechanism.* Proc Natl Acad Sci U S A, 1996. **93**(9): p. 4030-5.

65. Brune, M., et al., *Mechanism of inorganic phosphate interaction with phosphate binding protein from Escherichia coli.* Biochemistry, 1998. **37**(29): p. 10370-80.

66. Brune, M., et al., *Direct, real-time measurement of rapid inorganic phosphate release using a novel fluorescent probe and its application to actomyosin subfragment 1 ATPase.* Biochemistry, 1994. **33**(27): p. 8262-71.

67. Kreuzer, K.N. and C.V. Jongeneel, *Escherichia coli phage T4 topoisomerase.* Methods Enzymol, 1983. **100**: p. 144-60.

68. Corsepius, N.C., *Experimental, computational, and theoretical analysis of the GroEL-GroES catalytically cycle.* 2014, University of Maryland: College Park.

69. Clark, A.C., R. Ramanathan, and C. Frieden, *Purification of GroEL with low fluorescence background.* Methods Enzymol, 1998. **290**: p. 100-18.

70. Voziyan, P.A. and M.T. Fisher, *Chaperonin-assisted folding of glutamine synthetase under nonpermissive conditions: off-pathway aggregation propensity does not determine the co-chaperonin requirement.* Protein Sci, 2000. **9**(12): p. 2405-12.

71. Eisenstein, E., P. Reddy, and M.T. Fisher, *Overexpression, purification, and properties of GroES from Escherichia coli.* Methods Enzymol, 1998. **290**: p. 119-35.

72. Zondlo, J., et al., *Monomer-heptamer equilibrium of the Escherichia coli chaperonin GroES.* Biochemistry, 1995. **34**(33): p. 10334-9.

73. Okazaki, A., et al., *The chaperonin GroEL does not recognize apo-alpha-lactalbumin in the molten globule state.* Nat Struct Biol, 1994. **1**(7): p. 439-46.

74. Johnson, K.A., *Kinetic Analysis of Macromolecules: A Practical Approach* first ed. The Practical Approach Series, ed. K.A. Johnson. 2003: Oxford University Press.

75. Paul F. Cook, W.W.C., *Enzyme Kinetics and Mechanism*. first ed. 2007: Garland Science.

76. Ueno, T., et al., *GroEL mediates protein folding with a two successive timer mechanism.* Mol Cell, 2004. **14**(4): p. 423-34.

77. Cliff, M.J., et al., *A kinetic analysis of the nucleotide-induced allosteric transitions of GroEL.* J Mol Biol, 1999. **293**(3): p. 667-84.

78. Geladopoulos, T.P., T.G. Sotiroudis, and A.E. Evangelopoulos, *A malachite green colorimetric assay for protein phosphatase activity.* Anal Biochem, 1991. **192**(1): p. 112-6.

79. Hirshberg, M., et al., *Crystal structure of phosphate binding protein labeled with a coumarin fluorophore, a probe for inorganic phosphate.* Biochemistry, 1998. **37**(29): p. 10381-5.

80. Shabala, L., et al., *Ion transport and osmotic adjustment in Escherichia coli in response to ionic and non-ionic osmotica.* Environ Microbiol, 2009. **11**(1): p. 137-48.

81. Terada, T.P. and K. Kuwajima, *Thermodynamics of nucleotide binding to the chaperonin GroEL studied by isothermal titration calorimetry: evidence for*

noncooperative nucleotide binding. Biochim Biophys Acta, 1999. **1431**(2): p. 269-81.

82. Subbarao, N.K. and R.C. MacDonald, *Experimental method to correct fluorescence intensities for the inner filter effect.* Analyst, 1993. **118**(7): p. 913-6.

83. Hackney, D.D., *Kinesin ATPase: rate-limiting ADP release.* Proc Natl Acad Sci U S A, 1988. **85**(17): p. 6314-8.

84. Hamm, H.E., *The many faces of G protein signaling.* J Biol Chem, 1998. **273**(2): p. 669-72.

85. Frank, G.A., et al., *Out-of-equilibrium conformational cycling of GroEL under saturating ATP concentrations.* Proc Natl Acad Sci U S A, 2010. **107**(14): p. 6270-4.

86. Rye, H.S., *Application of fluorescence resonance energy transfer to the GroEL-GroES chaperonin reaction.* Methods, 2001. **24**(3): p. 278-88.

87. Taguchi, H., et al., *BeF(x) stops the chaperonin cycle of GroEL-GroES and generates a complex with double folding chambers.* J Biol Chem, 2004. **279**(44): p. 45737-43.

88. Webb, M.R., *A continuous spectrophotometric assay for inorganic phosphate and for measuring phosphate release kinetics in biological systems.* Proc Natl Acad Sci U S A, 1992. **89**(11): p. 4884-7.

89. Luo, G.X. and P.M. Horowitz, *The stability of the molecular chaperonin cpn60 is affected by site-directed replacement of cysteine 518.* J Biol Chem, 1994. **269**(51): p. 32151-4.

90. Ryabova, N., et al., *Chaperonin GroEL Reassembly: An Effect of Protein Ligands and Solvent Composition.* Biomolecules, 2014. **4**(2): p. 458-73.

91. Ybarra, J. and P.M. Horowitz, *Refolding and reassembly of active chaperonin GroEL after denaturation.* J Biol Chem, 1995. **270**(38): p. 22113-5.

92. Chaudhry, C., et al., *Role of the gamma-phosphate of ATP in triggering protein folding by GroEL-GroES: function, structure and energetics.* EMBO J, 2003. **22**(19): p. 4877-87.

93. Thomas Engel, P.R., *Thermodynamics, statistical thermodynamics, & kinetics*. second ed. 2010: Pearson Education, Inc.

94. Sun, Z., D.J. Scott, and P.A. Lund, *Isolation and characterisation of mutants of GroEL that are fully functional as single rings.* J Mol Biol, 2003. **332**(3): p. 715-28.

95. Yifrach, O. and A. Horovitz, *Two lines of allosteric communication in the oligomeric chaperonin GroEL are revealed by the single mutation Arg196-->Ala.* J Mol Biol, 1994. **243**(3): p. 397-401.

96. Cui, Q. and M. Karplus, *Allostery and cooperativity revisited.* Protein Sci, 2008. **17**(8): p. 1295-307.

97. Eaton, W.A., et al., *Evolution of allosteric models for hemoglobin.* IUBMB Life, 2007. **59**(8-9): p. 586-99.

98. Eaton, W.A., et al., *Is cooperative oxygen binding by hemoglobin really understood?* Nat Struct Biol, 1999. **6**(4): p. 351-8.

99. Erman, B., *A fast approximate method of identifying paths of allosteric communication in proteins.* Proteins, 2013. **81**(7): p. 1097-101.

100. Suel, G.M., et al., *Evolutionarily conserved networks of residues mediate allosteric communication in proteins.* Nat Struct Biol, 2003. **10**(1): p. 59-69.

101. Motlagh, H.N., et al., *The ensemble nature of allostery.* Nature, 2014. **508**(7496): p. 331-9.

102. Horwich, A.L., et al., *Construction of single-ring and two-ring hybrid versions of bacterial chaperonin GroEL.* Methods Enzymol, 1998. **290**: p. 141-6.

103. Sot, B., et al., *Ionic interactions at both inter-ring contact sites of GroEL are involved in transmission of the allosteric signal: a time-resolved infrared difference study.* Protein Sci, 2005. **14**(9): p. 2267-74.

104. Kumar, S. and R. Nussinov, *Relationship between ion pair geometries and electrostatic strengths in proteins.* Biophys J, 2002. **83**(3): p. 1595-612.

105. Fersht, A., *Structure and Mechanism in Protein Science*. fourth ed. 2002, New York: W.H.Freeman and Company. P 527.

106. Brocchieri, L. and S. Karlin, *Conservation among HSP60 sequences in relation to structure, function, and evolution.* Protein Sci, 2000. **9**(3): p. 476-86.

107. Burston, S.G., N.A. Ranson, and A.R. Clarke, *The origins and consequences of asymmetry in the chaperonin reaction cycle.* J Mol Biol, 1995. **249**(1): p. 138-52.

108. Horowitz, P.M., G.H. Lorimer, and J. Ybarra, *GroES in the asymmetric GroEL14-GroES7 complex exchanges via an associative mechanism.* Proc Natl Acad Sci U S A, 1999. **96**(6): p. 2682-6.

109. Chen, J., et al., *Folding of malate dehydrogenase inside the GroEL-GroES cavity.* Nat Struct Biol, 2001. **8**(8): p. 721-8.

110. Cliff, M.J., et al., *Elucidation of steps in the capture of a protein substrate for efficient encapsulation by GroE.* J Biol Chem, 2006. **281**(30): p. 21266-75.

111. *Fluorescence Resonance Energy Transfer (FRET)—Note 1.2*. Available from: http://www.lifetechnologies.com/us/en/home/references/molecular-probes-the-handbook/technical-notes-and-product-highlights/fluorescence-resonance-energy-transfer-fret.html.

112. Lin, Z., et al., *Repetitive protein unfolding by the trans ring of the GroEL-GroES chaperonin complex stimulates folding.* J Biol Chem, 2013. **288**(43): p. 30944-55.

113. Bennett, B.D., et al., *Absolute metabolite concentrations and implied enzyme active site occupancy in Escherichia coli.* Nat Chem Biol, 2009. **5**(8): p. 593-9.

114. Lorimer, G.H., *A quantitative assessment of the role of the chaperonin proteins in protein folding in vivo.* FASEB J, 1996. **10**(1): p. 5-9.

115. Ranson, N.A., et al., *Chaperonins can catalyse the reversal of early aggregation steps when a protein misfolds.* J Mol Biol, 1995. **250**(5): p. 581-6.

116. Mendoza, J.A., et al., *Chaperonins facilitate the in vitro folding of monomeric mitochondrial rhodanese.* J Biol Chem, 1991. **266**(20): p. 13044-9.

117. Sharma, S.K., P. Christen, and P. Goloubinoff, *Disaggregating chaperones: an unfolding story.* Curr Protein Pept Sci, 2009. **10**(5): p. 432-46.

118. Saidi, Y., et al., *Controlled expression of recombinant proteins in Physcomitrella patens by a conditional heat-shock promoter: a tool for plant research and biotechnology.* Plant Mol Biol, 2005. **59**(5): p. 697-711.

119. Saidi, Y., et al., *Activation of the heat shock response in plants by chlorophenols: transgenic Physcomitrella patens as a sensitive biosensor for organic pollutants.* Plant Cell Environ, 2007. **30**(6): p. 753-63.

120. Zimmerman, S.B. and S.O. Trach, *Estimation of macromolecule concentrations and excluded volume effects for the cytoplasm of Escherichia coli.* J Mol Biol, 1991. **222**(3): p. 599-620.

121. Walters, B.T., et al., *Folding of a large protein at high structural resolution.* Proc Natl Acad Sci U S A, 2013. **110**(47): p. 18898-903.

122. Hu, W., et al., *Stepwise protein folding at near amino acid resolution by hydrogen exchange and mass spectrometry.* Proc Natl Acad Sci U S A, 2013. **110**(19): p. 7684-9.

123. Ranson, N.A., et al., *Allosteric signaling of ATP hydrolysis in GroEL-GroES complexes*. Nat Struct Mol Biol, 2006. **13**(2): p. 147-52.

124. Viitanen, P.V., A.A. Gatenby, and G.H. Lorimer, *Purified chaperonin 60 (groEL) interacts with the nonnative states of a multitude of Escherichia coli proteins.* Protein Sci, 1992. 1(3): p. 363-9.

125. Hilton, G.R. and J.L. Benesch, *Two decades of studying non-covalent biomolecular assemblies by means of electrospray ionization mass spectrometry.* J R Soc Interface, 2012. **9**(70): p. 801-16.